

NASA
TMX
69909

74-26274

A Model of the Trapped Electron Population for Solar Minimum



April 1974



NATIONAL SPACE SCIENCE DATA CENTER

NATIONAL AERONAUTICS AND SPACE ADMINISTRATION • GODDARD SPACE FLIGHT CENTER, GREENBELT, MD.

N74-26274

TECH LIBRARY KAFB, NM



0155182

NSSDC 74-03

A Model of the Trapped Electron Population
for Solar Minimum

by

Michael J. Teague
James I. Vette

National Space Science Data Center
National Aeronautics and Space Administration
Goddard Space Flight Center
Greenbelt, Maryland 20771

April 1974

CONTENTS

	<u>Page</u>
1. INTRODUCTION	1
2. THE SOLAR MINIMUM MODEL - GRAPHIC AND TABULAR PRESENTATION	3
3. THE SOLAR MINIMUM MODEL - ASSOCIATED COMPUTER PROGRAMS	7
4. DERIVATION OF MODEL AE-5 1975 PROJECTED	9
5. COMPARISON OF THE PRESENT INNER ZONE ELECTRON MODELS WITH NEW DATA SETS	17
APPENDIX A - MODEL FORMS AVAILABLE TO USERS	29
APPENDIX B - PROGRAM MODEL, VERSION 2.0	31
APPENDIX C - PROGRAM ORP, VERSION 2.0	33
C.1 Program Documentation	33
C.2 Accuracy of the Orbit-Integrated Fluxes	37
APPENDIX D - PROGRAM ORB	45
ACKNOWLEDGMENTS	51
REFERENCES	53

TABLES

<u>Table</u>		<u>Page</u>
1	Omnidirectional Flux Confidence Codes for Model AE-5 1975 Projected	55
2	Omnidirectional Flux Confidence Codes for Model AE-5 1967	56
3	Energy Ranges of Data Sets	57
4	Required Orbits for Accumulation Error to be Less Than a Factor of Two	58
5	Coefficients for Time Interval T_i	59
6	Coefficients for Total Time T_p	59
7	Accuracy of Orbit-Accumulated Fluxes	60

ILLUSTRATIONS

<u>Figure</u>		<u>Page</u>
1-9	Solar Minimum Flux Carpet Plots	61-86
10-13	Orbit-Integrated Flux Carpet Plots	87-94
14-16	B-L Flux Maps	95-97
17-19	R- λ Flux Maps	98-100
20-21	Effect of Revising OV3-3 Spectrometer Efficiencies	101-102
22-25	Inner Zone Electron Radial Profiles	103-106
26-27	Radial Profiles in the Interface Region (L \sim 2.6 Earth Radii)	107-108
28-34	Equatorial Pitch Angle Distributions for L \leq 1.8 Earth Radii	109-115
35-38	Differential Spectra for L \leq 1.8 Earth Radii	116-119
39-46	Equatorial Pitch Angle Distributions for L \geq 2.0 Earth Radii	120-127
47-49	Omnidirectional Flux Distributions for E > 1.5 MeV	128-130
50	Pre-Starfish Radial Profiles Measured by Explorers 4 and 12	131
51	Point-by-Point Table, ORP Version 2.0	132
52	L-band Summary Table, ORP Version 2.0	133
53	Intensity Summary Table, ORP Version 2.0	134
54	Peak Flux Per Orbit Table, ORP Version 2.0	135
55	ORB Output	136

1. INTRODUCTION

The purpose of this document is to present a model of the trapped electron environment for solar minimum conditions. Solar maximum models have been presented for the inner radiation zone by Teague and Vette (1972A and B) and for the outer radiation zone by Singley and Vette (1972A and B). These models are known respectively as AE-5 1967 and AE-4 1967. The solar minimum model presented in this document consists of an inner zone model (AE-5 1975 Projected) with an epoch of 1975, and an outer zone model with an epoch of 1964. With only minor modifications this latter model is identical to the AE-4 1964 model presented previously by Singley and Vette (1972A and B). The model, however, has not previously been issued in computer form. AE-4 1964 is based upon satellite data, while the inner zone solar minimum model AE-5 1975 Projected consists entirely of extrapolations from AE-5 1967. While the two components of the solar minimum model have epochs 11 years apart, it is assumed that any differences between the successive solar minima are smaller than the model error, and the complete model is associated with an epoch of 1975.

This document is presented in two parts. Those readers interested only in the model fluxes are directed to Sections 2 and 3 of the report. Section 2 contains carpet plots of the model flux and the orbit-integrated flux for circular orbits with altitudes in the range from 150 n.m. (278 km) to 18,000 n.m. (33,300 km). In addition, this section refers to confidence codes for AE-5 1975 Projected and presents revised codes for AE-5 1967. Section 3 presents a brief description of the latest model-associated computer programs issued by the National Space Science Data Center (NSSDC). Detailed documentation of each computer program is given in Appendixes B through D. These sections assume that the reader is in possession of the previous program documentation presented by Teague and Vette (1972A). A summary of the forms of the solar minimum model available to a user is given in Appendix A.

Sections 4 and 5 of this document are intended for those readers interested in the derivation of the extrapolated model AE-5 1975 and the agreement between the existing electron models and data that have become available since the generation of the models.

In Section 4, the derivation of the inner zone model is discussed. Two distinct temporal variations are identified in the inner zone: decay of artificial electrons and solar-cycle-associated changes. Model AE-5 1967 contains a significant artificial flux component at low L values and intermediate energies (~ 750 keV). The Starfish model presented by Teague and Stassinopoulos (1972) is used to estimate the natural background flux, and AE-5 1975 is therefore considered to be free of artificial electrons. Solar-cycle-associated changes over the period 1967 to 1975 are estimated from observations made over the time period 1964 to 1967.

In Section 5, the inner zone models AE-5 1967 and AE-5 1975 Projected are compared with a number of data sets that have become available since those models were generated. A number of data sets are regarded as provisional for reasons discussed in Section 4. Data from the following satellites are presented: OGO 5 (West, et al, 1973), OV3-3 (Vampola 1969), OV1-13 (Rothwell, et al, 1972), OSO 4 (Knox 1972), AZUR (Achtermann, et al, 1970), Explorer 4 (McIlwain 1963 and Vette 1966) and Explorer 12 (Ackerson, et al, 1966). In addition, the models are compared with OGO 3 (Pfitzer 1968) data. This data set was used for model AE-5 1967. In general, it is seen that the agreement between the existing electron models and the new data is acceptable.

2. THE SOLAR MINIMUM MODEL - GRAPHIC AND TABULAR PRESENTATION

The solar minimum model describes the trapped electron omnidirectional flux environment for L values in the range $1.2 \leq L/(\text{earth radii}) \leq 11.0$ and for threshold energies in the range $0.04 \leq E_T/(\text{MeV}) \leq 5.0$. The model epoch is 1975.

Omnidirectional flux plots are presented in Figures 1 through 9 for threshold energies $E_T = 40, 100, 250, 500, \text{ and } 750 \text{ keV}$ and 1, 2, 3, and 4 MeV. The omnidirectional flux is shown as a function of magnetic field strength B (units of gauss) and L value (units of earth radii) in carpet plot form. The use of this type of plot has been previously described by Teague and Vette (1972B). With the exception of 40-keV electrons, the inner and outer zones are mapped with three carpet plots. The first map covers the inner zone up to the slot region minimum, the second map covers the slot region to the outer zone maximum, and the final map covers the maximum up to the edge of the outer zone. It will be noted that the equator lines are not shown in Figures 1 through 9. These lines may be obtained by drawing the envelope of the high-flux side of the lines of constant L value.

Singley and Vette (1972A and B) have discussed the temporal variations observed in the outer zone due to magnetic storms. These variations are described by statistical models associated with AE-4 1964 and AE-4 1967. The outer zone plots presented in this document are applicable to an average storm situation. For fluxes at other levels of magnetic activity, the reader is referred to Singley and Vette (1972A). In addition, the inner zone plots presented in this document are appropriate to an average storm situation.

For L values greater than approximately five earth radii, distortion of the geomagnetic cavity by the solar wind becomes significant,

and the B-L coordinate system based upon an internal field becomes a geometric system only. Consequently, a third variable, local time, must be introduced to describe the flux. A local time model has been presented by Singley and Vette (1972A and B); in the present document, however, the plots presented are averaged over longitude, and for local time variations the reader is referred to Singley and Vette (1972A).

Orbit-integrated flux carpet plots are presented in Figures 10 through 13. The flux accumulated per day is shown as a function of energy threshold (MeV) and orbit altitude for circular orbits at inclinations of 0, 30, 60, and 90 degrees. The altitude range from 150 n.m. (278 km) to 18,000 n.m. (33,300 km) is covered in two plots at each inclination to facilitate interpolation. In Figure 10, note that no flux is shown for 150 n.m. (278 km) at 0-degree inclination, since at this altitude flux is accumulated in the anomaly region only. The data presented in Figures 10 through 13 were obtained by "flying" the orbits through the solar minimum model using Program ORP. This program is available from NSSDC and is discussed and documented in Appendix C.

The carpet plots depicted in Figures 1 through 13 are available from NSSDC in the form of black-and-white 35-mm microfilm. They may be obtained using the order numbers MT-26C in the Nonsatellite Data File (NSDF) for Figures 1 through 9 and MT-26B (NSDF) for Figures 10 through 13 (see Appendix A).

B-L and R- λ flux maps are presented in Figures 14 through 19 for threshold energies of 40 keV, 500 keV, and 1 MeV. These plots are shown for the inner zone only. Outer zone plots have been presented previously by Singley and Vette (1972A).

At each energy a single flux contour is shown from the solar maximum model AE-5 1967 for comparison with AE-5 1975 Projected. In Figures 14 and 17 the 1×10^8 -electrons/cm²-sec flux contour is shown for 40 keV.

At this energy the two models differ as a result of solar-cycle-related long-term changes in the inner zone. In Figures 15 and 18, the 1×10^7 -electrons/cm²-sec contour for 500 keV is shown. The double-peaked nature of this contour is evident from both figures. The inner peak reflects the artificial (Starfish) flux component in AE-5 1967. This component has decayed completely by 1975 (Teague and Stassinopoulos 1972). The outer peak is caused by natural electrons. However, the flux does not reach this level in the 1975 estimate, due to reduced magnetic activity at solar minimum. For 1 MeV, the 3×10^6 -electrons/cm²-sec contour is shown in Figures 16 and 19. At this energy there is also a significant artificial flux component in AE-5 1967; this, too, decays completely by 1975. The reader is referred to Sections 4 and 5 for a more detailed discussion of the differences between AE-5 1967 and AE-5 1975 Projected. In addition, a document entitled "Comparison of the Electron Models AE-4 and AE-5 with AE-2 and AE-3" is shortly to be issued by NSSDC (Hilberg, et al, 1974). This document will discuss the differences between the old and the new generation of inner and outer zone electron models.

To enable the user to assess the reliability of the solar minimum inner zone model, a system of confidence codes has been adopted. These codes are shown in Table 1. A similar table has been presented for the solar maximum model AE-5 1967 by Teague and Vette (1972A), where a scale of 1 to 10 was used. A code of 10 corresponds to the highest reliability, with an expected error of a factor of two or less, and a code of 1 to the least reliability, with an expected error in excess of a factor of 10. To maintain compatibility, the same codes are used here, although it is evident from Table 1 that the highest confidence code is 8.

It is clear from Table 1 that the most inaccurate regions of AE-5 1975 Projected are the high-energy regions ($E \geq 3$ MeV), which were derived entirely by extrapolation (even for AE-5 1967). The most accurate

regions are at low energy and low L value, for which temporal variations are small. For additional discussions of the Table 1 confidence codes, the reader is referred to Sections 4 and 5. As a product of the comparison of model AE-5 1967 with new data sets (Section 5), updated confidence codes for this model have been generated. These are shown in Table 2. They replace those previously presented by Teague and Vette (1972A). Discussion of these confidence codes may be found in Section 5.

3. THE SOLAR MINIMUM MODEL - ASSOCIATED COMPUTER PROGRAMS

Three model-associated computer programs are now issued by the National Space Science Data Center (NSSDC): Programs MODEL, ORP, and ORB. The first two of these programs have been issued previously by NSSDC in earlier versions (1.0). Documentation of these has been presented by Teague and Vette (1972A). Program MODEL provides the user with the model flux at an arbitrary energy for an arbitrary point in B-L space. Program ORP allows the user to fly an arbitrary orbit through any of the models issued by NSSDC. The major modification to these two programs has been to include the solar minimum model. Detailed documentation of the modifications to Programs MODEL and ORP is given in Appendixes B and C. In addition, a discussion of the accuracy of orbit-integrated fluxes is given in Appendix C. Appendixes B and C are presented on the assumption that the reader has access to the program documentation presented by Teague and Vette (1972A). The third program issued by NSSDC, ORB, is a new program and is primarily designed to generate orbit tapes for Program ORP. Detailed documentation of this program is given in Appendix D. A summary of the available computer programs and model products is given in Appendix A.

4. DERIVATION OF AE-5 1975 PROJECTED

As noted in the Introduction, the solar minimum model presented in this document is composed of two parts. The outer zone part of the model is identical to the AE-4 1964 model presented by Singley and Vette (1972A), except that smoothing has been performed to remove irregularities in the average differential spectrum output by Program MODEL, and to make the interface region between the outer and inner zones smooth. The inner zone part of the solar minimum model is referred to as AE-5 1975 Projected, and is derived solely from the inner zone solar maximum model AE-5 1967, presented by Teague and Vette (1972B).

In the context of temporal variations, the inner zone in 1967 may be divided into three regions, each with a dominant temporal variation. At low L values, ($L \leq 1.6$ earth radii), a decaying artificial flux component exists for energies $E > 400$ keV. This artificial component is the residue of the particles injected by the Starfish nuclear explosion of July 1962. At intermediate L values (from 1.6 to 1.8 earth radii), the characteristic variation is a steady solar-cycle-related change in the flux of particles with energies less than 500 keV. This variation is characterized by the solar cycle parameters presented by Teague and Vette (1972A). At high L values (greater than 1.8 earth radii), the dominant temporal variation for $E > 100$ keV is due to magnetic storms. Compared to the outer zone, magnetic storms occur in the inner zone with a relatively low frequency, and it is possible to determine a "quiet day" flux level between storms for most energies. The change in the flux level at storm time, however, is sufficiently large for magnetic storms to be the dominant factor in determining the model in the outer edge of the inner radiation belt. It is clear that storm-time flux changes at high L and steady changes that occur at intermediate L values have the same source and are

separated only as a matter of convenience. In deriving AE-5 1975 Projected from AE-5 1967, efforts were made to account for the three temporal variations discussed in this paragraph.

An additional factor concerning the OV3-3 electron spectrometer data (Vampola 1969) affected the derivation of AE-5 1975 Projected. The energy ranges covered by this spectrometer are shown in Table 6. At the time AE-5 1967 was generated, the only data set available in the time period 1966-67 for $L > 1.6$ earth radii and $E > 700$ keV was equatorial perpendicular flux as a function of time at various L values, measured by OV3-3. This data set was supplied by Vampola. At lower energies and L values a number of other data sets were available (Teague and Vette 1972A). Subsequent to the derivation of AE-5 1967, the estimated values of efficiency of the OV3-3 spectrometer were increased by a factor of four (Vampola 1972), with the result that the flux levels were reduced by the same factor. Consequently, the fluxes given by AE-5 1967 for $L > 1.6$ earth radii and $E > 700$ keV must be regarded as high estimates. In the derivation of AE-5 1975 Projected, an attempt was made to allow for the correction in the estimated efficiency of the OV3-3 spectrometer. The importance of the correction can be assessed from Figures 20 and 21, in which various differential energy spectra are shown for L values of 1.4 and 1.8 earth radii, respectively. In each figure, the "uncorrected" OV3-3 data are those data that were available at the time of the generation of AE-5 1967. The "corrected" OV3-3 data comprise the latest OV3-3 data set available at NSSDC. This data set was not used for the generation of either AE-5 1975 Projected or the Starfish model (Teague and Stassinopoulos 1972), and is shown for comparison purposes only. Comparing the "corrected" and "uncorrected" OV3-3 data sets in Figures 20 and 21, it can be seen that the two sets of data differ, in general, by less than a factor of four. The discrepancy is thought to have arisen as a result of differing assumptions concerning the pitch-angle distribution used to normalize

the data to the equator, and as a result of scattering of the data. Further discussion of the corrected OV3-3 data is given in the following section.

In Figure 20, AE-5 1967 for $E > 700$ keV is substantially a fit to the uncorrected OV3-3 data, with a decay factor included for the difference of epochs. The following procedure was adopted for determining model AE-5 1975 Projected for those energies and L values ($E > 700$ keV, $L < 1.6$ earth radii) for which AE-5 1967 contained a significant Starfish residual flux. A "corrected" AE-5 1967 spectrum was obtained on the basis of a compromise between a small amount of OGO 3 data (Figure 20) and the uncorrected OV3-3 data, divided by four to account for the efficiency change. The Starfish model of Teague and Stassinopoulos (1972), which was not affected by the efficiency change in the OV3-3 spectrometer, was then used to remove the artificial flux component. The broken line in Figure 20 indicates the results of this procedure. Summations of the solar minimum model and of the Starfish model for September 1966 indicate reasonable agreement with corrected OV3-3 data from the same time period.

The above procedure was used for $L < 1.6$ earth radii and $E > 700$ keV. In this region, AE-5 1975 Projected is intended to reflect the natural electron environment. Teague and Stassinopoulos (1972) have shown that the artificial Starfish electrons are longest lived in the inner zone at $L=1.3$ earth radii and $E=1.6$ MeV, approximately, and reach the natural background approximately 8 years (July 1970) after Starfish injection. Since the only data available for low L values and high energies contain a significant artificial component, estimation of the solar minimum model in these regions is an inaccurate process. This is reflected in the confidence limits given in Table 1.

In Figure 21 for $L=1.8$ earth radii, it is clear that the AE-5 1967 spectrum for $E > 700$ keV is a simple fit to the OV3-3 uncorrected data set. For $L > 1.8$ earth radii at these energies, as noted at the beginning of this section, the effects of magnetic storms become important. Teague and Vette (1972B) showed that the ratio of average storm flux to quiet day flux over an 18-month time period near solar maximum peaked in the region of 1 MeV. This ratio increased from 1.2 at $L=1.8$ earth radii to 35 at $L=2.4$ earth radii. It has not been possible, however, to make meaningful estimates of how these ratios may vary with solar cycle, nor is it known how the quiet day flux varies at high energies. Consequently the solar minimum model in these regions was obtained from AE-5 1967 by correcting for the change in the efficiency of the OV3-3 spectrometer. That is, AE-5 1967 for $L \geq 1.3$ earth radii and $E > 700$ keV was divided by four to obtain AE-5 1975 Projected, which may be regarded as a high estimate of the average storm flux at solar minimum.

For energies $E < 500$ keV, the inner zone exhibits a steady increase in the quiet day flux from solar minimum to solar maximum. Teague and Vette (1972A) have made a quantitative estimate of this steady increase in flux from 1964 to 1967.

The ratio of the flux in late 1967 to that in late 1964 reaches a peak at $L = 2.0$ earth radii, where it varies from 2.8 for particles with energies between 36 keV and 133 keV, to 22 for particles with energies between 292 keV and 690 keV. In terms of integral energies, the solar-cycle ratios vary at $L = 2.0$ earth radii from 3.6 at 40 keV to 6.9 at 250 keV.

Assuming that the 1975 solar minimum flux is similar to the 1964 solar minimum, these estimates may be used to obtain AE-5 1967 from AE-5 1975 Projected. This procedure was adopted for all L values and energies $E < 250$ keV.

Examples of the inner zone radial profiles for Models AE-5 1967 and AE-5 1975 Projected are shown in Figures 22 through 25 for 40, 250, and 500 keV, and 1 MeV. The profiles at these energies illustrate the various procedures used to derive AE-5 1975 Projected.

In Figure 22, the two models at 40 keV are related by the solar cycle parameters discussed previously. Magnetic storm effects are observable at 40 keV, particularly at high L values, but the magnitude of the effects is not sufficient to affect the model significantly. At 250 keV, storm effects become more important, but the effect on the model remains minor even at high L values. With the exception of a small Starfish component for $L \leq 1.6$ earth radii, the two model curves in Figure 23 are related by the solar cycle parameters.

At 500 keV, the situation becomes more complex (as shown in Figure 24) because of an increased Starfish component and the impact of the OV3-3 data. The solar minimum flux at 500 keV was primarily determined by smoothing the spectrum between higher and lower energies where the solar minimum flux was better defined; however, some explanation of the differences between the two models should be given. For $L \leq 1.6$ earth radii, where a significant Starfish component existed, AE-5 1967 was determined as a compromise between the uncorrected OV3-3 data and the OGO 3 data. Correcting for the OV3-3 data yields the dotted curve shown in Figure 24. Using the Starfish model of Teague and Stassinopoulos (1972), the artificial flux component can be removed and the broken line in Figure 24 may be regarded as an estimate of the natural solar maximum flux at 500 keV. The solar cycle parameters have been used to obtain AE-5 1975 Projected at $L \leq 2.0$ earth radii. It should be noted that whenever the solar cycle parameters were used to determine the solar minimum condition, a smoothing of the radial profiles was performed to obtain an acceptable model. In general, this smoothing resulted in small changes in the solar minimum flux. However, more substantial (approximately 80 percent) changes were necessary in the

region around $L = 1.8$ earth radii at 500 keV. For $L > 2.0$ earth radii at 500 keV, magnetic storm effects become significant and the solar minimum radial profile is largely determined by smoothing with other energies and L values.

For higher energies such as 1 MeV, shown in Figure 25, the Starfish component in AE-5 1967 at low L values becomes more significant (an estimated 90 percent of the total flux at $L = 1.4$ earth radii). For $L \leq 1.7$ earth radii, the same procedure for estimating the solar minimum flux was adopted at this energy as was used at 500 keV, except that solar parameters were not used. However, the accuracy of the model is significantly reduced at 1 MeV because of the large Starfish component in AE-5 1967. This is reflected in Table 1. For $L > 1.7$ earth radii, AE-5 1967 was determined on the basis of uncorrected OV3-3 data. As noted earlier in this section, the solar minimum model was determined simply by dividing by four. This procedure was adopted for energies up to 3 MeV. Minor corrections were made for smoothing. At 4 MeV, correction was made for the Starfish component only, but at this energy the model is most inaccurate, as indicated by Table 1.

As noted earlier, the outer zone portion of the model presented in this document is substantially the same as the AE-4 1964 model presented by Singley and Vette (1972A and B). However, a certain amount of smoothing has been performed, particularly at the inner edge of the outer zone at high energies, to make the outer zone portion of the model compatible with the inner zone portion. The interface region between the two portions of the solar minimum model is shown in Figures 26 and 27. The dotted line indicates the interpolation performed for the interface region, and the broken lines show the modification that has been made to the outer zone model AE-4 1964. A minor amount of smoothing has been performed on AE-4 1964 at higher L values than those shown in

Figures 26 and 27. This was done to make the average differential spectrum smooth. In no case was AE-4 1964 changed by more than 30 percent.

Changes to the radial profiles and spectra between solar maximum and minimum have been discussed in the preceding paragraphs. No modification has been made to the B dependence of the fluxes. Models AE-5 1967 and AE-5 1975 Projected have identical B dependences. Teague and Vette (1972B) showed that there were small differences in the B dependence of the artificial and natural flux distributions at certain L values and energies. However, in the regions where AE-5 1967 contains a large artificial component, the B dependence is not well known, and no effort has been made to include B dependence variations.

5. COMPARISON OF THE PRESENT INNER ZONE ELECTRON MODELS WITH NEW DATA SETS

In this section the inner zone models AE-5 1967 and AE-5 1975 Projected are compared with data from the following satellites: OGO 5 (West, et al, 1973), OV1-13 (Rothwell 1972), OSO 4 (Knox 1972), AZUR (Achtermann 1970), OV3-3 (Vampola 1969), OGO 3 (Pfitzer 1968), Explorer 12 (Ackerson, et al, 1966) and Explorer 4 (McIlwain 1963, Vette 1966). The electron data from OGO 5, OV1-13, OSO 4, and AZUR were not used in the development of AE-5 1967 or AE-5 1975 Projected since they have only recently become available to the National Space Science Data Center (NSSDC). The OGO 5, Explorer 12, and Explorer 4 data have previously been compared with the Starfish model of Teague and Stassinopoulos (1972). As discussed in the previous section, some OV3-3 data were used in the development of AE-5 1967, but a more complete and more correct data set is presented here. The OGO 3 data comprised the prime data set used for AE-5 1967 and are presented here for comparison with the new data sets.

Information concerning the type of detectors and their energy ranges is presented in Table 3. This table summarizes the data available to NSSDC at the present time. Only a portion of these data sets is presented in this document. Some analysis of the data sets and experiments listed in Table 3 has been performed at NSSDC. The calibration parameters used for the OGO 3 electron spectrometer are those presented by Teague (1970). The efficiencies and energy ranges of each channel differ from those presented by Pfitzer (1968). The resulting fluxes presented here (and those used for determining AE-5 1967) are lower than those given by Pfitzer by a factor of approximately two in Channel 1 and by 25 to 30 percent in the higher channels. The OV3-3 data set has been determined using the calibration parameters given by Vampola (1969) after correction for the factor-of-four efficiency change (Vampola 1972). Correction has been made for the variation of local pitch angle with time over the spectrometer cycle

time. This correction resulted in a maximum change of 10 percent in the flux observed at any given equatorial pitch angle. Analysis of the OV1-13 and AZUR data sets is in progress, and the data presented here are provisional. Data at higher energies than those indicated in Table 3 are available from the OV1-13 detector. These data are not shown at the present time because of problems with the calibration parameters. Similarly, AZUR data are available for 4.5-MeV electrons but are not displayed because of calibration problems. In addition, no effort has been made to remove the 20-MeV proton contribution from the 1.5-MeV electron flux measured by AZUR, owing again to calibration problems. These data are presented as upper limits of the electron flux only.

The data sets discussed in the previous paragraphs are compared with models AE-5 1967 and AE-5 1975 Projected in Figures 28 through 50. Figures 28 through 34 show examples of differential flux equatorial pitch angle distributions for $L \leq 1.8$ earth radii, as measured by OGO 5, OSO 4, OV1-13, OV3-3, and OGO 3. Examples of equatorial spectra are shown in Figures 35 through 38 for $L \leq 1.8$ earth radii. For these L values, magnetic storm effects are relatively unimportant, and a good comparison between the model and the data can be anticipated. At higher L values, storm effects are dominant. However, the model estimates an average storm condition, with the result that comparison of data and model is qualitative only. Examples of the equatorial pitch angle distributions at these higher L values are shown in Figures 39 through 46 for data from OGO 5, OV1-13, OV3-3, and OGO 3. In Figures 47 through 49, examples of the B dependence of the omnidirectional flux by AZUR are shown for various L values. Figure 50 illustrates the radial profiles measured by Explorers 4 and 12.

In general, where comparison can be made, the data from the OGO 3, OV3-3, OV1-13, and OGO 5 experiments show substantial agreement.

However, there are a number of areas where conflict is apparent, notably for the low-energy OV3-3 data. This may be seen from Figure 30 and Figures 35 through 38. In the latter set of figures, each data point has been normalized to the equator, where possible, by using the pitch angle distribution given by that data set. In some cases, notably with the OGO 3 data, the model pitch angle distribution has been used. With the exception of the two highest energy channels of the OGO 3 detector and the highest energy channel of the OGO 5 detector, the pitch angle coverage in the region of the equator is good, and the standard deviation of the equatorial values is less than a factor of two. For the exceptions, a standard deviation of a factor of three may be appropriate. It is clear from Figure 30 and Figures 35 through 38 that the fluxes from channels 8 and 9 (Table 3) are low in relation to the other data sets. Further, the average differential flux measured by channel 8 (475 keV) is lower than that measured by channel 7 (approximately 250 keV higher), when in all other cases the spectrum is monotonic at these energies. Also, in Figure 30 substantial differences in the equatorial pitch angle distribution observed in Channel 8 of the OV3-3 detector and other satellites is evident. OV3-3 indicates an isotropic distribution for $\alpha_0 \geq 50$ degrees approximately, whereas OGO 5, OV1-13, and OGO 3 show a clear decrease in flux for $\alpha_0 < 65$ degrees approximately. In the region of the cutoff, however, substantial agreement can be seen among all data sets. Similar observations may be made for both Channels 8 and 9 when $L \leq 1.8$ earth radii. At high L values, however, such as that shown in Figure 41, the pitch angle coverage is such that equatorial observations are not made. Since data from channels 8 and 9 were used to generate AE-5 1967, some discussion of the impact upon this model is in order.

Referring to Figure 30, it can be seen that model AE-5 for epoch 1967 is in substantial agreement with the OGO 3 data for late 1967. In general, AE-5 for this epoch was a fit to the OGO 3 data and was

not influenced by OV3-3 data. As a result the accuracy of AE-5 1967 at low energies ($E < 500$ keV) was not compromised. However, data taken at earlier epochs, such as mid-1966 shown in Figure 30, were used in the determination of the solar cycle parameters and the Starfish model. The Starfish model presented by Teague and Stassinopoulos (1972) and used for the generation of AE-5 1975 Projected has been corrected for these effects. In Figure 30, AE-5 1967, back-dated to June 1966 by using the Starfish model and the solar cycle parameters, shows good agreement with OGO 3 data obtained at the same time period. This results from the fact that the uncorrected OV3-3 data available at the time AE-5 1967 was generated were a factor of four higher at the equator than the OV3-3 data shown in Figure 30, and apparently showed good agreement with the OGO 3 data.

The conclusions concerning the low-energy OV3-3 data are that channels 8 and 9 are apparently anomalous, both in terms of the equatorial value and the pitch angle distribution, for reasons that are presently not understood. However, the accuracy of AE-5 1967 at low energies is not compromised, since this model generally favored the OGO 3 data that subsequently showed good agreement with OGO 5 and OV1-13 data.

The high-energy OV3-3 data (Channels 1 through 7 in Table 6) generally show reasonable agreement with other data sets. This may be seen for Figures 29, 34, and 35 through 38. At low L values where the flux is influenced by Starfish electrons, good agreement can be seen between the OGO 3 and OV3-3 data (Figures 35 and 36). At higher L values (Figures 37 and 38), there is reasonable agreement among the OV1-13, OGO 5, and OV3-3 data, except for $E > 1$ MeV at $L = 1.6$ earth radii, where a decaying Starfish component is present in late 1966. In Figure 34 the pitch angle distributions observed by OV1-13 and OV3-3 are seen to be very similar. In Figure 29, however, some differences between the OV1-13 and OV3-3 equatorial flux can be seen for electrons with

energies in the neighborhood of 700 keV. The OV3-3 data for the earlier epoch are believed to contain a small Starfish component, so the differences between the two data sets may be explained by a solar cycle effect occurring after the artificial component decayed. This supposed solar cycle effect is not observed at the same energy at $L = 1.8$ earth radii (Figure 34), however.

The OGO 5, OV1-13, and OGO 3 data may be compared in Figures 30, 32, and 35 through 38. The experimenter's calibration parameters have been used for OGO 5 and OV1-13, and no assessment of these parameters has been made by NSSDC. For the OGO 3 spectrometer, however, the calibration values given by Teague (1970) have been used. Differences between these values and those given by Pfitzer (1968) result in differences of a factor of two in the flux at low energies and differences of a smaller factor at high energies. For $E \leq 400$ keV, the OGO 5 data tends to be higher than the OGO 3 data. This tendency may be observed in Figure 30 and Figures 35 through 38. At $L = 1.4$ earth radii, the difference is as high as a factor of two.* For energies in the neighborhood of 550 keV, the OGO 5 data is slightly higher than the OV1-13 data (Figures 35 through 38), and in most cases slightly higher than the OGO 3 data. Again, in the region of 900 keV, the OGO 5 data is higher than the OV1-13 data by a small amount.

*In the course of review of the document, it was pointed out by Dr. H. West that the apparent differences between the OGO 3 and OGO 5 low-energy fluxes suggest that Pfitzer's calibration values for the lowest energy channels may be more appropriate than those used in this document. At some L values ($L = 1.4$ earth radii, for example, in Figure 36) the use of Pfitzer's low-energy calibration value would improve the agreement between the two data sets. In other cases, however, such as $L = 1.6$ or 1.8 earth radii (Figures 37 and 38), this is not the case. It should be stated that with electron modeling, it has generally been the experience of the authors that agreement within a factor of two between two given data sets is the best that can be expected.

Pitch angle distributions observed by OGO 3, OGO 5, OV3-3, and OV1-13 at $L = 2.0$ and 2.4 earth radii are shown in Figures 39 through 46. At these L values the comparison between various data sets must take into account the degree of magnetic activity for $E > 100$ keV, approximately, and these figures are intended to give an indication of the variability of the absolute-flux levels with magnetic activity. Although the data shown here for magnetically active periods have poor equatorial pitch angle coverage, in general the shape of the pitch angle dependences in this region of space are not strongly energy dependent and, with the exception of the first few days following a major event, this shape is given by that for energies $E < 100$ keV. In Figures 39 through 46, data are shown for periods before and after the September 1966 magnetic storm (peak $|Dst| = 229$ on day 247, 1966) and before and after the June 1968 storm (peak $|Dst| = 94$ on day 163, 1968). In the neighborhoods of 80 keV and 158 keV, no storm effects are evident from the OGO 5 data (Figures 39 and 40). At $E \approx 280$ keV, clear storm effects are evident in both the OGO 5 data (shown for times before and after the 1968 event) and the OV3-3 data (shown for two periods after the 1966 event). Storm effects became most pronounced between the energy levels of 500 keV and 900 keV, shown in Figures 42 through 44. In these plots OGO 5 and OV1-13 data may be compared for the relatively quiet period before the June 1968 event, and these data may be compared with OV3-3 and OGO 3 data from relatively quiet periods in 1966. It should be noted that some of the OGO 5 data shown in these figures were taken 30 days after the mild event occurring in February 1968 (peak $|Dst| = 123$ on day 42). These data show no enhancement over the general quiet background, while ten days after the June event, however, considerable enhancement is evident. These observations indicate that a rapid (less than 30 days) depletion of storm-time flux can occur at these L values. Markedly longer depletion times are evident at lower L values. In Figures 42 through 44, fair agreement may be observed between the various quiet-time data sets, but some spread of the data resulting from

varying degrees of magnetic activity is evident. In Figure 45 the 1.22-MeV OV3-3 data are shown at $L = 2.0$ earth radii for two epochs following the 1966 event. Magnetic storm effects are evident. However, at 1.76 MeV, shown in Figure 46, little or no storm effects can be seen, indicating the reduced affect of storms at very high energies. This has been noted previously by Teague and Vette (1972B), who reported a peak storm effect at $E \sim 900$ keV.

In comparing the new data sets presented here with the models, it should be noted that the epochs of most of the data are comparable with that of AE-5 1967. As a result, the confidence codes for AE-5 1967 are modified, and these in turn affect the projected model AE-5 1975. The atmospheric cutoff region of AE-5 for $L \leq 1.8$ earth radii is confirmed by the OSO 4 data (Figures 28 through 34). In most cases new data from other satellites are available for comparison in this region, and these are in general agreement with the model cutoff. A possible exception is $L = 1.7$ earth radii, shown in Figures 32 and 33, where the equatorial pitch angle of the model cutoff is apparently too high. This effect is more pronounced at the low energies, shown in Figure 32, than at the higher energies, shown in Figure 33. At higher L values ($L > 1.9$ earth radii), no new data are available in the cutoff region, and the model cutoff cannot be confirmed.

For energies less than 500 keV, AE-5 1967 was primarily determined from the OGO 3 data. The equatorial flux given by AE-5 1967 is therefore seen to be slightly lower than the OGO 5 data at most L values. The possible reasons for the small differences between the OGO 3 and OGO 5 data have been discussed previously. At high L values ($L > 2$ earth radii), the OGO 3 data provided poor pitch angle coverage. In Figure 39 it can be seen that the model pitch angle distribution at $L = 2.4$ earth radii underestimates the equatorial flux at 80 keV. At a slightly higher energy at the same L value (Figure 40), however, the model pitch angle distribution shows good agreement with the data.

At most energies and L values the shape of the pitch angle distribution given by AE-5 1967 agrees very well with that given by the new data sets. This pitch angle distribution is unchanged for AE-5 1975 Projected.

Some deficiencies may be present in the equatorial fluxes given by AE-5 1967 for energies greater than 700 keV, largely as a result of the use of uncorrected OV3-3 data in determining this model. The differences between the model and the data at high energies may be observed in Figures 29, 31, and 33 through 38. In each case, AE-5 1967 is too high by a factor between 1.2 and 4. This model must be regarded as a high estimate of the 1967 flux for energies greater than 700 keV, as noted in the previous section. A change in the OV3-3 spectrometer efficiency by a factor of four has been incorporated into AE-5 1975.

In Figures 35 through 37, the Starfish model of Teague and Stassinopoulos has been used with AE-5 1975 Projected to obtain the high-energy model flux for the two epochs September 1966 and March 1968. The model and the data agree within a factor of two at these epochs. For $L = 1.8$ earth radii, shown in Figure 38, good agreement is seen between the high-energy AE-5 1975 Projected spectrum and the OV1-13 and corrected OV3-3 data.

For the high L values, shown in Figures 41 through 46, magnetic storm effects dominate. The model represents an average storm flux. As a result, the level of agreement between model and data is dependent upon the degree of magnetic activity. In the course of developing AE-5 1967, an estimate of the quiet-day flux at high L values was made. This estimate was based upon uncorrected OV3-3 data for energies greater than 500 keV. Correcting for the efficiency changes in the OV3-3 spectrometer (a factor of four), the quiet-day flux estimates shown in Figures

42 through 44 were obtained. It can be seen that these estimates lie below the quiet-time data by a factor of two to three. In general, the magnetically distributed data shown in Figures 41 through 46 are in the region of the AE-5 1967 model curve, and it would seem likely that this model is a high estimate of the average storm flux in 1967.

A comparison is made between the AE-5 models and the AZUR 1.5-MeV data in Figures 47 through 49. The B dependences of the omnidirectional flux are shown for $L = 1.8, 2.0, \text{ and } 2.4$ earth radii. As indicated by Table 3, the AZUR detector also measured 20-MeV protons. Protons have not been removed from the data shown in these figures because of uncertainties with proton counting efficiency; it is estimated that as much as 60 percent of the observed counts may be due to protons. In view of the probable proton contribution, the agreement between the AZUR data and the models is considered to be good. However, the data do indicate a slightly flatter B dependence than that given by the model, particularly at $L = 2.4$ earth radii.

The only available estimate of the natural electron population of the inner zone before the artificial injection event of 1962 has been provided by the Explorer 4 and Explorer 12 satellites. As indicated by Table 3, both detectors were sensitive to protons and electrons. At the time the Explorer 4 measurements were made, it was assumed that the total inner zone counting rate came from energetic protons (McIlwain, 1963). An upper limit to the electron flux is obtained by assuming all counts came from electrons, as Ackerson and Frank (1966) have done for the Explorer 12 inner zone measurements. These upper limit radial profiles for 1.6-MeV and 2-MeV electrons are shown in Figure 50. However, it is estimated that at least 50 percent of the observed count rate is due to protons. For $L > 1.4$ earth radii, the Explorer 4 data have been extrapolated to the equator, using the B dependence of the proton model (Vette 1966). For $L > 1.6$ earth radii, the Explorer 12 data have been extrapolated to the equator.

The equatorial values presented by Ackerson and Frank (1966) are shown in Figure 50; it is estimated that these equatorial values are accurate to within 50 percent. The 1.5-MeV AZUR data are shown for an epoch of December 1969. With the possible exception of $L = 1.3$ and 1.4 earth radii, where a small artificial flux component may remain, the AZUR data are considered to be an upper estimate of the natural electron flux at 1.5 MeV. The agreement between the AZUR and Explorer 12 data with similar electron and proton thresholds is reasonable. Model AE-5 1975 Projected shows reasonable agreement with the data at 1.6 MeV. At low L values the Explorer 12 data appear higher than the model. A large proton contribution is expected in this region. At high L values the Explorer 12 data also appear higher than the model. It is possible, therefore, that these data are affected by the large magnetic storm event of July 1961 (peak $|Dst| = 144$ on day 208, 1961). At 2 MeV, model AE-5 1975 Projected appears higher than the data at most L values, particularly when it is considered that the data contain a significant proton contribution. There is some doubt, however, about the electron energy threshold of the Explorer 4 detector, and therefore the 2-MeV value quoted may be regarded as a minimum energy threshold.

In conclusion, it should be stated that the best accuracy that can be expected for an electron model is a factor of two. Consequently, differences of less than this factor between model and data set or between data set and data set can be regarded as relatively unimportant from a modeling point of view. Thus, in most cases, the agreement between the various data sets presented, and that between model AE-5 1967 and the data sets, is regarded as good. The two exceptions are: (1) the two low-energy channels of the OV3-3 detector, which seem anomalously low in relation to the other data sets, and (2) the high-energy ($E > 700$ keV) portion of AE-5 1967, which is higher by a factor of three to four than the corrected OV3-3 data set. In respect to the last item, it should be noted that the confidence code quoted by

Teague and Vette (1972A) for the high-energy AE-5 1967 spectrum denoted accuracy within a factor of three or four.

The results of the comparison between the new data sets and the solar maximum model AE-5 1967 have been used to reevaluate the confidence codes presented by Teague and Vette (1972A). The new codes are shown in Table 2. These differ from those presented previously, primarily as a result of the general good agreement between AE-5 1967 and the new data for L values between 1.3 and 1.9, for $E < 700$ keV. The B dependence of the model at high energies ($E > 700$ keV) has been confirmed, but no improvement in the confidence code results because of the correction to the OV3-3 spectrometer efficiency. Similarly, the B dependence of the model at low energies and high L values ($L > 2$ earth radii) has been confirmed in some cases, but in others minor differences between the model and data are observed, and no change in the confidence code is given. Confidence codes have been estimated for AE-5 1975 Projected and are shown in Table 1. The same scale of 1 to 10 is adopted, although the highest confidence code that occurs is 8.

APPENDIX A
MODEL FORMS AVAILABLE TO USERS

The following forms of model-related information are available from the National Space Science Data Center.

Documents:

1. AE-4 outer zone electron model documentation. Singley and Vette 1972 A and B.
2. AE-5 solar maximum inner zone electron model documentation. Teague and Vette 1972 A and B.
3. Starfish Electron Model. Teague and Stassinopoulos 1972.
4. Comparison of the new generation of electron models, AE-4 and AE-5, with the old electron models, AE-2 and AE-3. Hilberg, et al, 1974.

Computer Programs:

1. Program MODEL, Version 2.0. BCD and EBCDIC punch. Available with any or all of the model BLOCK DATA subprograms: AE-5 solar maximum (AE5MAX), AE-4 solar maximum (AE4MAX), AE-5 solar minimum (AE5MIN), AE-4 solar minimum (AE4MIN) and a smoothed version of the proton models AP-5, AP-6 and AP-7 (PROTON).
2. Program ORP, Version 2.0. BCD and EBCDIC punch. Available with any or all of the model BLOCK DATA subprograms described in Program MODEL.
3. Program ORB, Version 1.0. BCD and EBCDIC punch. Two versions are available: Version 1.1 with a Brouwer orbit generator for eccentricities greater than 0.1, and Version 1.2 with a Lyddane orbit generator for eccentricities smaller than 0.1.

Microfilm:

The following information is available on 35-mm microfilm:

1. Carpet plots as Figures 1 through 9 in black and white. Use

reference number MT-26C in the Nonsatellite Data File.

2. Carpet plots as Figures 10 through 13 in black and white. Use reference number MT-26B in the Nonsatellite Data File.

APPENDIX B
PROGRAM MODEL, VERSION 2.0

The major modification to Version 1.0 of MODEL has been the inclusion of the solar minimum model presented in this document. The BLOCK DATA subprograms are designated AE4MIN and AE5MIN for models AE-4 1964 and AE-5 1975 Projected, respectively. The COMMON statements are included in subroutine TYPE. With reference to page 14 of Teague and Vette (1972A), the solar minimum model may be accessed by setting the variable MTYPE in column 9 of card a to 3. The appropriate header information is generated by MAIN. The meanings of other input variables for Version 1.0 remain unchanged in Version 2.0. The same restrictions on the average differential flux calculations for the solar maximum model are applicable to the solar minimum model (page 12 of Teague and Vette 1972A).

The second modification concerns the default B intervals used in the output tables for IDEF=0. In Version 1.0, linear B intervals are used at each L value, with the interval size being set to give approximately 25 B values at each L value. This algorithm provides poor resolution at high B values. Version 2.0 contains a semi-logarithmic algorithm for reducing the B interval at high B values where $L > 2.8$ earth radii. A final minor modification is that the lines of the output tables corresponding to different B values are numbered in Version 2.0.

A summary of the computer decks available with Program MODEL Version 2.0 is given in Appendix A.



APPENDIX C
PROGRAM ORP, VERSION 2.0

C.1 Program Documentation

Substantial changes have been made to the input and output of Program ORP, Version 1.0. Changes have been made to the input of Version 2.0 to give ORP the potential of executing in less computer time. Ultimately, however, the execution time is dependent upon the time period covered by the input orbit tape and the time increment used for the orbit. In the latter part of this section, consideration is given to the relation between these parameters and the accuracy of the output tables provided by ORP.

Two new input parameters are included in Version 2.0 of Program ORP. The first parameter, ISKIP, controls the number of points read from the input orbit tape and passed to the model interpolation routines. This parameter may be used when it is known that too many points are stored on the input tape. When ISKIP is set at 2, one-half of the points read from the tape are passed on to the model; if ISKIP is set at 5, one-fifth of the points will be passed to the model interpolation routine. Considerable savings in execution time will result from the use of this parameter. Use of this parameter, though, might also affect the accuracy of the resulting output tables. This problem will be discussed later in this section.

A second parameter, ITAPE, allows the input of either binary or BCD tapes. In general, binary tapes are preferred, since substantially less computer time is required to input unformatted tapes than formatted ones. When a list of items is being read or written under format control, each item in the list must be passed to special programs in the FORTRAN I/O package for the necessary conversion. The use of binary input tapes bypasses this conversion. Tests performed on an IBM 360/75

with ORP indicated that as much as 25 percent of the execution time can be saved by using binary input tapes.

With reference to page 25 of Teague and Vette (1972A), the field of input card a for ORP has been extended to include the two new parameters:

<u>Card No.</u>	<u>Variable Name</u>	<u>Cols</u>	<u>Format</u>	<u>Function</u>
a cont	ISKIP	71-72	I2	Controls number of input points passed to model (one in every ISKIP). If field is blank, ISKIP=1.
	ITAPE	73-74	I2	ITAPE = 0 for binary input tape; = 1 for BCD input tape.

The format of the BCD input tape remains as described on pages 22 and 23 of Teague and Vette (1972A). Either binary or BCD tape is input on logical unit 10. The first record of the tape must contain arbitrary header information. Subsequent records must contain the six variables: longitude (degs), latitude (degs), altitude (km), magnetic field strength (gauss), McIlwain L parameter (earth radii) and time from start of orbit (hours). The end of the orbit is recognized by an altitude of -100 km or less. The orbit generation Program ORB documented in Appendix D is designed to output orbit tapes in the correct format for input to Program ORP Version 2.0.

The solar minimum model described in Section 2 of this document may be obtained by setting the parameter MODEL on card a equal to 3 (Teague and Vette 1972A, page 24). To avoid unnecessary subroutine calls, sub-

routine TYPE has been eliminated from ORP Version 2.0 and the COMMON statements for the BLOCK DATA subprograms AE4MIN and AE5MIN are entered into MAIN. A summary of the computer decks available with Program ORP Version 2.0 is given in Appendix A.

Program ORP is able to output any or all of the following six tables under control of the parameter TABCON described on page 23 of Teague and Vette (1972A): Point by Point (PP) Table, L-band Summary (LS) Table, Integrated Flux (IF) Table, Intensity Summary (IS) Table, Peak Flux per orbit (PF) Table, and the Four-Orbit Summary (FOS) Table. Modifications have been made to all tables except the IF and FOS Tables. Some of the modifications are cosmetic, but a number of new indices have been added to the tables to enable the user to assess the reliability of the orbit-integrated fluxes.

An example of the PP Table output by Version 2.0 is shown in Figure 51. The point flux is output at three energies determined by the energy ET, input on card a (Teague and Vette 1972A, page 24). The center energy is the energy nearest to ET contained in the E energy array, input on cards b and c. The next lower and higher energies in this array are also output in the PP Table. If the length of the E array is less than three, the point flux is given for each energy E. Program ORP automatically rejects points for which B and L are zero. That is, these points are not passed to the model interpolation routines, with a consequent saving of computer time. As will be discussed in Section 3.3, Program ORB is able to write zeros on the tape for B and L when it is known that the satellite orbit is outside the radiation belts. These points are automatically omitted in the PP Table, and a statement of the number of omitted points is given.

An example of the LS Table is shown in Figure 52. This table differs from the Version 1.0 table primarily because of the addition of three sets of sample sizes NP1, NP2, and NSIZE, each defined in the

table footnote. The energy array used for the LS Table is that input on cards b and c. NP1 is the number of non-zero fluxes encountered in the L band given for the lowest energy of this array. NP2 is given for that energy in the E array nearest to ET, input on card a. NSIZE is the number of orbit points lying in each L band. The use of these indices is discussed in subsequent paragraphs. The L ranges used for the LS Table are specified in subroutine STORE. The parameter 'Time Interval' output at the top of the LS Table refers to the last two points on the orbit. For highly eccentric orbits the time interval may vary considerably with altitude, and the value output for 'Time Interval' will be of limited use.

An example of the IS Table is shown in Figure 53. The intensity ranges used for this table are specified by a DATA statement in subroutine FLITAB. The sample size of each accumulated flux is printed out as described in the table footnote. Discussion of the use of this parameter is given in later paragraphs.

An example of the PF Table is shown in Figure 54. A nominal orbital period, T, has been added to this table. This is computed using the expression

$$T = T_c (1 + h_{av})^{3/2},$$

where T_c is the Schuler Period, equal to 84.347 minutes (Nelson and Loft 1962), and h_{av} is the average altitude in earth radii determined by summing at successive orbit points over the total orbit time. This period may be in error for a small number of revolutions of eccentric orbits if the last revolution is partial. ORP computes a revolution in differing fashions for zero and non-zero inclinations. For zero inclination, 0 hours local mean time is used, while for non-zero inclinations a south-to-north equatorial crossing is used. In Version 2.0 of ORP, the appropriate longitude of the end of each revolution is

given with the appropriate header information. It is very likely that the last revolution is a partial revolution only; in this case an appropriate message is output as shown in Figure 54. The PF Table will terminate at 50 revolutions with an appropriate message.

C.2 Accuracy of the Orbit-Integrated Fluxes

In this section a discussion of the accuracy and utility of the tabular output of ORP is given. The solar minimum model accuracy is summarized in Table 2 of this document, and the similar table given by Teague and Vette (1972A) for the inner zone solar maximum model has been updated in Table 2. It is clear that at best the orbit-integrated fluxes are no better than the models used with the orbit. However, a number of other effects may result in additional errors in the accumulated fluxes. For instance, table accumulation errors may result from basing the sample size on an orbit of finite length. For certain orbits accumulating a significant portion of the integrated flux from regions of steep gradients in flux, the type of orbit generator used may become important. The distinction is drawn between "errors" in the accumulated fluxes and "limitations" of the accumulated fluxes. The latter item is discussed first.

"Limitations" of the accumulated fluxes arise as a result of various time averagings performed in the model. The variation in the flux level due to magnetic storm effects is known to be considerable in the outer zone and the outer edge of the inner zone ($L > 1.8$ earth radii). A variation about the average flux of approximately one order of magnitude may be regarded as typical in the outer zone. The BLOCK DATA subprograms issued by NSSDC represent the average storm situation in the radiation belts. The orbit-integrated fluxes, therefore, represent the same average situation, and the question arises of the time required for the satellite to accumulate this average. The frequency of occurrence of magnetic storms in the outer zones is high, and it is not

possible to isolate magnetically undisturbed periods. As a result the satellite accumulates the storm-averaged integrated fluxes to a reasonable degree of accuracy in a matter of weeks for outer-zone-dominated fluxes. As noted by Teague and Vette (1972B), in the outer edge of the inner zone region the frequency of occurrence of magnetic storms is low in relation to the outer zone frequency, but considerable enhancement of the flux is observed when a storm does occur. For instance, over the period mid-1966 to late-1967 only three significant excursions of the flux above a quiet-day value were observed for $L > 1.8$ earth radii. However, these three excursions were largely responsible for determining AE-5 1967 for energies between 0.5 and 2 MeV (Teague and Vette 1972B). For orbits accumulating a significant percentage of the flux from the outer edge of the inner zone (low-inclination circular orbits in the region of 7000 km, for instance), the actual mission time required to accumulate the storm's average orbit-integrated flux given by the model subprograms may be as high as one year. In addition to these orbit-integrated effects, the tables providing information concerning point fluxes must be kept in perspective. In particular, the Peak Flux per orbit (PF) and the Point by Point (PP) Tables provide averaged fluxes that may differ from the actual observed value by an order of magnitude (up or down) due to magnetic storm variation.

A second averaging process has been performed for the model contained in the BLOCK DATA subprogram. The outer zone model has been local time or longitudinally averaged. The local time parameter is included in the outer zone model for $L > 5$ earth radii, approximately, to account for cavity distortion. By using a local-time-averaged model for accumulating orbit-integrated fluxes, it is implicitly assumed that the satellite averages over local time in its orbit; that is, it samples all local times with equal weighting. This is clearly not correct for many orbits and for those orbits for which it is a reasonable assumption that the actual mission time required to observe the average obtained from the model subprogram may be considerable. It is

not possible to estimate what this time might be, but the observed flux can differ from the averaged flux by a maximum of the local time variation contained in the outer zone model. However, it is very probable that the actual effect is less severe than this. Stassinopoulos (1974) has investigated a synchronous orbit with eccentricity 0.18 and inclination 45 degrees. This orbit does not sample all local times equally, and a comparison of the local-time-averaged orbit-integrated fluxes with those accumulated accounting for the variation of local time showed typical differences of factors of two or three.

In the previous two paragraphs, "limitations" of the orbit-integrated fluxes have been discussed. It is not easy to interpret these in terms of "errors" in the accumulated fluxes since these are based upon items that are not quantitatively well defined. However, one source of error can be referred to as table accumulation error. This results from the use of a finite orbit to estimate the actual coverage of the arbitrary accumulation bins encountered by the satellite. The magnitude of this effect may be estimated by varying both the length of time the orbit is flown (total time) and the time increment between successive orbit points (time interval) and observing the effect on the tabular output of ORP. In general, accumulation errors are dependent on the size of the accumulation bin and the number of independent variables used for the accumulation. That is, the IS and LS Tables are more susceptible to accumulation error than the IF Table, since the former accumulates on two independent variables (intensity and energy, L-band and energy) whereas the latter uses only one (energy). Using the accumulation bins shown in Figures 52 and 53, the total times and time intervals required for accumulation errors in the IS and LS tables to be less than a factor of two were determined for circular equatorial and polar orbits at altitudes of 150, 1500, 5000, and 15,000 n.m. (approximately 278, 2778, 9260, and 27,780 km, respectively). For higher L-values than those shown in the LS Table (Figure 52), 0.1-unit increments in L were used up to L=3

earth radii, 0.2-unit increments up to L=6 earth radii, and 0.5-unit increments for higher L-values. The required time intervals and total times are shown in Table 4. These times are those for the maximum error to be less than a factor of two. Most accumulated fluxes will be more accurate than this, and determining which fluxes are subject to accumulation error will be discussed in a following paragraph. From Table 4, it is clear that there is considerable variation of the required time interval and total time with orbit. High-inclination orbits require more total points and more points per revolution than low-inclination orbits. Further, low altitudes require more total points than high altitudes. The first requirement results from the fact that higher inclination orbits spend a smaller proportion of each revolution inside the belts than the lower inclinations. The second requirement results from the fact that low-altitude orbits are influenced significantly by the South Atlantic anomaly region, which is traversed for a comparatively small proportion of some revolutions. At 150 n.m. (278 km), flux is accumulated in the anomaly region only, and the figures in Table 4 at this altitude are given for 30 degrees inclination. To reduce the maximum accumulation error in the IS and LS Tables to a factor of two or below requires a considerable increase in the total number of orbit points. To reduce the maximum error to 30 percent, the number of orbit points must be doubled or even tripled, thereby increasing the computer time by an almost equal amount. In view of the limitations of these tables, this increase is entirely unwarranted. As noted above, tables other than the IS and LS Tables have small accumulation errors only, and fewer orbit points are needed for these tables. In Table 4, the values in parentheses are those required to give a maximum accumulation error of 30 percent in the FOS and IS tables.

As a guide to suitable values of time interval, T_i , and total time, T_p , the following expression,

$$\log_{10} T_i \text{ or } \log_{10} T_p = a_1 \log_{10} (\text{altitude}) - a_2 \times (\text{inclination}) - a_3 - 2,$$

may be used with the coefficients given in Tables 5 and 6 for time interval and total time, respectively. In this equation, T_i is given in minutes, T_p in days, altitude in nautical miles, and inclination in degrees. These coefficients provide suitable circular orbit parameters for the IS and LS Tables. For the remaining tables, the total time may be reduced by a factor of 1.5, and the time interval increased by the same amount. For eccentric orbits, equation 2 may be used to determine the time interval at apogee and perigee; if Program ORB is used to generate the orbit, the time interval may be varied linearly with altitude between these extremes (Section 3.3). The total time used for the orbit should be that determined from equation 2 for apogee. If the orbit to be input to Program ORP is already in existence and the time interval is less than that given by equation 2, the ISKIP parameters discussed earlier in this section may be used to increase the time interval. If the time interval is greater than that given by equation 2, it should be appreciated that accumulation errors greater than a factor of two may result in the IS and LS Tables.

The indices included in the Intensity Summary and L-band Summary Tables may be used to assess the reliability of the accumulated fluxes. It is important to use these indices, as the accumulation errors discussed in previous paragraphs do not affect all accumulated fluxes. For the L-band Summary Table (Figure 52), L bands for which the spectrum is hard are suspect, particularly those for which NSIZE is less than 30. Small sample sizes (fewer than five samples) are suspect in general, as are accumulated fluxes in energy bins for which NP2 is considerably different from NSIZE or NP1. For the Intensity Summary Table (Figure 53), the accumulated fluxes that are most suspect are the smaller fluxes that occur with small sample sizes (fewer than 30 samples).

An additional item may affect the accumulated fluxes and the point fluxes determined by Program ORP. For orbits and energies where the

flux accumulation arises predominantly from regions of steep gradient in the model, the orbit generator used may significantly affect the tabular output of ORP. Orbits in this category include low-altitude satellites at low inclination that accumulate flux from the steep-gradient region at the inner edge of the inner zone, and satellites that accumulate flux from the horns of the outer zone where the flux is varying rapidly with B. In general, orbits for which the orbit generator used may be important are also orbits for which the model error is particularly high, and thus the use of a sophisticated orbit generator does not significantly improve the accuracy of the accumulated fluxes.

The question arises as to how differences between predicted and observed orbits affect the accumulated fluxes, that is, how much will the observed flux differ from the predicted accumulated flux due to small differences between assumed and observed orbits? Orbits for which the orbit generator used is important are also the orbits for which small deviations from assumed orbit will significantly vary the accumulated fluxes. Since in these cases the flux differences between planned and achieved orbits may be as great as those between different generators, even the most sophisticated orbit generator will probably not result in more accurate accumulated fluxes. In general, it is recommended that the simplest orbit generators be used to generate orbit tapes for input to Program ORP.

In summary, there are important limitations on the orbit-accumulated fluxes generated by Program ORP resulting from averaging processes in the model. In addition, there may be errors in the accumulated fluxes over and above those introduced by model error. Both the limitations and the errors are very orbit-dependent, and no generalized quantitative statement may be made about either. However, Table 7 is an attempt at estimating the error in the LS and IS Tables for circular orbits at 150, 1500, 5000, and 15,000 n.m. (approximately 277, 2778, 9260, and 27,780 km, respectively) and 0-degree and 90-degree

inclinations. The total times and time intervals shown in Table 4 were used for the orbits, and the accumulation bins described previously were used in the IS and LS Tables. The estimated maximum and minimum model error is shown for each orbit for the solar maximum and solar minimum electron models. In general, the maximum model error occurs at the highest energy encountered on each orbit, and the minimum model error occurs at the lowest energy encountered. The total maximum and minimum errors are given for solar maximum and solar minimum, including the effects of table accumulation errors. No error greater than a factor of 10 is estimated. It is emphasized that this table is not intended to give a definitive statement of the accuracy of the IS and LS Tables, but merely to give some indication of the accumulated fluxes. It is clear from Table 7 that the model error is the most significant contributor to the final total error for the orbit total times and time intervals used for this table. If the total time is reduced or the time interval is increased significantly, accumulation errors become relatively more significant. Conversely, accumulation errors become less significant if the accumulation bins are increased in size. The conclusion to be drawn from Table 7 is that the errors associated with the IS and LS Tables are sufficiently large for the accumulated fluxes to be regarded as approximate figures only.

APPENDIX D
PROGRAM ORB

Program ORB is a simple orbit generation and B-L calculation program that is primarily used for generating orbit tapes for input to Program ORP, described in the previous section. Program ORB is a FORTRAN IV program written for the IBM 360 series machines; however, the program is also operational on UNIVAC 1108 machines. The program exists in two versions, both sharing a common MAIN. The two versions, 1 and 2 respectively, contain a Brouwer orbit generator (Brouwer 1959) and a Lyddane orbit generator (Lyddane 1963). The former is more suited to orbits with eccentricities greater than 0.1, while the latter is better suited to less eccentric orbits. Both versions will operate for small eccentricities, but there are certain restrictions that will be discussed in a following paragraph.

Sample ORB output is shown in Figure 55. The line printer output is under control of the input parameter IPR. Using this parameter, either a point-by-point listing of the generated orbit may be obtained, or the first five and last five generated points may be output only, as shown in Figure 55. The tape output is under control of the input variable ITAPE, which allows either a binary or a BCD output tape to be written. Both output tapes are compatible with Program ORP.

As noted in the previous section, binary tape output is generally to be preferred, since less computer time is required for a binary WRITE. The time interval between successive points on the orbit tape is defined by the input parameter DSEC, and the total time covered by the generated orbit is specified by the parameter SEC MAX. For circular orbits, the time interval should remain constant, but for eccentric orbits it may be advantageous to vary the interval with altitude for radiation belt studies. If required, Program ORB will read in the parameters A and C and compute the time interval from the expression

$$\text{DSEC} = A + (C \times \text{altitude}).$$

If this option is used, DSEC is output as zero, and the above expression is written out on the line printer. The number of orbit points generated and the average altitude are written on the line printer together with the nominal period computed from equation 1.

ORB contains an algorithm for controlling the B and L values written on the output tape. The B-L calculation is performed at every orbit point using the routine INTEL (Sugiura and King, 1973) with the IGRF 1965 magnetic field model (IAGA 1969) updated to 1970. Under control of the parameter LIMIT these B and L values may be written to default values on the output tape if the point is outside the broad region of the radiation belt. Program ORB defines this region as

L > 11.0 earth radii
or L < 1.1 earth radii
or B > 0.2 + 0.05L gauss for L \leq 2.4 earth radii
or B > 0.604 gauss for L > 2.4 earth radii.

The default values DEFB and DEFL are specified to be zero by a DATA statement in Program MAIN. These default values are automatically rejected by Program ORP with a consequent saving of computer time (see Section 3.2).

A variable IORB determines the version of Program ORB to be used. Each deck contains one orbit generator only and includes dummy routines for the other. If the value of IORB and the generator included are incompatible, an appropriate error message is generated.

The input card format to ORB is as follows:

<u>Card No.</u>	<u>Variable Name</u>	<u>Cols.</u>	<u>Format</u>	<u>Function</u>
a	HEAD	1-76	19A4	Arbitrary header information output on both tapes and printer.
b		1-38	2D15.8, 4(2X,I2).	
	SECMAX	1-15	D15.8	Total Time of orbit in seconds. Program terminates for DSEC=-1.D0
	DSEC	16-30	D15.8	Time Interval in seconds. If DSEC=0.0D0, card C is read.
	IPR	33-34	I2	IPR=1 for point-by-point printer output; IPR=0 for first five and last five points only output on line printer.
	ITAPE	37-38	I2	ITAPE=0 for binary tape output; ITAPE=1 for no tape output; ITAPE=2 for BCD tape output.
	LIMIT	41-42	I2	LIMIT=0 for B-L algorithm; LIMIT=1 for no B-L restriction on tape.

<u>Card No.</u>	<u>Variable Name</u>	<u>Cols.</u>	<u>Format</u>	<u>Function</u>
	IORB	45-46	I2	IORB=0 for Version 1 (Brouwer generator); IORB=1 for Version 2 (Lyddane generator).
c		1-30	2D15.8	Card read for DSEC=0.0D0 only.
	A	1-15	D15.8	Coefficient for orbit time interval in sec- onds - (equation 3).
	C	16-30	D15.8	Coefficient for orbit time interval in sec- onds/km - (equation 3).
d		1-45	3D15.8	
	ELEM1(1,1)	1-15	D15.8	Semi-major axis in earth radii.
	ELEM1(1,2)	16-30	D15.8	Eccentricity.
	ELEM1(1,3)	31-45	D15.8	Inclination in degrees.
e		1-45	3D15.8	
	ELEM1(1,4)	1-15	D15.8	Mean anomaly in radians.
	ELEM1(1,5)	16-30	D15.8	Argument of perigee in radians.
	ELEM1(1,6)	31-45	D15.8	Right Ascension of ascending node in radians.
f	Same as card 1.			
g	Same as card 2 etc.			Program terminates for DSEC=-1.0D0

There are a number of restrictions on the values of ELEM1(1,2) and ELEM1(1,3). For Version 1.0, the eccentricity may not be entered as zero. If this version is used to generate circular orbits, ELEM1(1,2) should be entered in the range from 10^{-9} to 10^{-3} . For larger values of eccentricity, altitude and L variations become significant for lower altitudes. For smaller values, program interrupts occur, and spurious L values are generated. For Version 2.0, (the intended version for small eccentricities), eccentricity may be entered as 0.000. The inclination, ELEM1(1,3), may not be entered as zero in either version. A value in the range from 10^{-9} to 10^{-7} degrees should be used for zero-inclination orbits. Larger values result in nonzero latitudes, and smaller values result in program interrupts.

The output BCD tape (ITAPE=2, card b) is written on unit 10 and the format is as follows:

<u>Record</u>	<u>Variable</u>	<u>Format</u>	<u>Function</u>
1	HEAD	19A4	Orbit Header as input on card a.
2 to i+1		6E18.8	i successive orbit points.
	XXLONG	E18.8	Longitude (degrees)
	XXLAT	E18.8	Latitude (degrees)
	XALT	E18.8	Altitude (km)
	XB	E18.8	Magnetic field strength (gauss)
	XXL	E18.8	McIlwain L parameter (earth radii)
	XHOUR	E18.8	Time from start of orbit (hours)
i+2		36X,F5.0	
	TALT	F5.0	Written to -100.0 to indicate end of orbit.
i+3	Same as record 1 for next orbit.		

The variable TALT written to indicate the end of the orbit is set equal to -100.0 by a DATA statement in MAIN. This is recognized by Program ORP as an end-of-orbit flag.

The unformatted binary tape is written on logical unit 10. The variables are written in the same order as the BCD tape, with the exception that the i+2 record is a repeat of the i+1 record with altitude set equal to -100.0 km.

The suggested deck setup for IBM 360 series machines is as follows:

```
//Job Card
//EXEC FORTRANH,PARM='MAP,OPT=2',REGION.SOURCE=300K.
//SOURCE.SYSIN DD *
                Source Deck
/*
//EXEC LINKGO,REGION.GO=150K
//LINK.OBJECT DD * (if Object deck included)
                Object Deck (if any)
/* (if object deck included)
//GO.FT10F001 DD (output tape information appropriate to value of
                ITAPE input on card b)
//GO.SYSUDUMP DD SYSOUT=C
//GO.DATA5 DD *
                Data Deck
/*
//
```

Program ORB generates and outputs on tape approximately 5×10^4 orbit points on the IBM 360/75 in approximately 8 minutes of cpu time and 0.5 minutes of I/O time. These figures are appropriate to binary output. For BCD tape output, approximately 12 minutes of cpu time are required.

A summary of the ORB decks issued by NSSDC is given in Appendix A.

ACKNOWLEDGMENTS

Our thanks are due to Dr. Harry West, who provided valuable assistance in incorporating the OGO 5 data in this document, and to Drs. West and Al Vampola, who reviewed the document and suggested several improvements. In addition, we express our appreciation to Dr. L. Choy, who performed much of the analysis of the data presented in this document.

REFERENCES

1. Achtermann, E., B. Häusler, D. Hovestadt, G. Paschmann, E. Küneth, and P. Laeverenz, "The Experiments EI88 and EI93 for the Measurement of High-Energy Electrons, Protons and Alpha particles in the AZUR Satellite: Physical Properties and Test Measurements," The Max Planck Institute of Physics and Astrophysics, Research Report W70-67, Interplanetary Research.
2. Ackerson, K. L., and L. A. Frank, "Explorer 12 Observations of Charged Particles in the Inner Radiation Zone," University of Iowa 66-13, 1966.
3. Brouwer, D., "Solution of the Problem of Artificial Satellite Theory Without Drag," The Astronomical Journal, Vol. 64, 1959.
4. Hilberg, R., M. J. Teague, and J. I. Vette, "A Comparison of the Recent Electron Models AE-4 and AE-5 with AE-2 and AE-3," to be published in 1974.
5. IAGA, "International Geomagnetic Reference Field 1965.0," IAGA Commission 2 Working Group 4 Analysis of the Geomagnetic Field. J. Geophys. Res. 74 4407-4408, 1969.
6. Knox, R. J., "OSO-4 Electron Observations on the Edge of the Inner Radiation Zone," UCRL-51185 Feb. 1972.
7. Lyddane, R. H., "Small Eccentricities or Inclinations in the Brouwer Theory of Artificial Satellites," The Astronomical Journal, Vol. 68, 1963.
8. McIlwain, C. E., "Coordinates for Mapping the Distribution of Magnetically Trapped Particles," J. Geophys. Res. 66, 3681-4078, 1963.
9. Nelson, N. C., and E. E. Loft, "Space Mechanics," Prentice-Hall Space Technology Series, 1962.
10. Pfitzer, K. A., "An Experimental Study of Electron Fluxes from 50 keV to 4 MeV in the Inner Radiation Belt," University of Minnesota, Tech. Report CR-123, August 1968.
11. Rothwell, P. L., and W. R. Mooney, "Calibration of a Magnetic Spectrometer Designed to Measure 0.1- to 1.0-MeV Electrons in Space," AFCRL-72-0710, December 1972.
12. Singley, G. W., and J. I. Vette, "The AE-4 Model of the Outer Radiation Zone Electron Environment," NSSDC 72-06, 1972A.

13. Singley, G. W., and J. I. Vette, "A Model Environment for Outer Zone Electrons," NSSDC 72-13, 1972B.
14. Stassinopoulos, E. G., "Non-separability of Radial and Local-time Dependences in the Orbital Flux Integration of Synchronous Trajectories," NSSDC 74- , To be published.
15. Sugiura, M., and J. H. King, "Computer Programs Pertaining to the Earth's Magnetic Field and Magnetospheric Field Models," NSSDC 73-12, 1973.
16. Teague, M. J., "The Calibration Constants for the OGO 1/3 Electron Spectrometer," NSSDC 70-14, October 1970.
17. Teague, M. J., and J. I. Vette, "The Inner Zone Electron Model AE-5," NSSDC 72-10, 1972B.
18. Teague, M. J., and J. I. Vette, "The Use of the Inner Zone Electron Model AE-5 and Associated Computer Programs," NSSDC 72-11, 1972A.
19. Teague, M. J., and E. G. Stassinopoulos, "A Model of the Starfish Flux in the Inner Radiation Zone," NASA X-601-72-487, December 1972, 1972.
20. Vampola, A. L., "Energetic Electrons at Latitudes Above the Outer Zone Cutoff," J. Geophys. Res., 74(5), 1254-1269, 1969.
21. Vampola, A. L., private communication, December 1972.
22. Vette, J. I., "Models of the Trapped Radiation Environment. Volume 1 - Inner Zone Protons and Electrons," NASA SP 3024, 1966.
23. West, H. I., Jr., R. M. Buck, and J. R. Walton, "The LLL Electron and Proton Spectrometer on NASA's Orbiting Geophysical Observatory 5," UCRL-51385, May 1973.

Table 1. Omnidirectional Flux Confidence Codes for AE-5 1975 Projected

Code	B range	L range	E range	Comment
1	$>B_0^*$	<1.25	≥ 3 MeV	Extrapolation on B, L, and E
2	B_0	<1.25	≥ 3 MeV	Extrapolation on L and E
4	All B	≥ 1.3	≥ 3 MeV	Extrapolation on E and B
5	All B	1.3-1.6	0.5-3 MeV	Starfish model used to estimate artificial flux Agrees with pre-Starfish data at E ~ 1.6 MeV
5	All B	1.9-2.4	>250 keV	Storm effects. Corrected for OV3-3 data.
6	All B	1.3-1.9	0.7-2.5 MeV	Corrected for OV3-3 data
6	All B	1.9-2.4	40-250 keV	Solar cycle parameters used
7	All B	1.6-1.9	40-600 keV	Solar cycle parameters used
8	All B	1.3-1.6	40-500 keV	Solar cycle parameters used.

<u>Code</u>	<u>Model Accuracy</u>
8	Factor of 3 to 4
1	Order of Magnitude

$*B_0$ = Equatorial B value.

Table 2. Omnidirectional Flux Confidence Codes for AE-5 1967

Code	B range	L range	E range	Comment
1	$>B_0$	<1.25	≥ 3 MeV	Extrapolation on B, L, and E. No data
2	B_0	<1.25	≥ 3 MeV	Extrapolation on L and E. No data
4	All B	≥ 1.3	≥ 3 MeV	Extrapolation on E and B
4	All B	<1.25	< 3 MeV	Extrapolation on L and B
5	All B	1.9-2.4	> 250 keV	Magnetic storm effects present
6	B_0	1.9-2.4	< 250 keV	Conflicts with new data
6	All B	1.3-1.9	700-2000 keV	Too high due to OV3-3 data
8	$> B_0$	1.9-2.4	< 250 keV	Agrees with new data
10	All B	1.3-1.9	< 700 keV	Favorable comparison with new data.

<u>Code</u>	<u>Model Accuracy</u>
10	Factor of 2
1	Order of magnitude

Table 3. Energy Ranges of Data Sets

Satellite	Channel	Electron Energy Range (MeV)	Type of Measurement
OGO 3	1 2 3 4 5	0.036-0.133 0.133-0.292 0.292-0.690 0.690-1.97 1.97 -4.74	Unidirectional Differential Electron Flux. June 1966 - December 1967
OV3-3	1 2 3 4 5 6 7 8 9	2.147-2.472 1.88 -2.2 1.615-1.925 1.329-1.651 1.075-1.375 0.814-1.099 0.574-0.849 0.35 -0.6 0.225-0.375	Unidirectional Differential Electron Flux. August - December 1966
Explorer 4		> 2.0	Omnidirectional Integral Total Particle Flux. Protons > 43 MeV July - October 1958
Explorer 12		> 1.6	Omnidirectional Integral Total Particle Flux. Protons > 21 MeV August - September 1961
OGO 5	1 2 3 4 5 6 7	0.056-0.102 0.122-0.194 0.23 -0.302 0.427-0.531 0.637-1.007 1.27 -1.79 2.55 -3.09	Unidirectional Differential Electron Flux. March - June 1968
OSO 4	1 2 3 4 5	0.08 -0.121 0.121-0.171 0.171-0.258 0.258-0.537 0.537-0.900	Unidirectional Differential Electron Flux. March 1968
OV1-13	6 7 8	0.45 -0.55 0.62 -0.72 0.85 -0.95	Unidirectional Differential Electron Flux. May - June 1968
AZUR	1	> 1.5	Omnidirectional Integral Total Particle Flux. Pro- tons > 20 MeV December 1969

Table 4. Required Orbits for Accumulation Error to be Less Than a Factor of Two

Inclination (degs)	30	0			90			
Altitude (n.m.)	150	1500	5000	15000	150	1500	5000	15000
Total Time (Days)	1.5 (1.0)	0.5 (0.5)	1.0 (1.0)	12.0 (12.0)	1.5 (1)	1.0 (1.0)	4.0 (2.0)	48.0 (24.0)
Time Interval (Minutes)	0.5 (2.0)	1.0 (3.0)	4.0 (6.0)	48.0 (72.0)	0.5 (2)	0.5 (3.0)	2.0 (6.0)	12.0 (72.0)
Total Number of Points	4320 (720)	720 (240)	360 (240)	360 (240)	4320 (720)	2880 (480)	2880 (480)	5760 (480)
Number of Points per Revolution	180 (45)	144 (48)	88 (58)	22 (15)	180 (45)	288 (48)	176 (58)	88 (15)

Figures in parentheses are for 30 percent FOS and IF tables.

Table 5. Coefficients for Time Interval T_i

altitude (n.m.)	a_1	a_2	a_3
150 - 1500	0.301	3.344×10^{-3}	0.956
1500 - 12000	1.193	3.344×10^{-3}	3.79
12000 - 18000	5.154	3.344×10^{-3}	19.95

Table 6. Coefficients for Total Time T_p

altitude (n.m.)	a_1	a_2	a_3
150 - 1500	-0.176	0	-0.559
1750 - 4500	0.567	-3.344×10^{-3}	1.840
5000 - 12000	0.567	-6.690×10^{-3}	1.840
12000 - 18000	6.874	-6.690×10^{-3}	27.568

Table 7. Accuracy of Orbit-Accumulated Fluxes

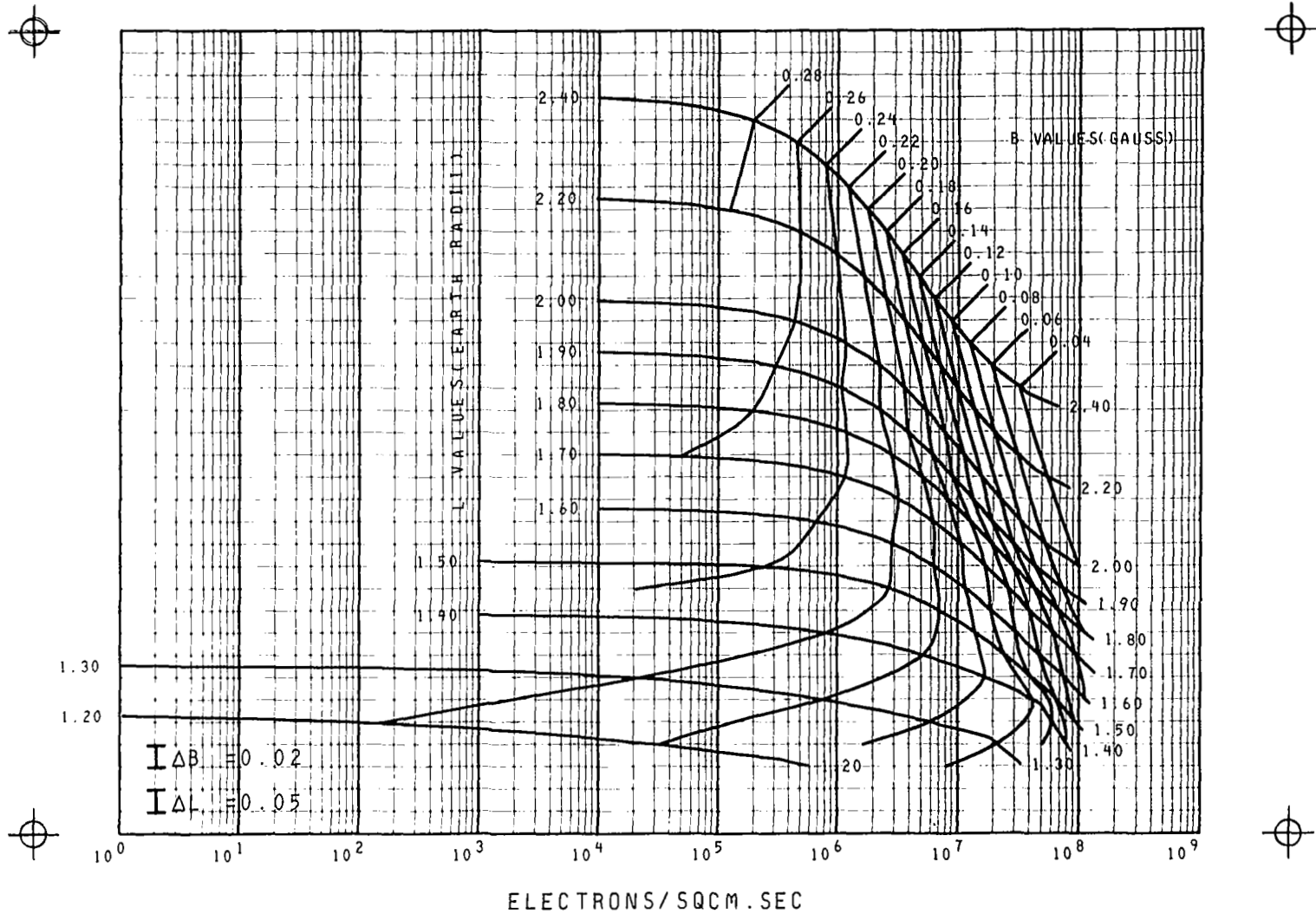
Inclination (degs)	30	0			90			
Altitude (n.m.)	150	1500	5000	15000	150	1500	5000	15000
Max. Model Error	10 (10)	10 (8)	9 (8)	6 (6)	10 (10)	7 (7)	8 (8)	10 (10)
Min. Model Error	7 (6)	3 (2)	5 (4)	4 (4)	4 (4)	5 (5)	5 (5)	5 (5)
Max. Table Error	10 (10)							
Min. Table Error	8 (7)	3 (3)	6 (5)	5 (5)	5 (5)	6 (6)	6 (6)	6 (6)

The figures in this table are factor errors; i.e., "7" indicates an error of a factor of 7. The figures in parentheses are for the solar maximum electron model AE-5 1967. The figures not in parentheses are for model AE-5 1975 Projected.

OMNIDIRECTIONAL INTEGRAL FLUX MAP
 40 KEV ELECTRONS L LE 2.4
 MODEL AE5 SOLAR MINIMUM PROJECTED

FIG. 1

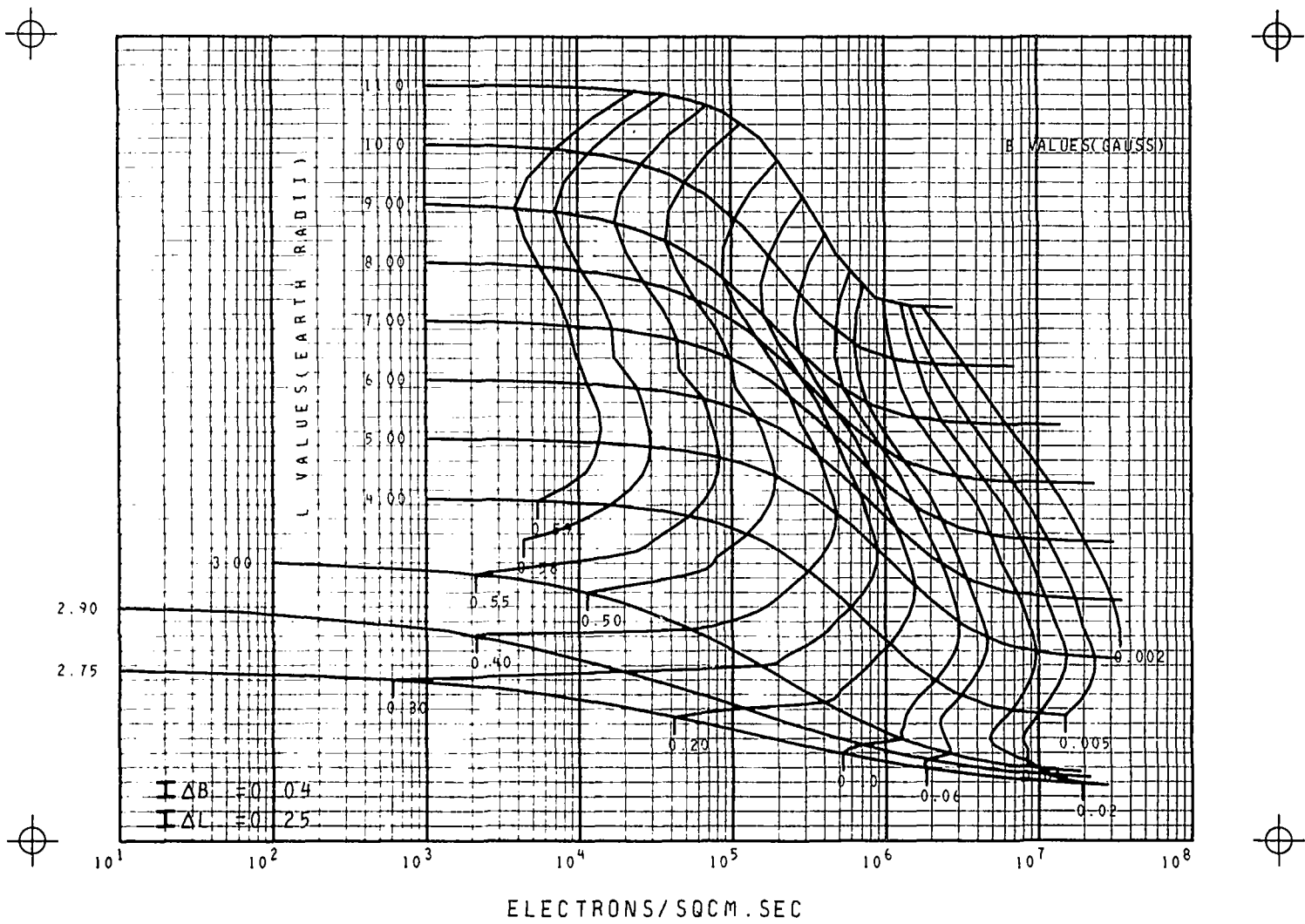
19



OMNIDIRECTIONAL INTEGRAL FLUX MAP
 40 KEV ELECTRONS L GT 2.75
 MODEL AE4 SOLAR MINIMUM PROJECTED

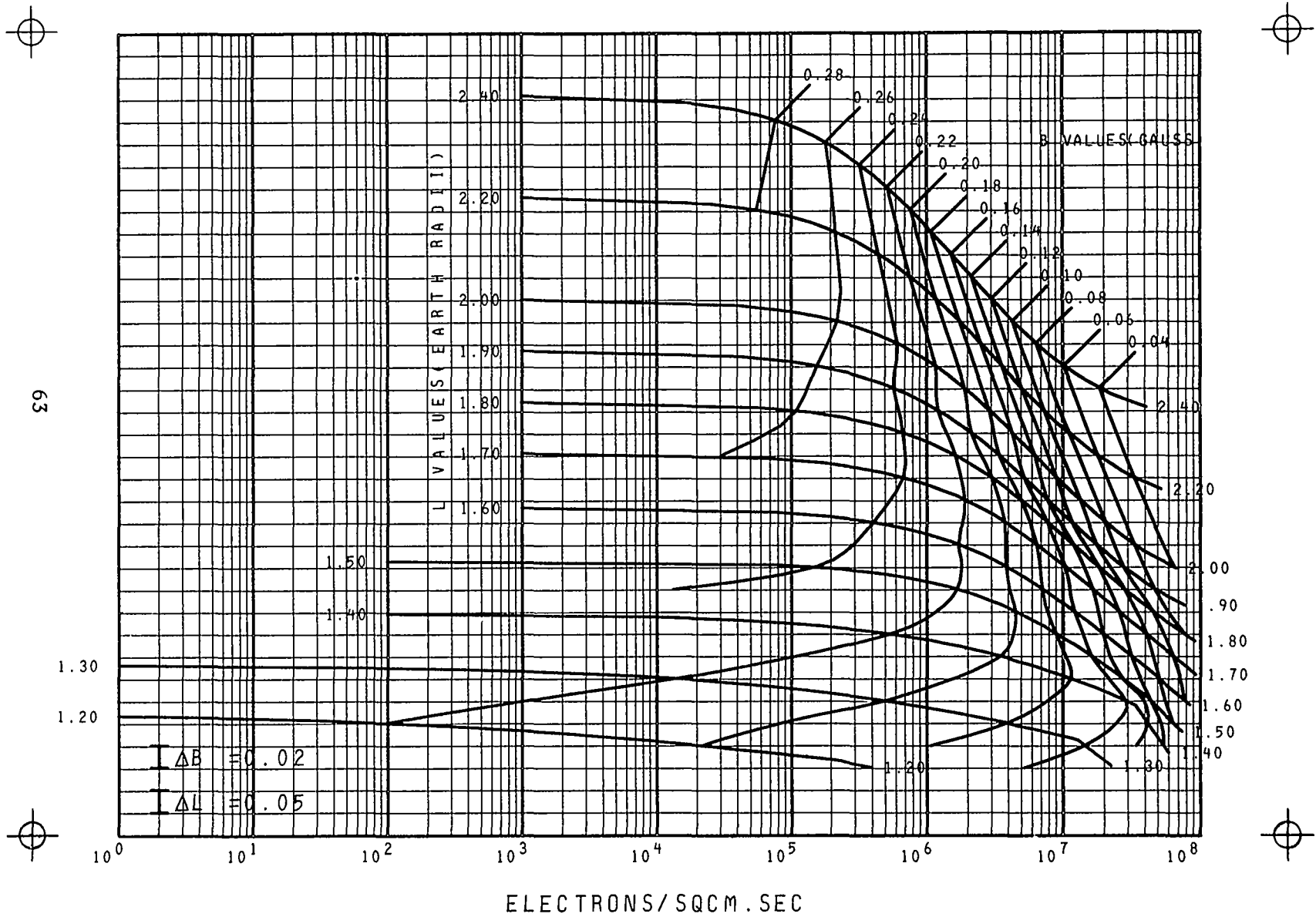
FIG.1 CONT

62



OMNIDIRECTIONAL INTEGRAL FLUX MAP
 100 KEV ELECTRONS L LE 2.4
 MODEL AE5 SOLAR MINIMUM PROJECTED

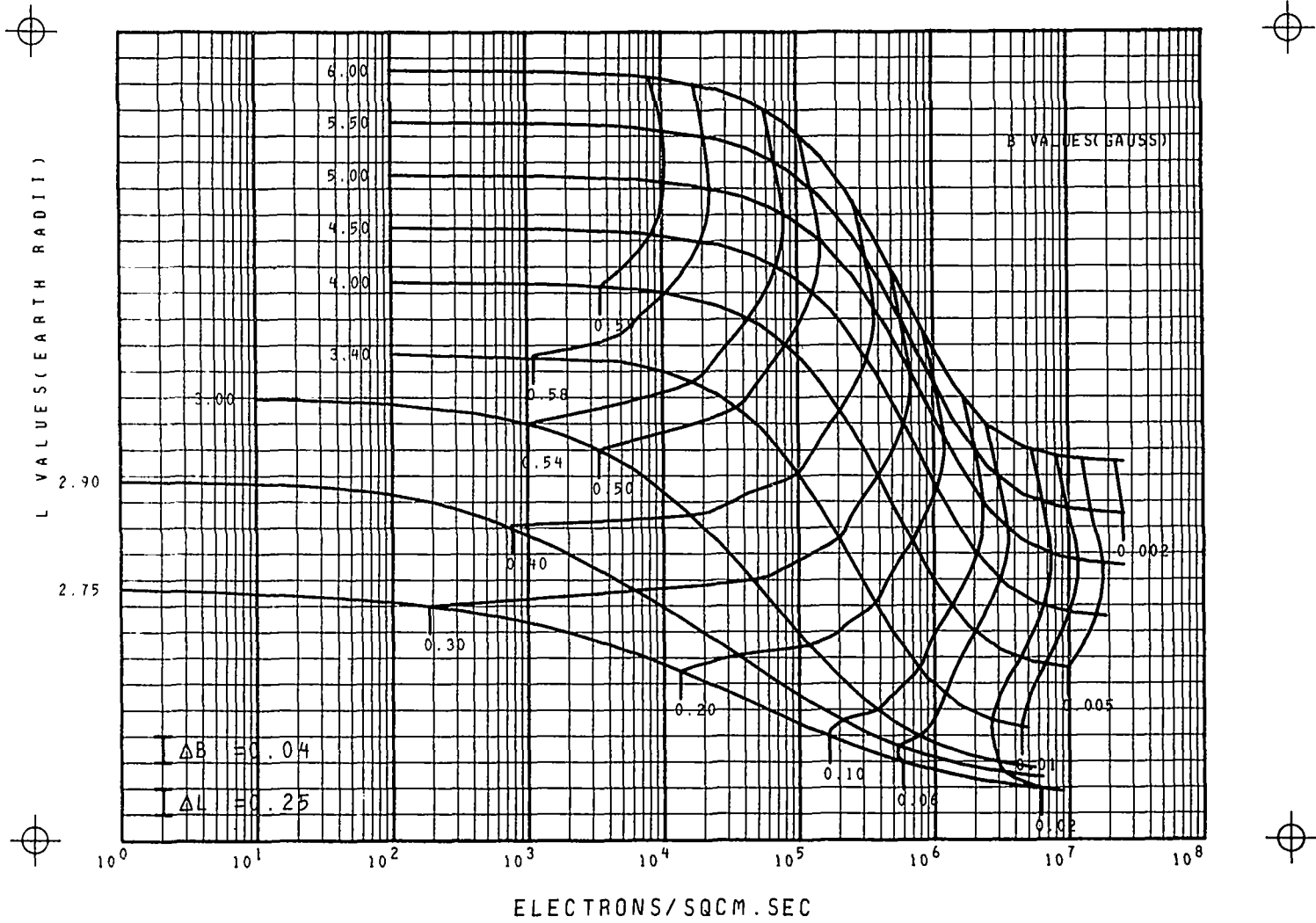
FIG. 2



OMNIDIRECTIONAL INTEGRAL FLUX MAP
100 KEV ELECTRONS L 2.75 TO 6
MODEL AE4 SOLAR MINIMUM PROJECTED

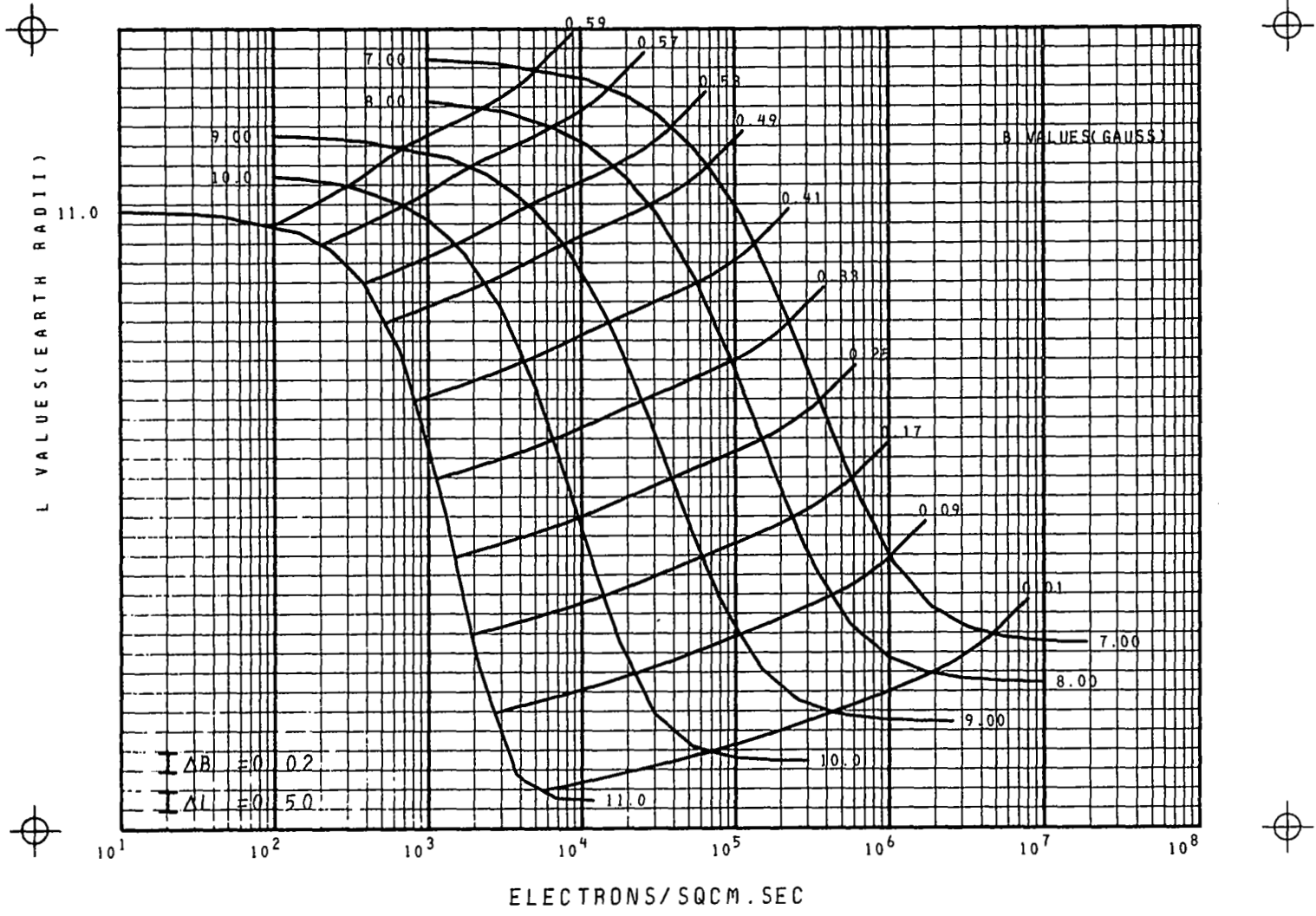
FIG.2 CONT

64



OMNIDIRECTIONAL INTEGRAL FLUX MAP
 100 KEV ELECTRONS L GE 7
 MODEL AE4 SOLAR MINIMUM PROJECTED

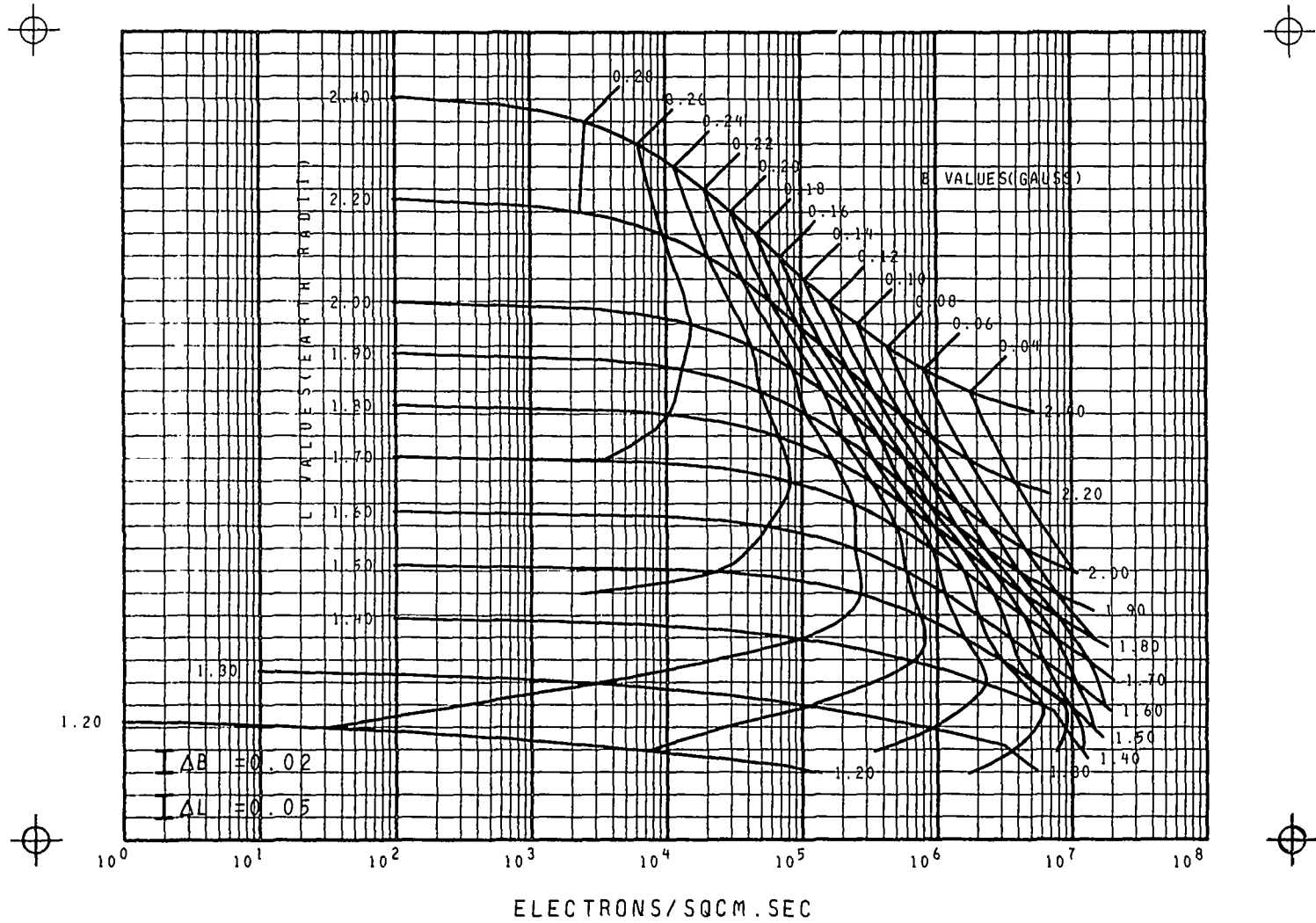
FIG.2 CONT



OMNIDIRECTIONAL INTEGRAL FLUX MAP
 250 KEV ELECTRONS L LE 2.4
 MODEL AE5 SOLAR MINIMUM PROJECTED

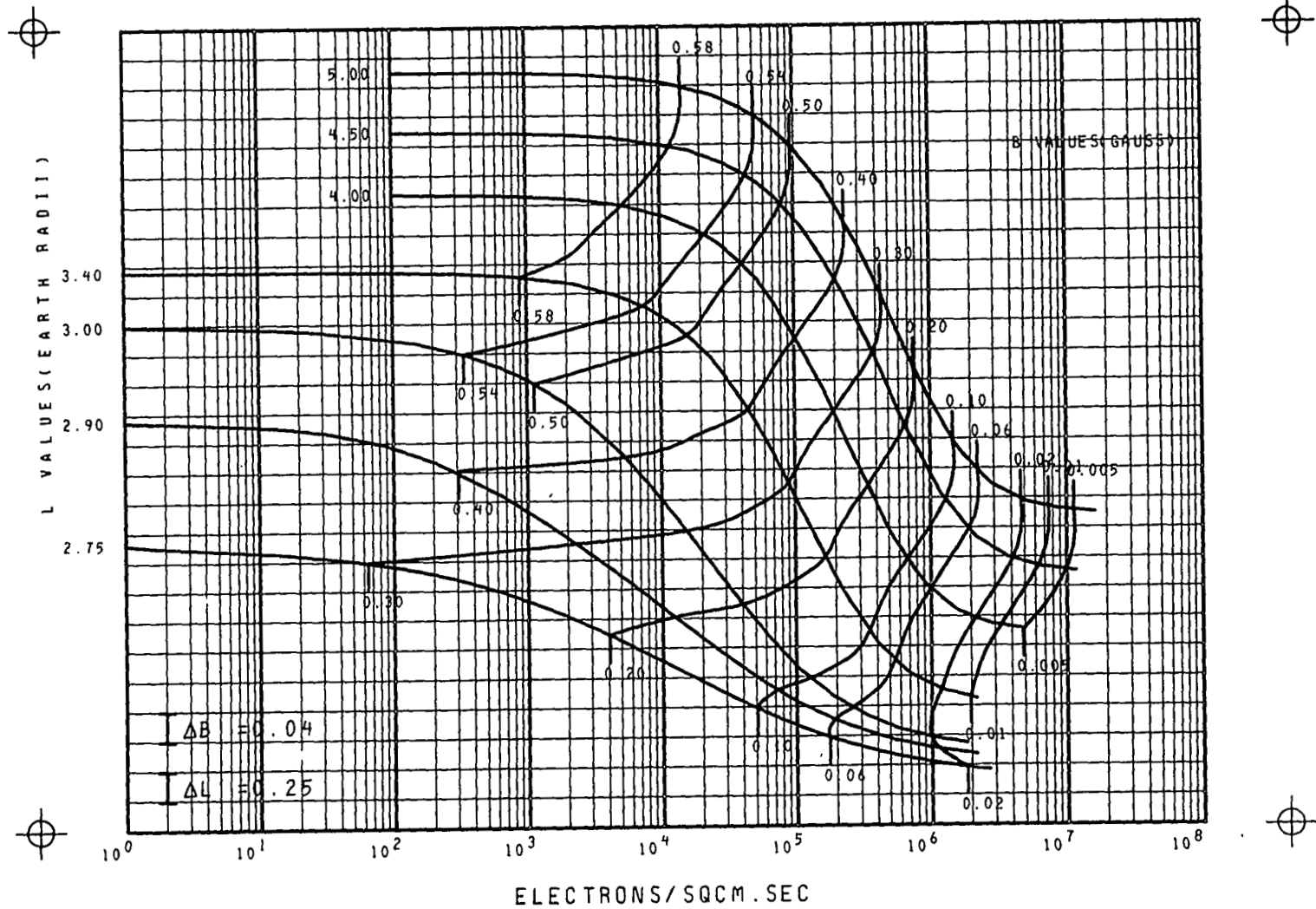
FIG. 3

69



OMNIDIRECTIONAL INTEGRAL FLUX MAP
250 KEV ELECTRONS L 2.75 TO 5
MODEL AE4 SOLAR MINIMUM PROJECTED

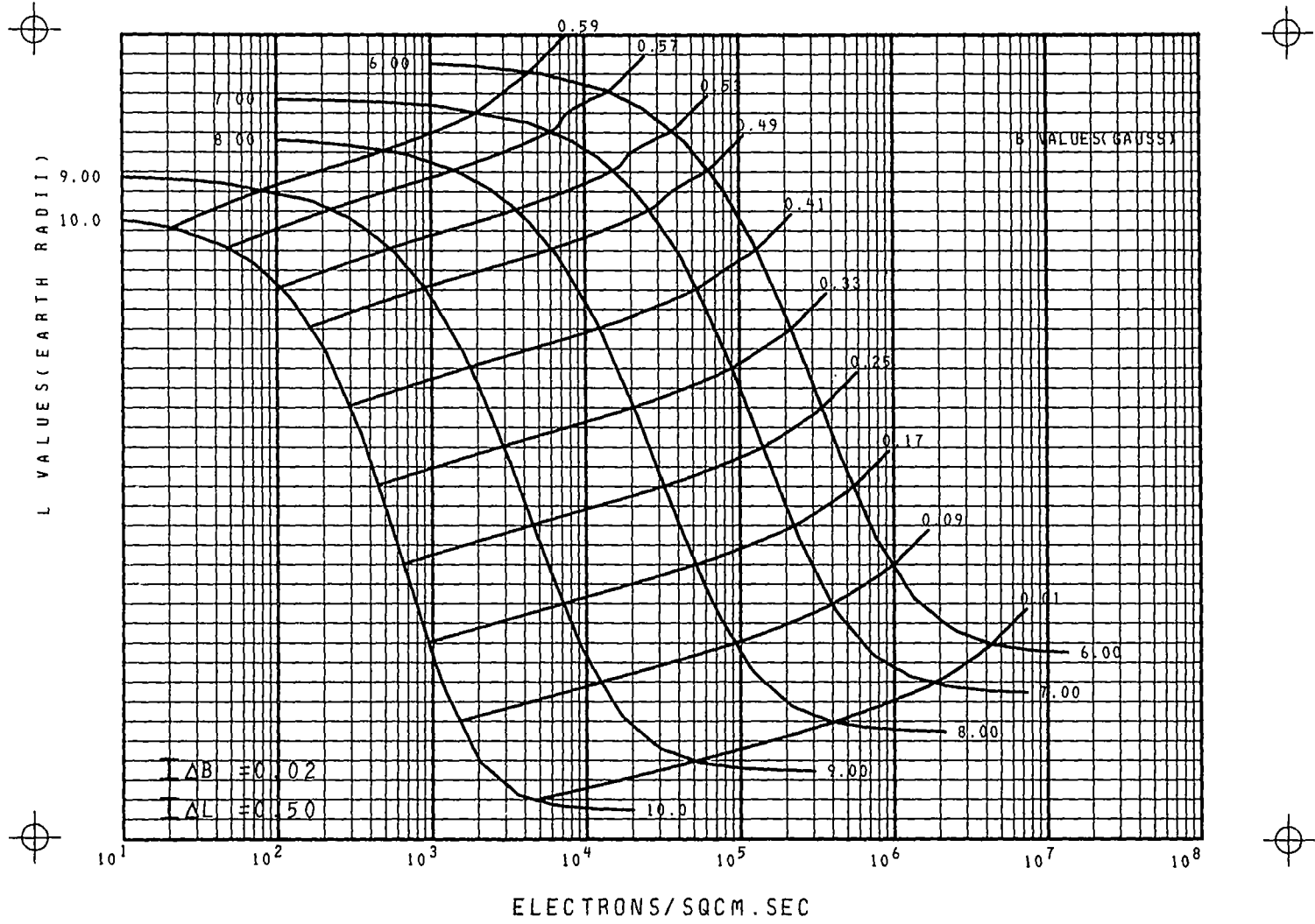
FIG.3 CONT



OMNIDIRECTIONAL INTEGRAL FLUX MAP
 250 KEV ELECTRONS L GE 6
 MODEL AE4 SOLAR MINIMUM PROJECTED

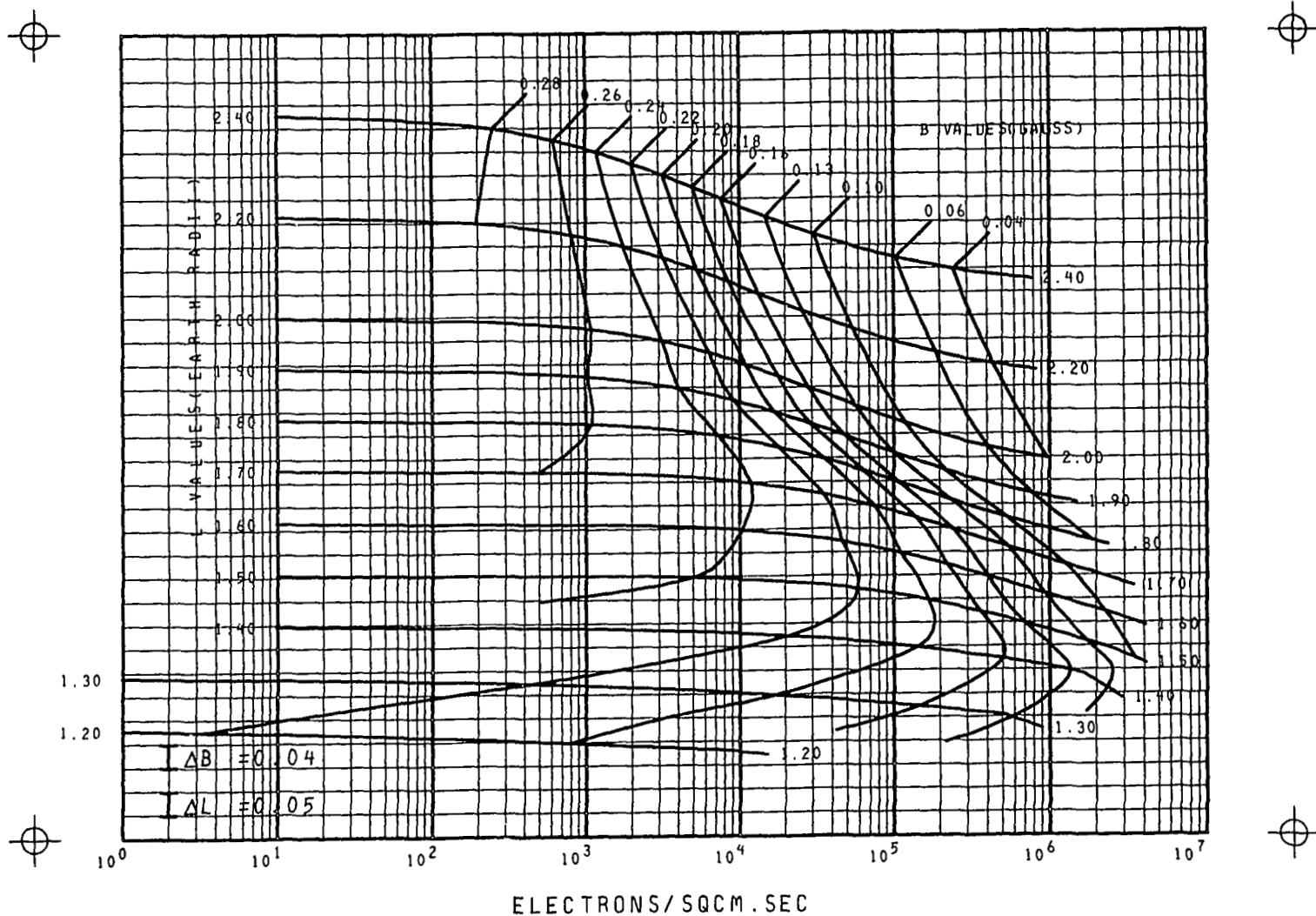
FIG. 3 CONT

89



OMNIDIRECTIONAL INTEGRAL FLUX MAP
 500 KEV ELECTRONS L LE 2.4
 MODEL AE5 SOLAR MINIMUM PROJECTED

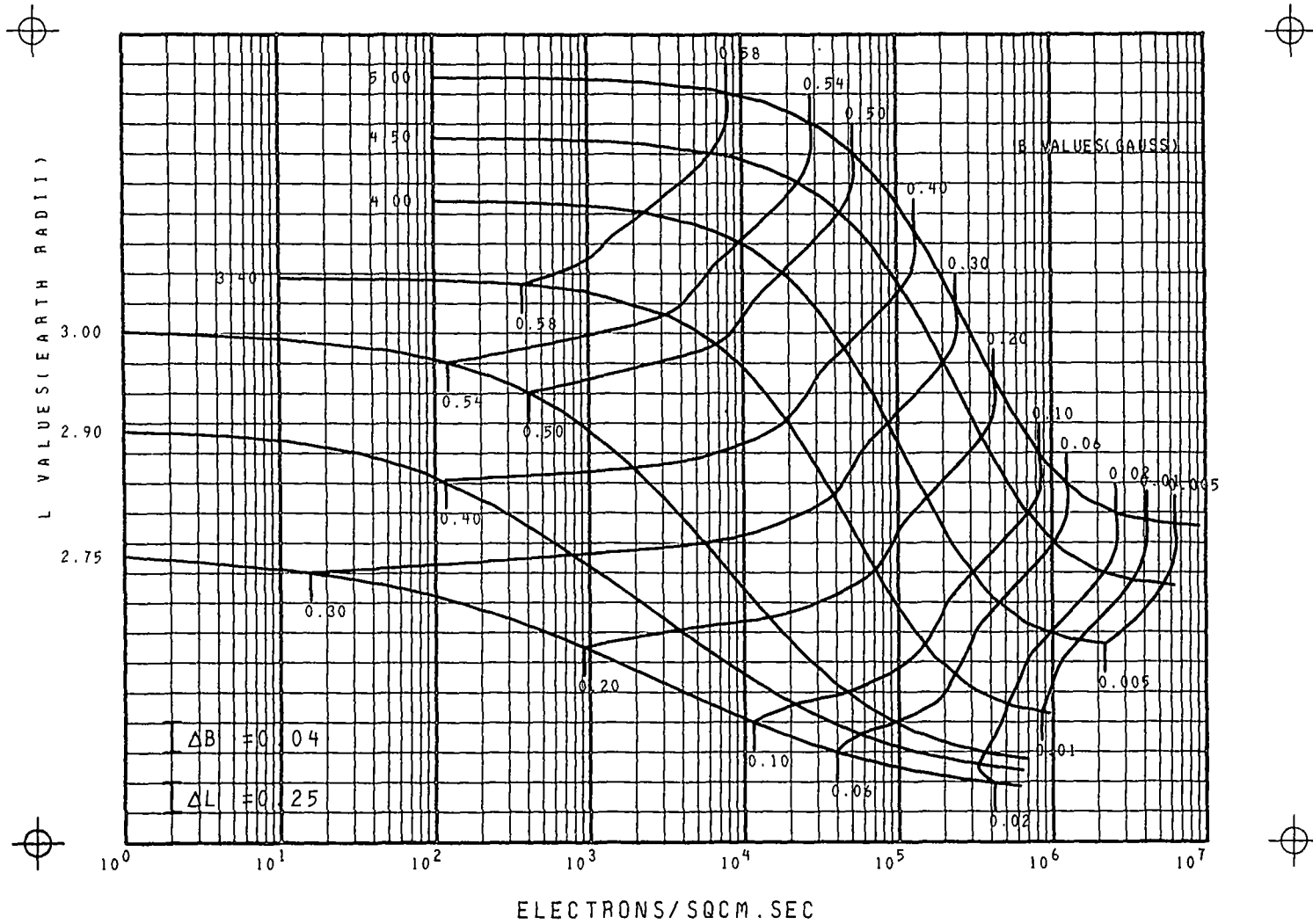
FIG. 4



OMNIDIRECTIONAL INTEGRAL FLUX MAP
 500 KEV ELECTRONS L 2.75 TO 5
 MODEL AE4 SOLAR MINIMUM PROJECTED

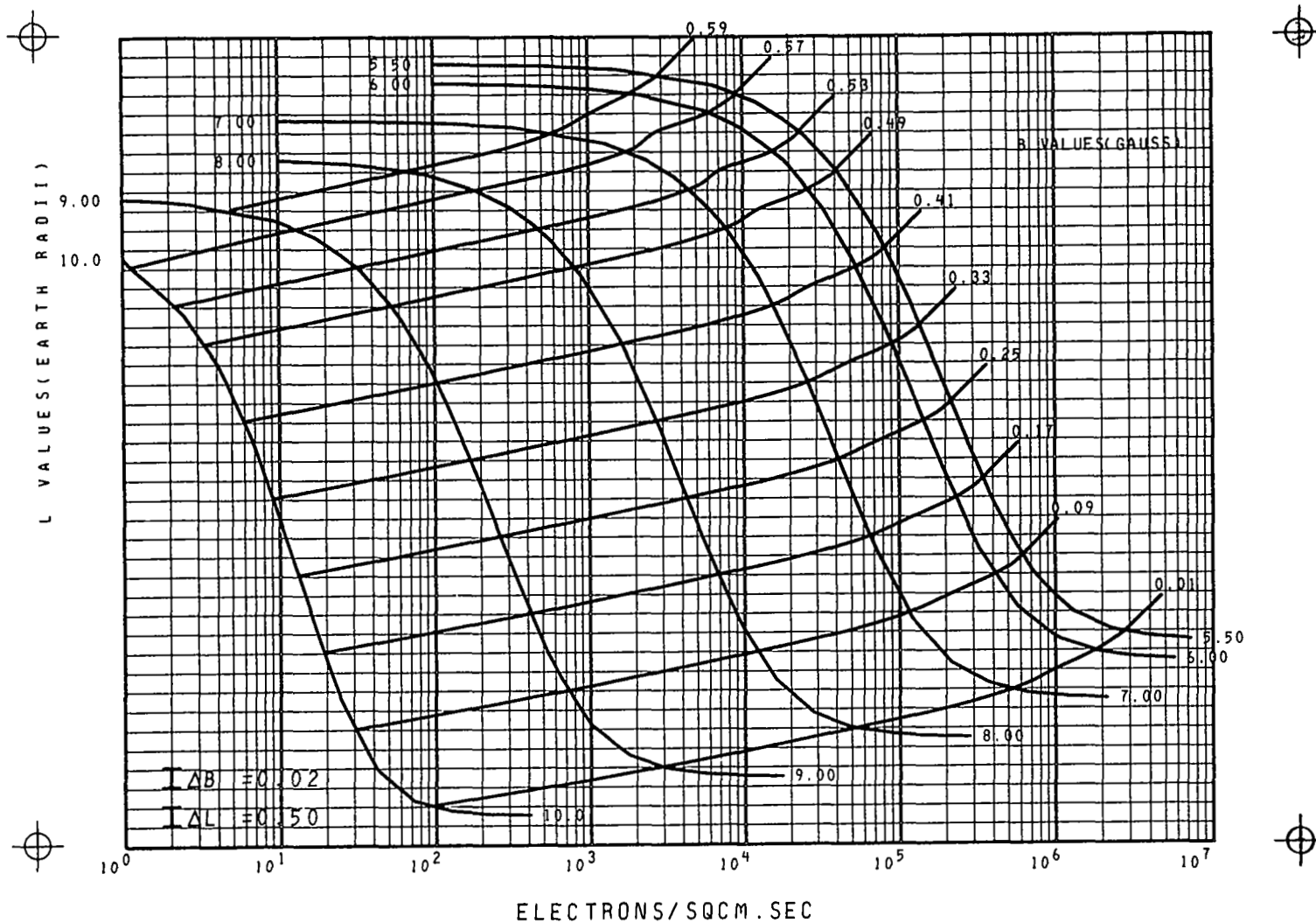
FIG.4 CONT

70



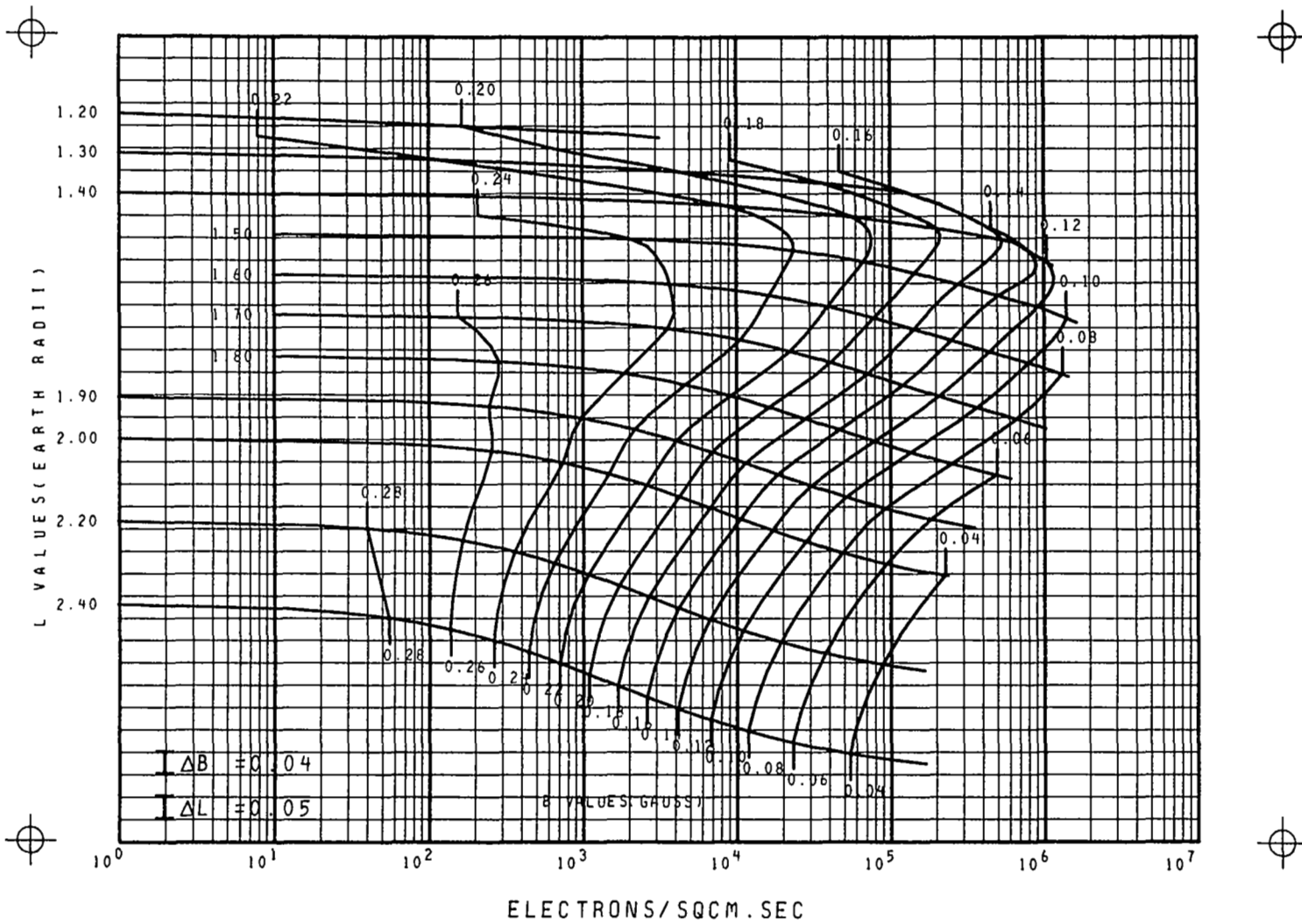
OMNIDIRECTIONAL INTEGRAL FLUX MAP
 500 KEV ELECTRONS L GE 5.5
 MODEL AE4 SOLAR MINIMUM PROJECTED

FIG.4 CONT



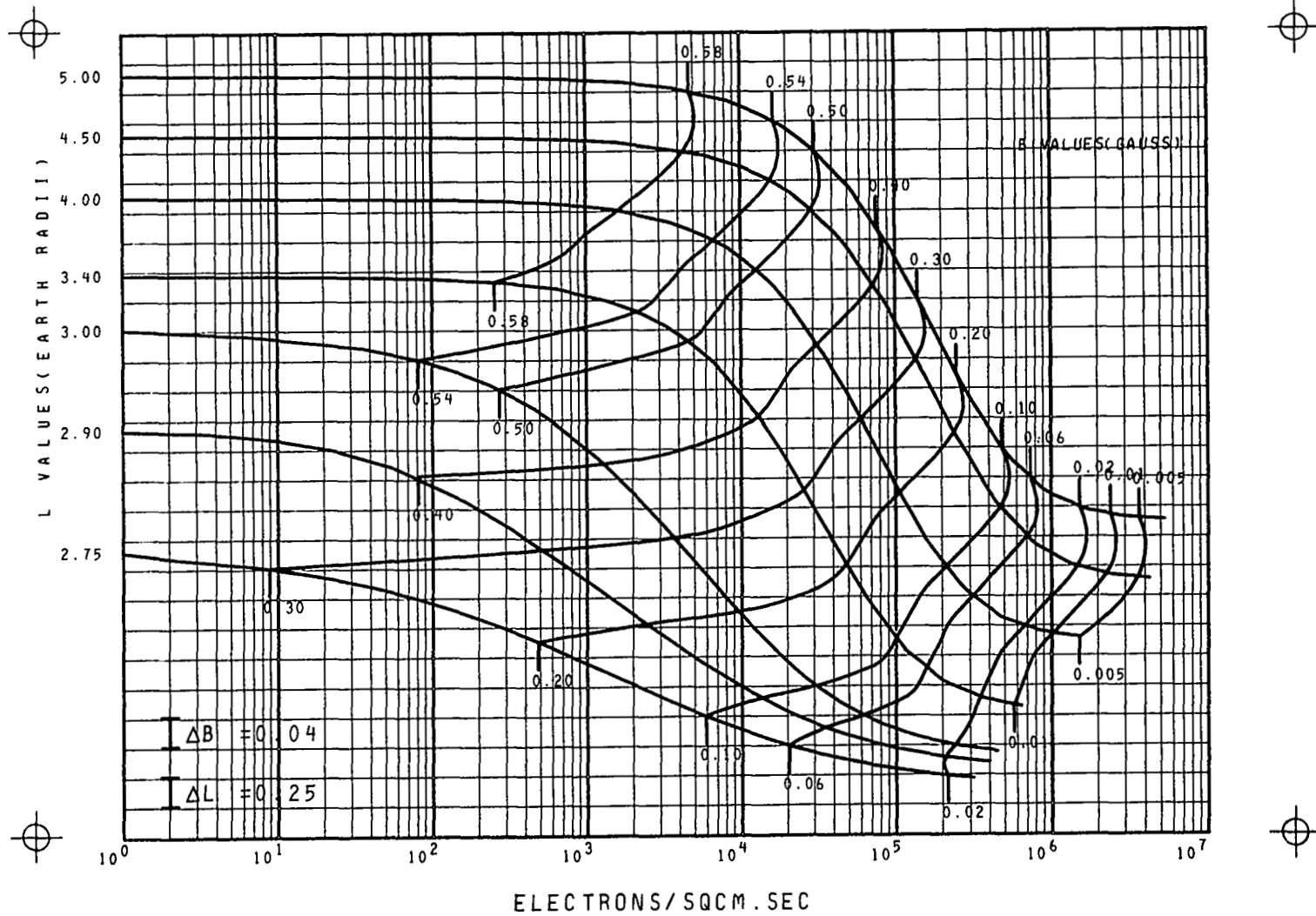
OMNIDIRECTIONAL INTEGRAL FLUX MAP
 750 KEV ELECTRONS L LE 2.4
 MODEL AE5 SOLAR MINIMUM PROJECTED

FIG. 5



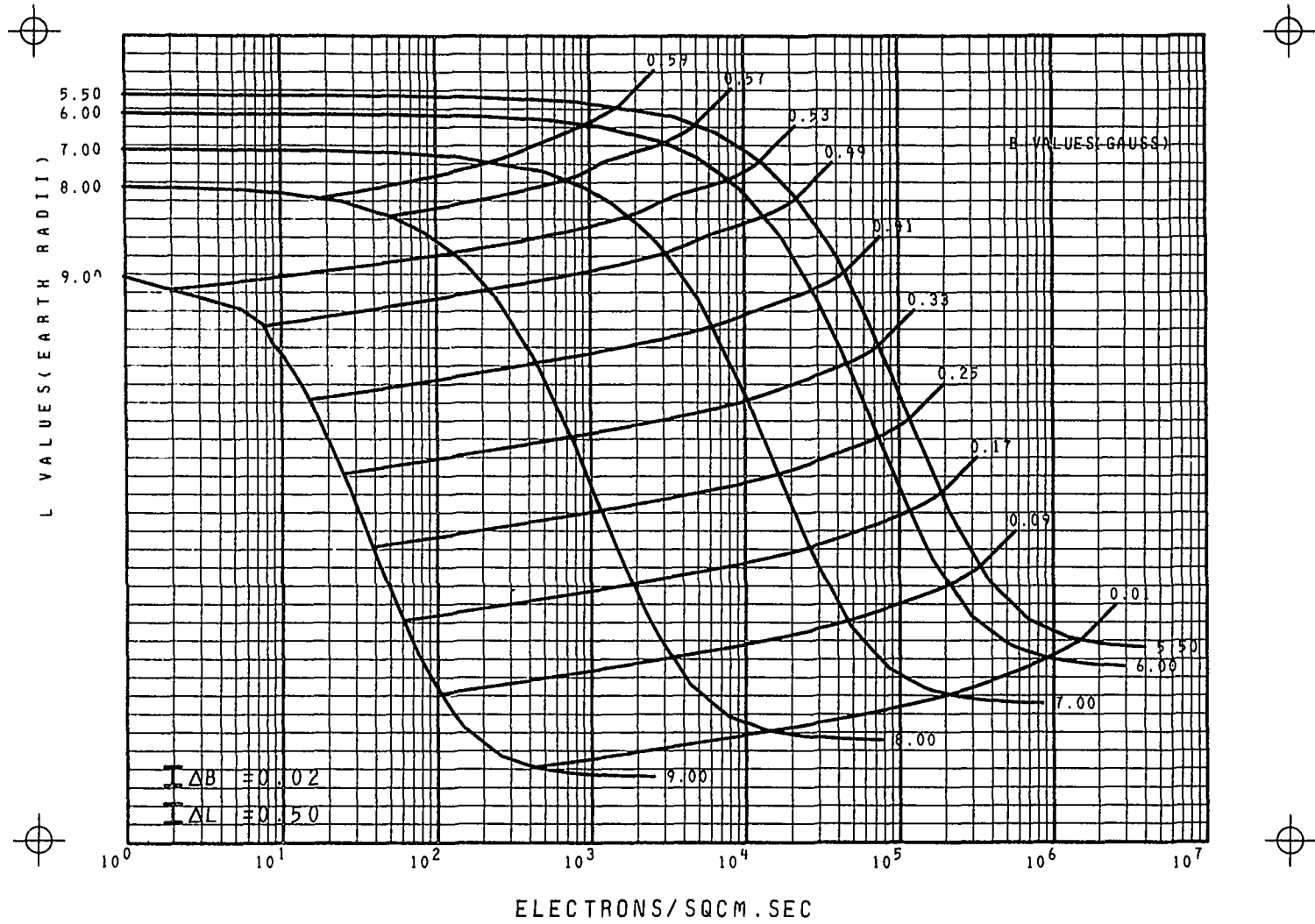
OMNIDIRECTIONAL INTEGRAL FLUX MAP
 750 KEV ELECTRONS L 2.75 TO 5
 MODEL AE4 SOLAR MINIMUM PROJECTED

FIG.5 CONT



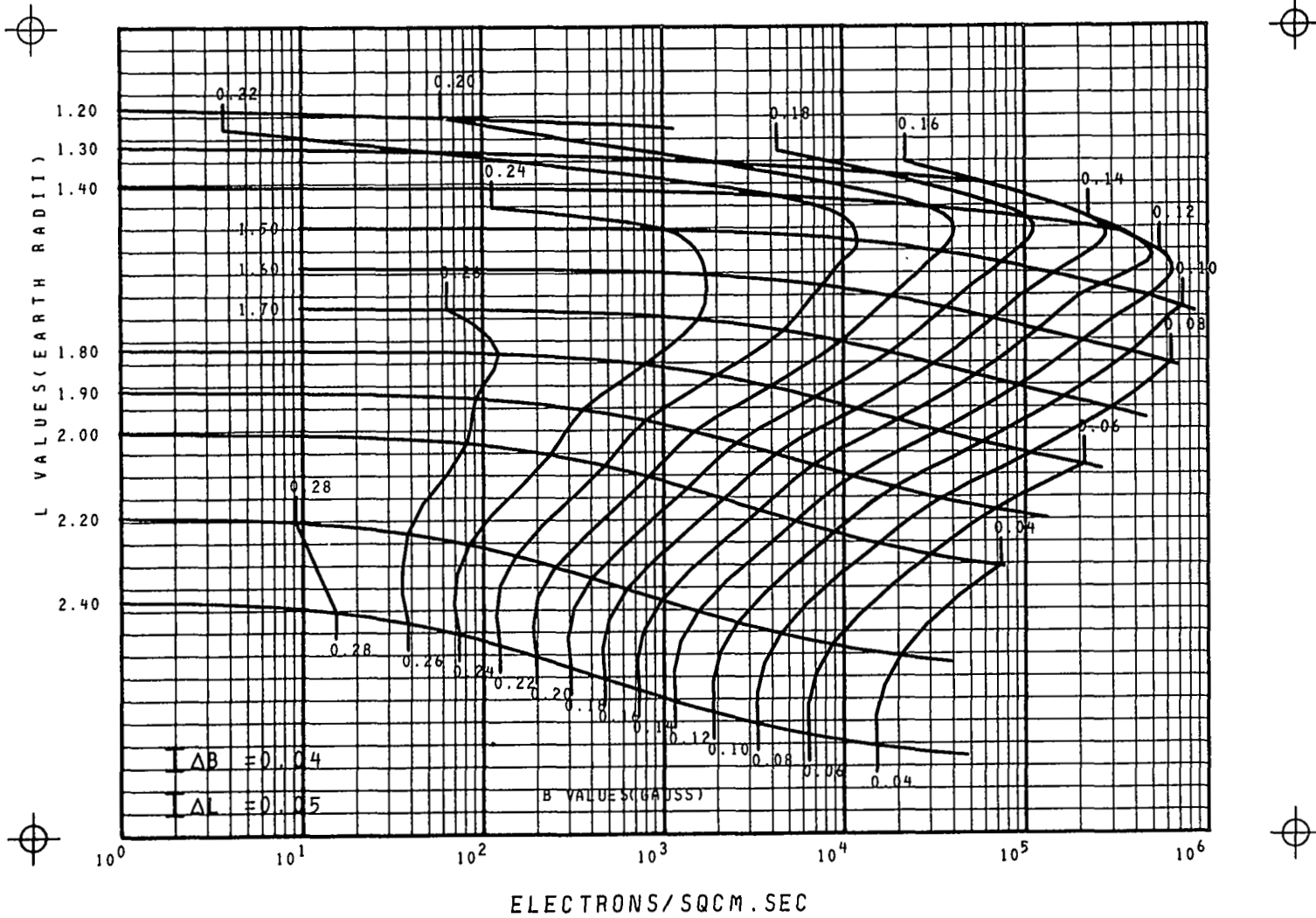
OMNIDIRECTIONAL INTEGRAL FLUX MAP
 750 KEV ELECTRONS L GE 5.5
 MODEL AE4 SOLAR MINIMUM PROJECTED

FIG.5 CONT



OMNIDIRECTIONAL INTEGRAL FLUX MAP
 1 MEV ELECTRONS L LE 2.4
 MODEL AE5 SOLAR MINIMUM PROJECTED

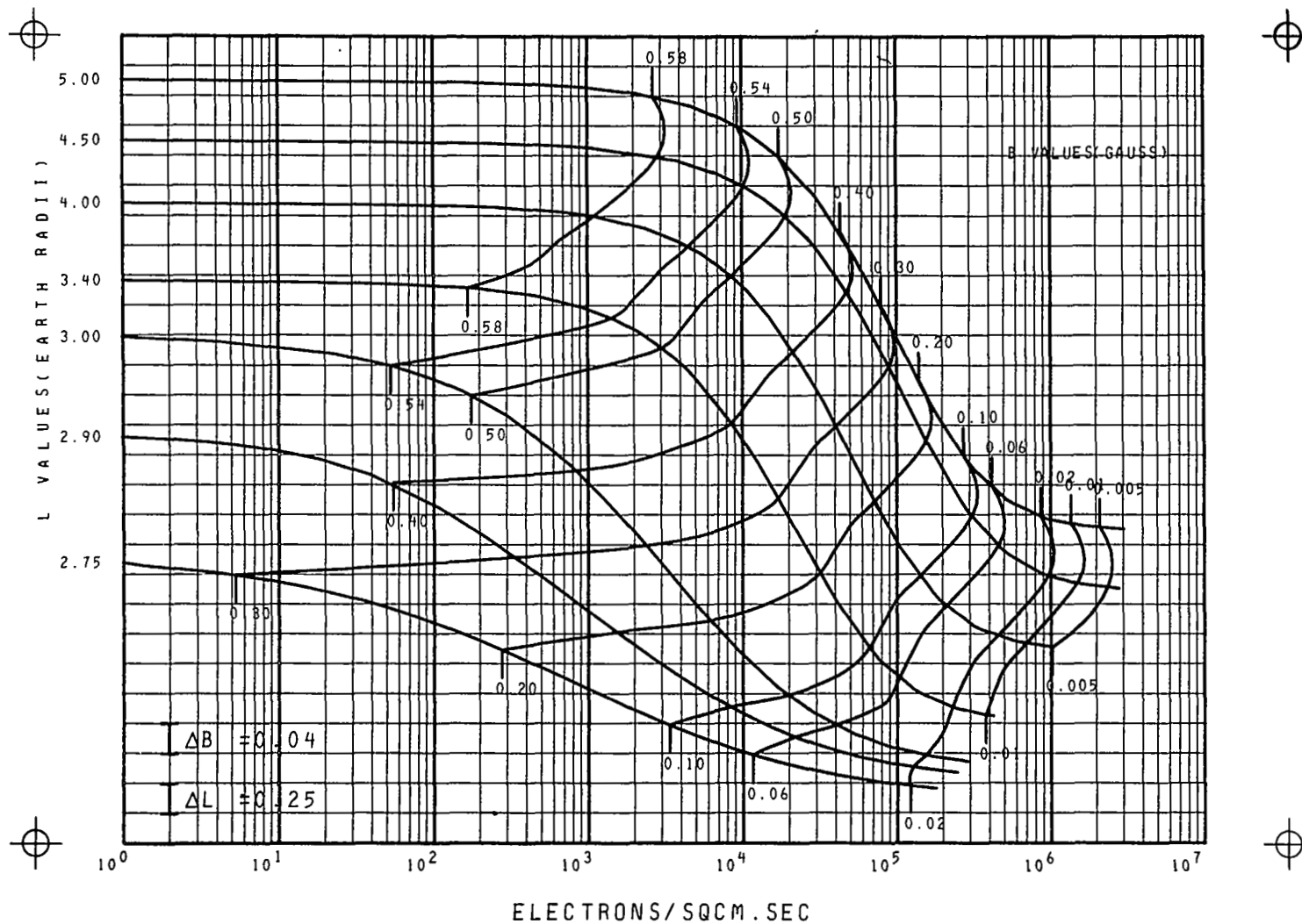
FIG. 6



75

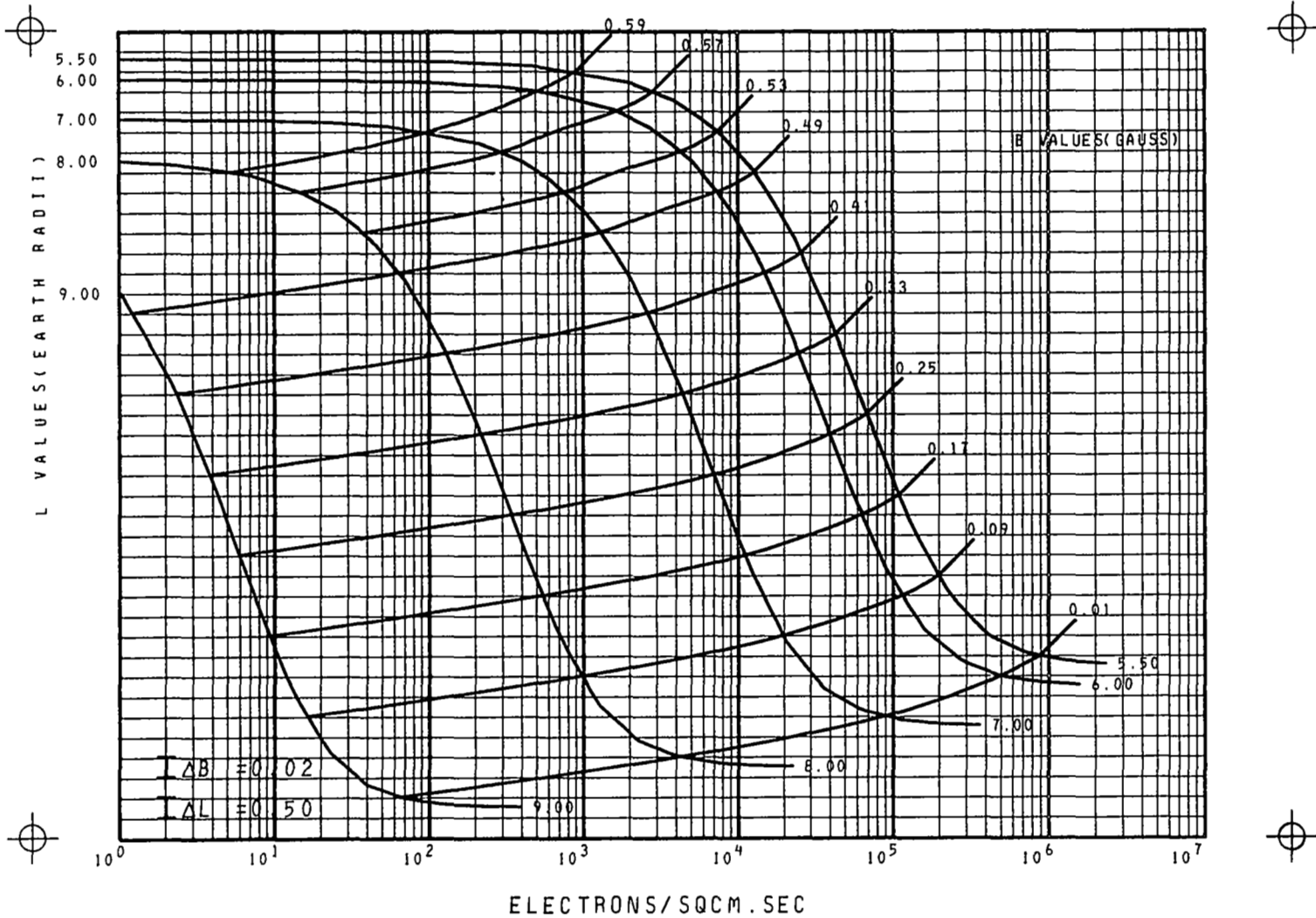
OMNIDIRECTIONAL INTEGRAL FLUX MAP
 1 MEV ELECTRONS L 2.75 TO 5
 MODEL AE4 SOLAR MINIMUM PROJECTED

FIG.6 CONT



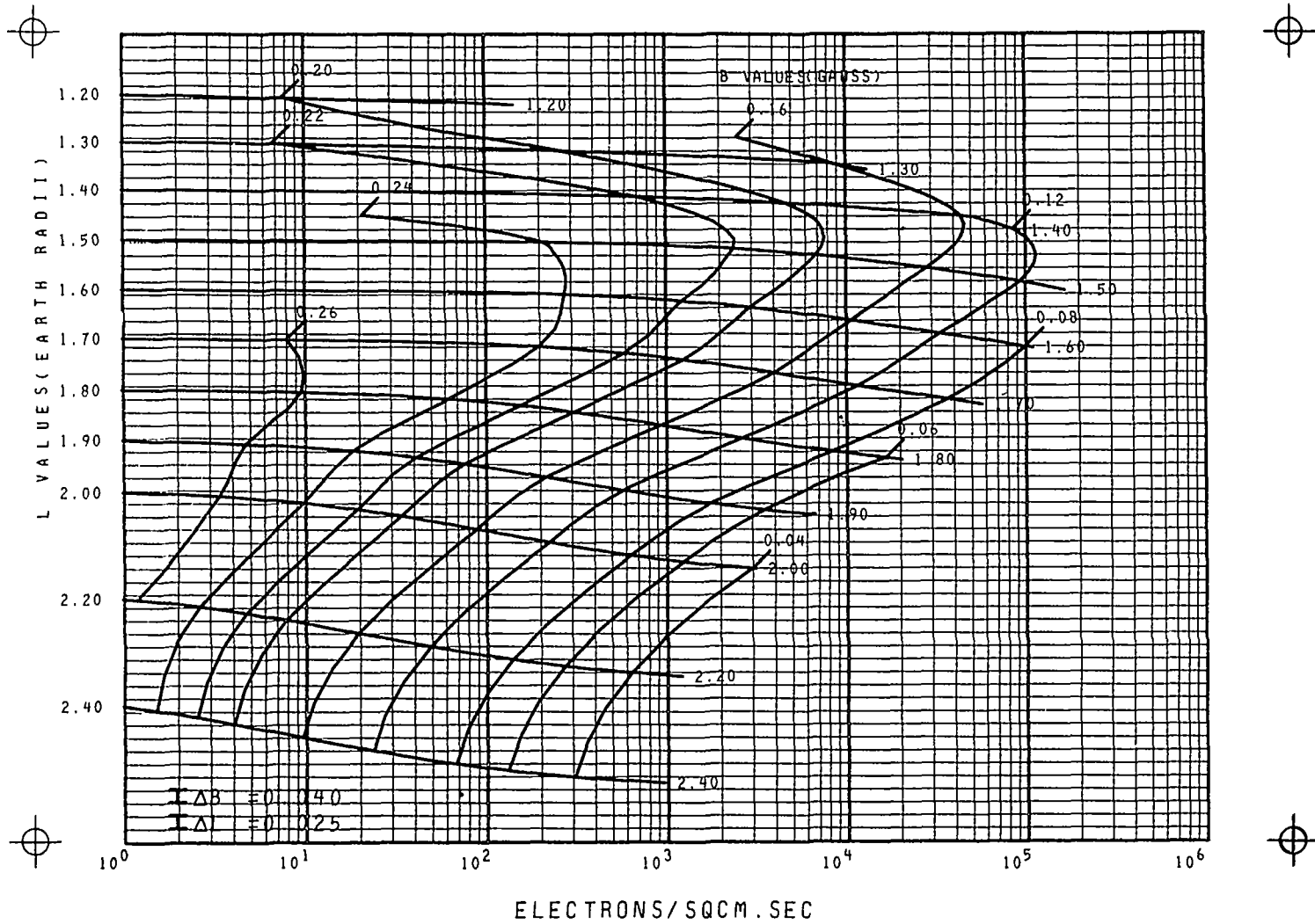
OMNIDIRECTIONAL INTEGRAL FLUX MAP
 1 MEV ELECTRONS L GE 5.5
 MODEL AE4 SOLAR MINIMUM PROJECTED

FIG. 6 CONT



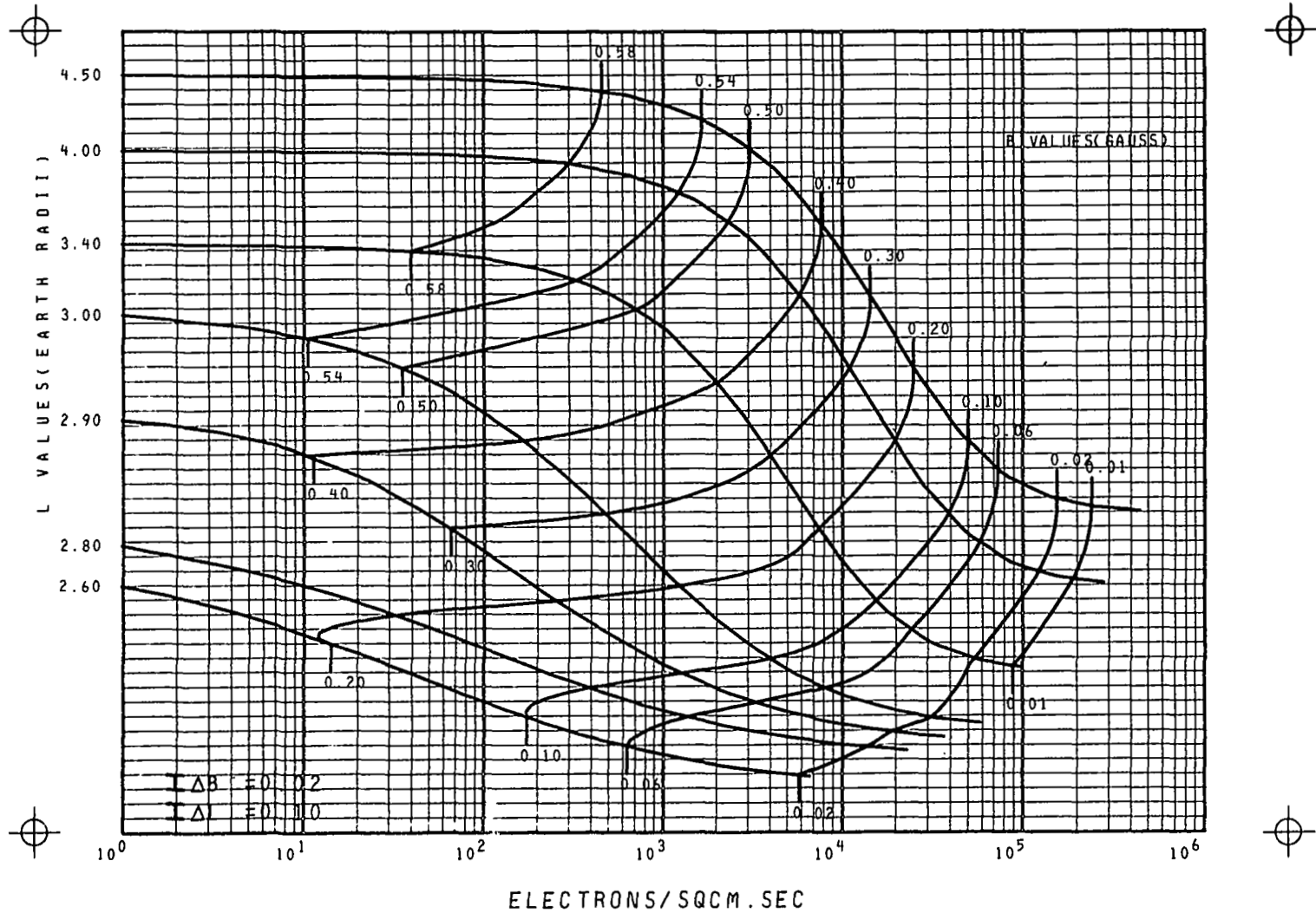
OMNIDIRECTIONAL INTEGRAL FLUX MAP
 2 MEV ELECTRONS L LE 2.4
 MODEL AE5 SOLAR MINIMUM PROJECTED

FIG. 7



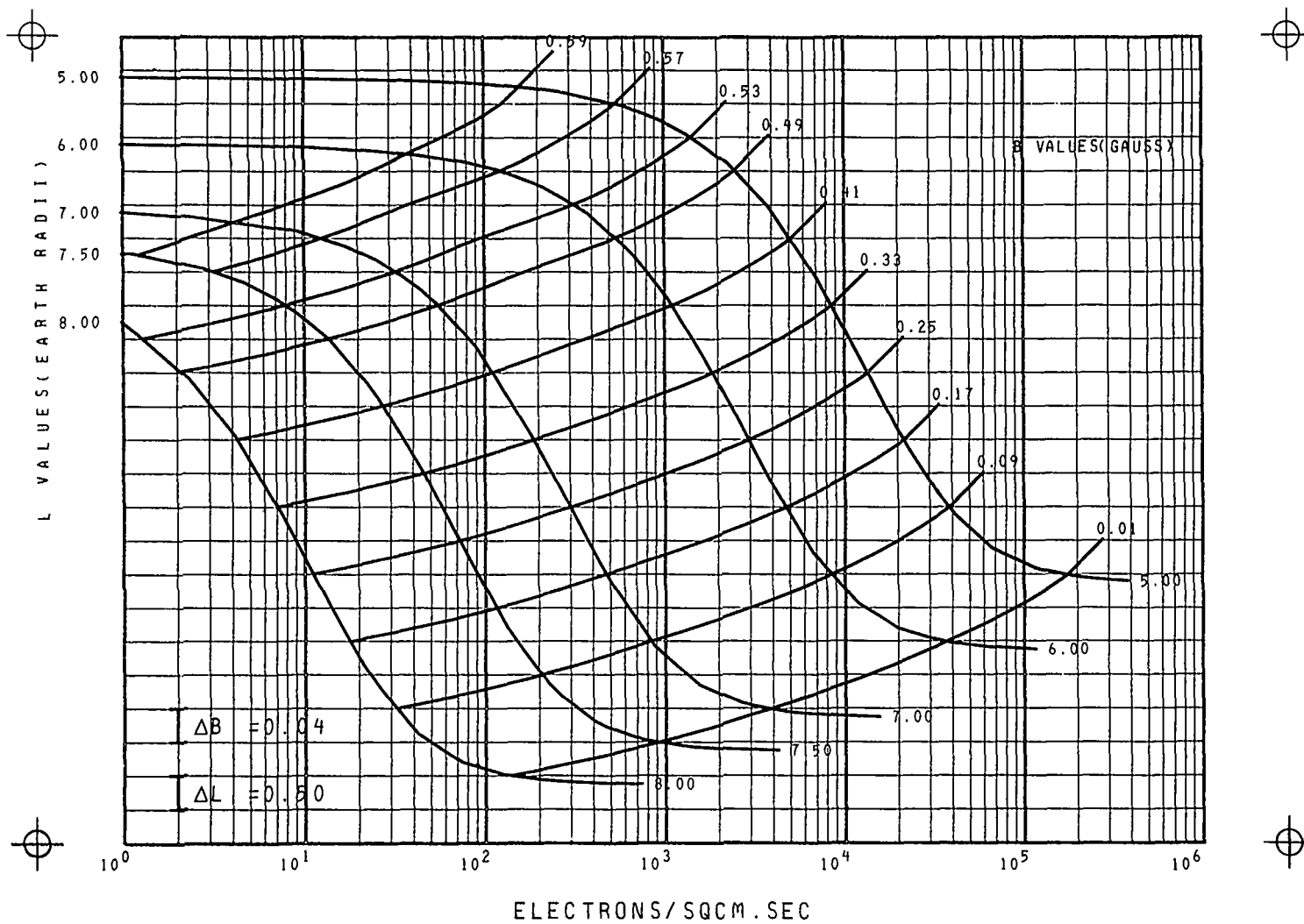
OMNIDIRECTIONAL INTEGRAL FLUX MAP
 2 MEV ELECTRONS L 2.6 TO 4.5
 MODEL AE4 SOLAR MINIMUM PROJECTED

FIG. 7 CONT



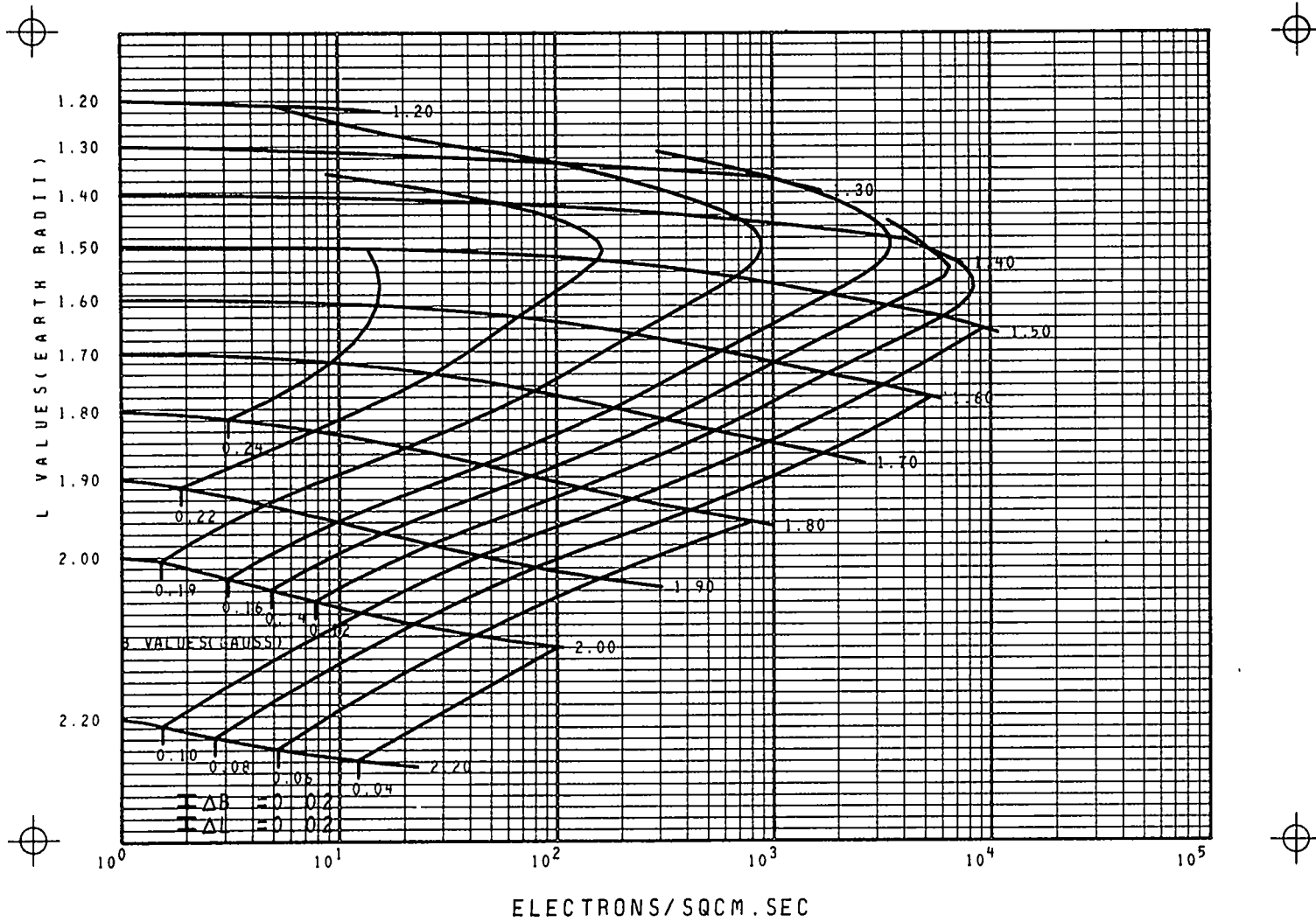
OMNIDIRECTIONAL INTEGRAL FLUX MAP
 2 MEV ELECTRONS L GE 5
 MODEL AE4 SOLAR MINIMUM PROJECTED

FIG. 7 CONT



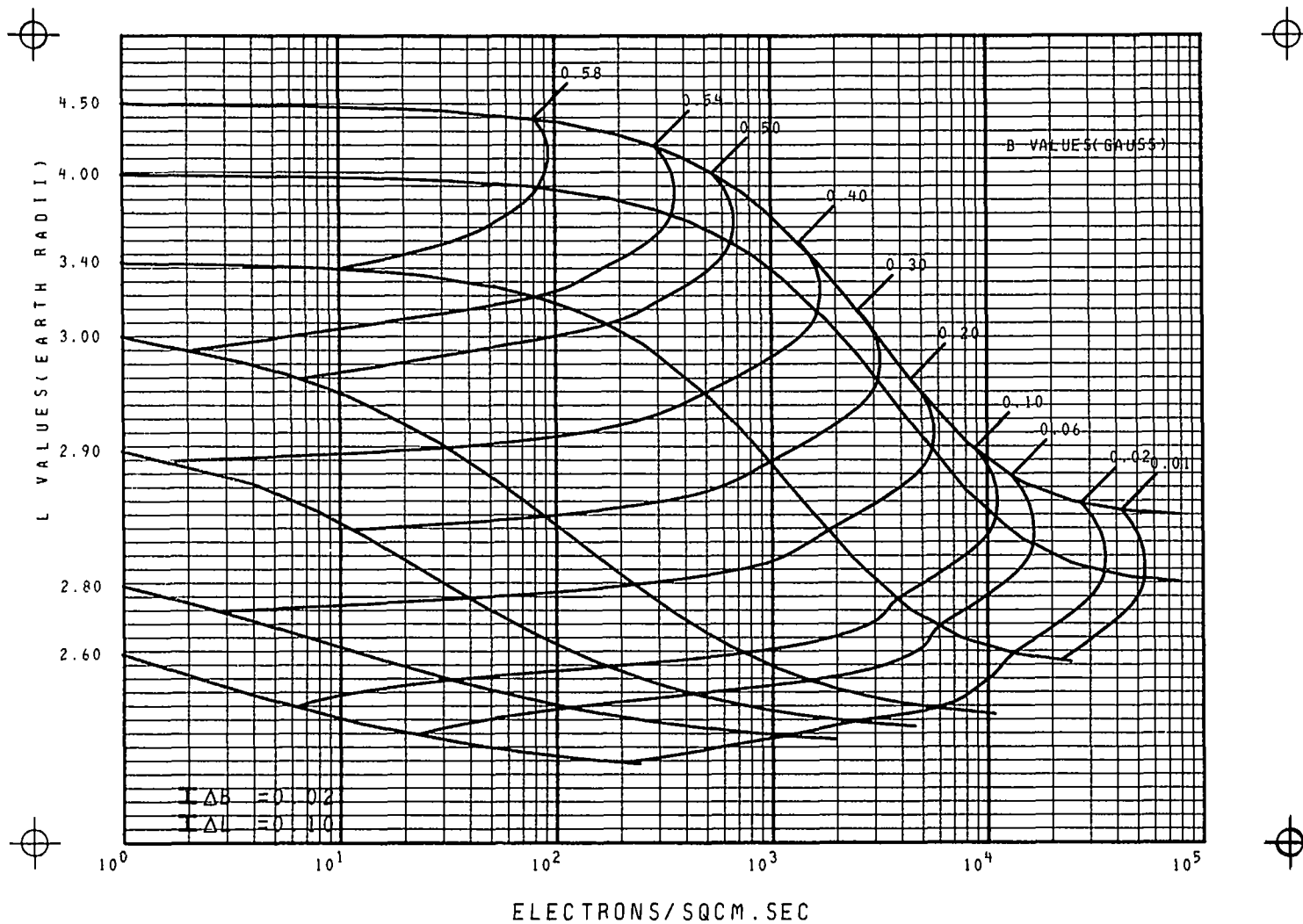
OMNIDIRECTIONAL INTEGRAL FLUX MAP
 3 MEV ELECTRONS L LE 2.4
 MODEL AE5 SOLAR MINIMUM PROJECTED

FIG. 8



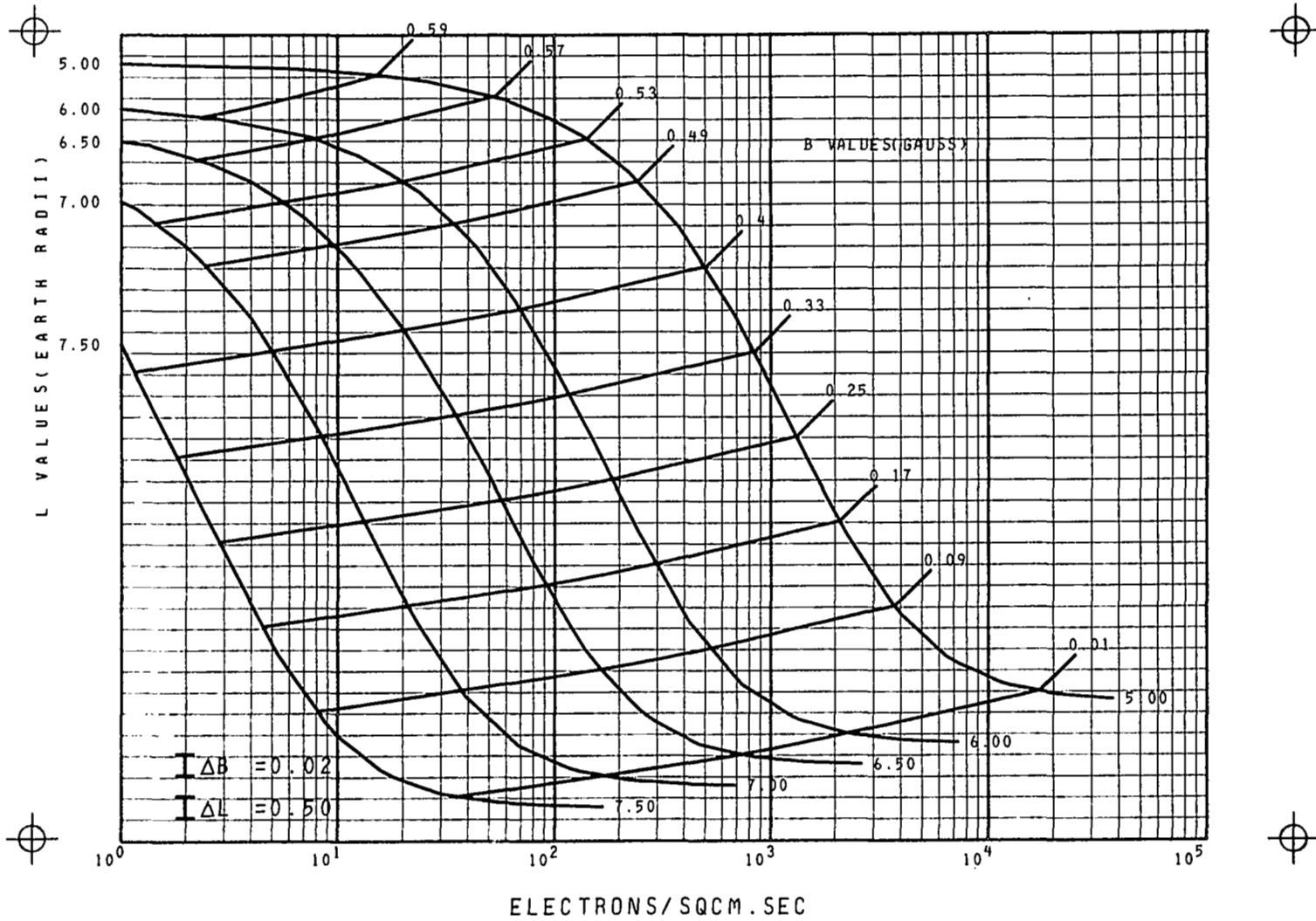
OMNIDIRECTIONAL INTEGRAL FLUX MAP
 3 MEV ELECTRONS L 2.6 TO 4.5
 MODEL AE4 SOLAR MINIMUM PROJECTED

FIG. 8 CONT



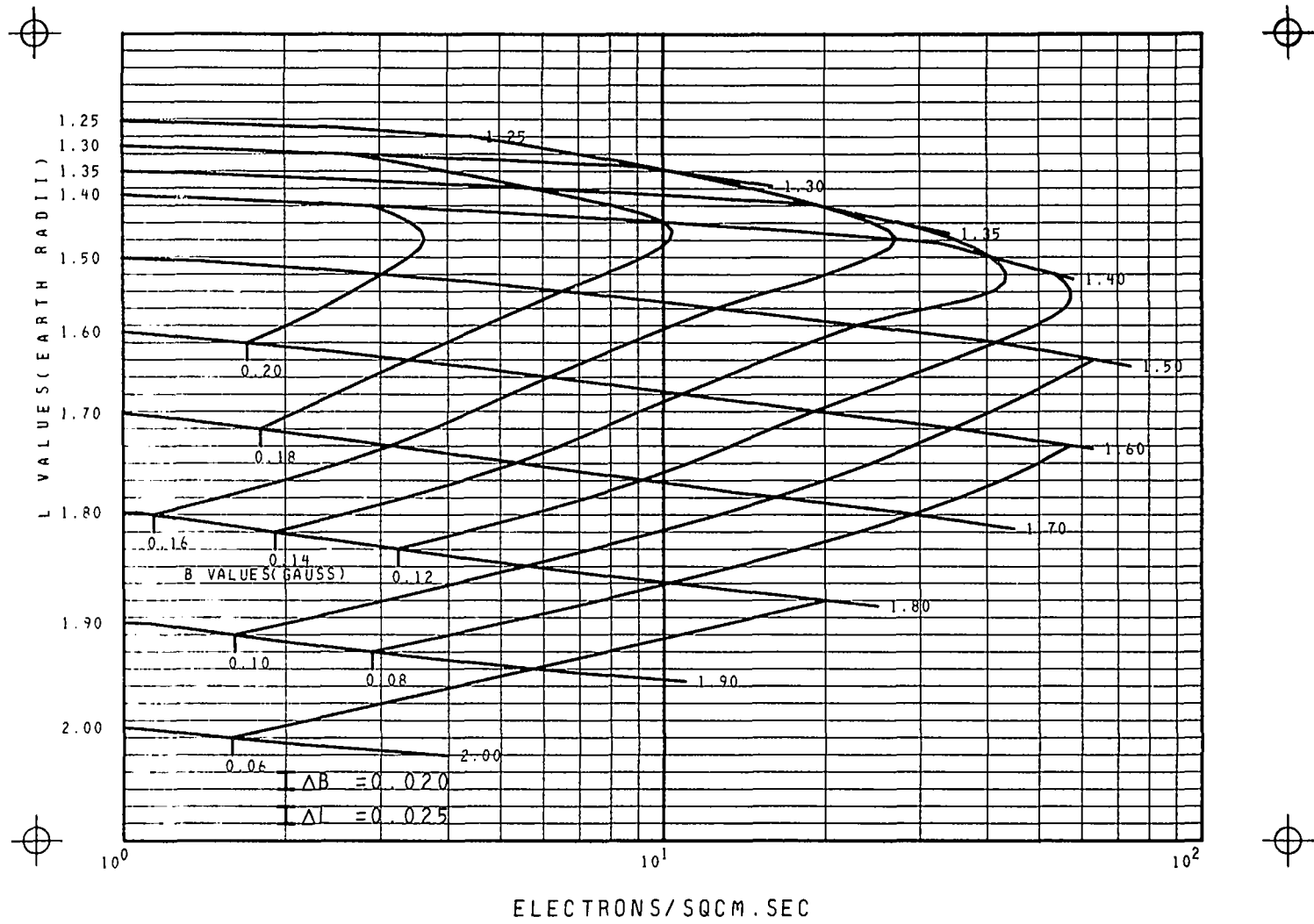
OMNIDIRECTIONAL INTEGRAL FLUX MAP
 3 MEV ELECTRONS L GE 5
 MODEL AE4 SOLAR MINIMUM PROJECTED

FIG. 8 CONT



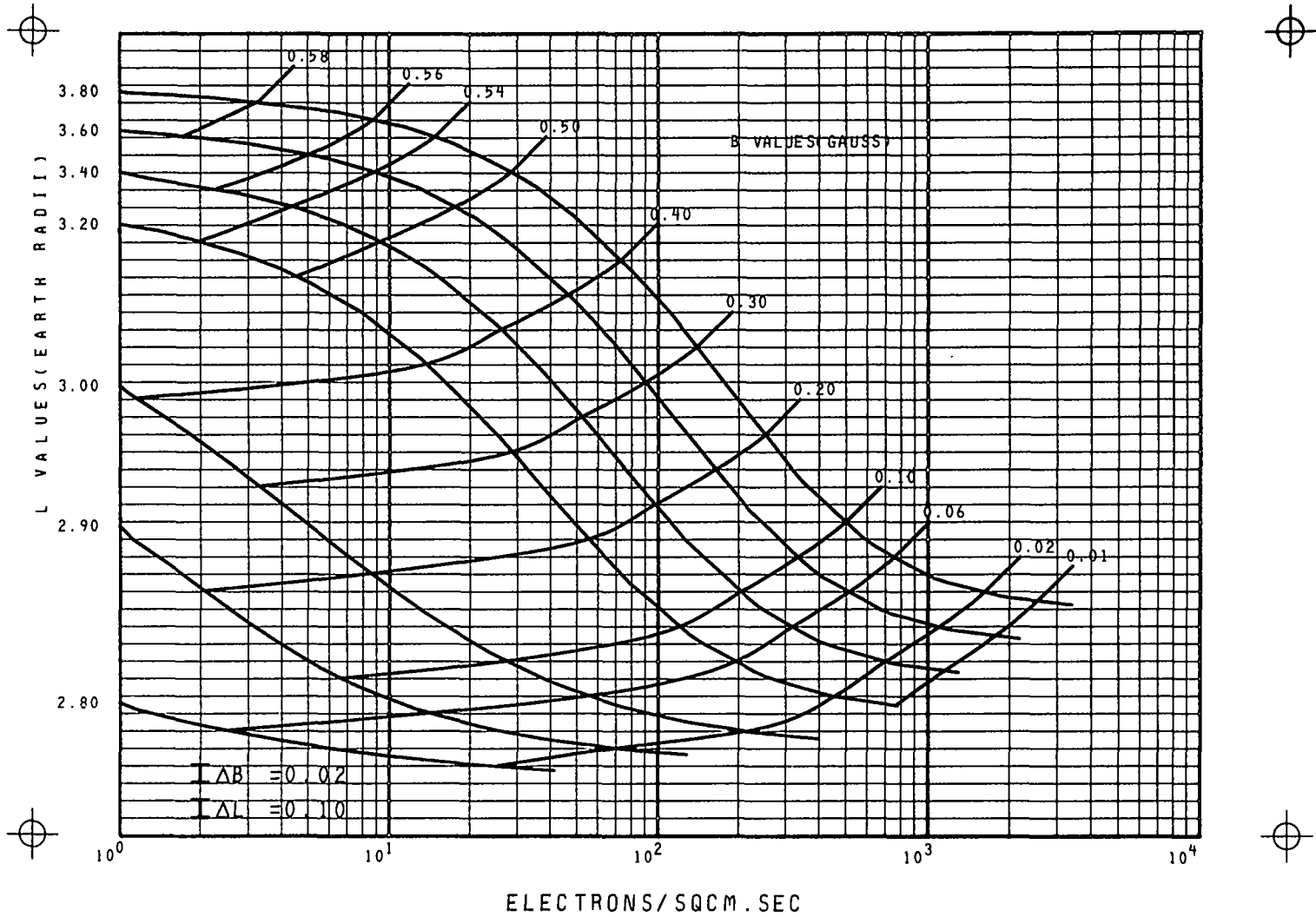
OMNIDIRECTIONAL INTEGRAL FLUX MAP
 4 MEV ELECTRONS L LE 2.4
 MODEL AE5 SOLAR MINIMUM PROJECTED

FIG. 9



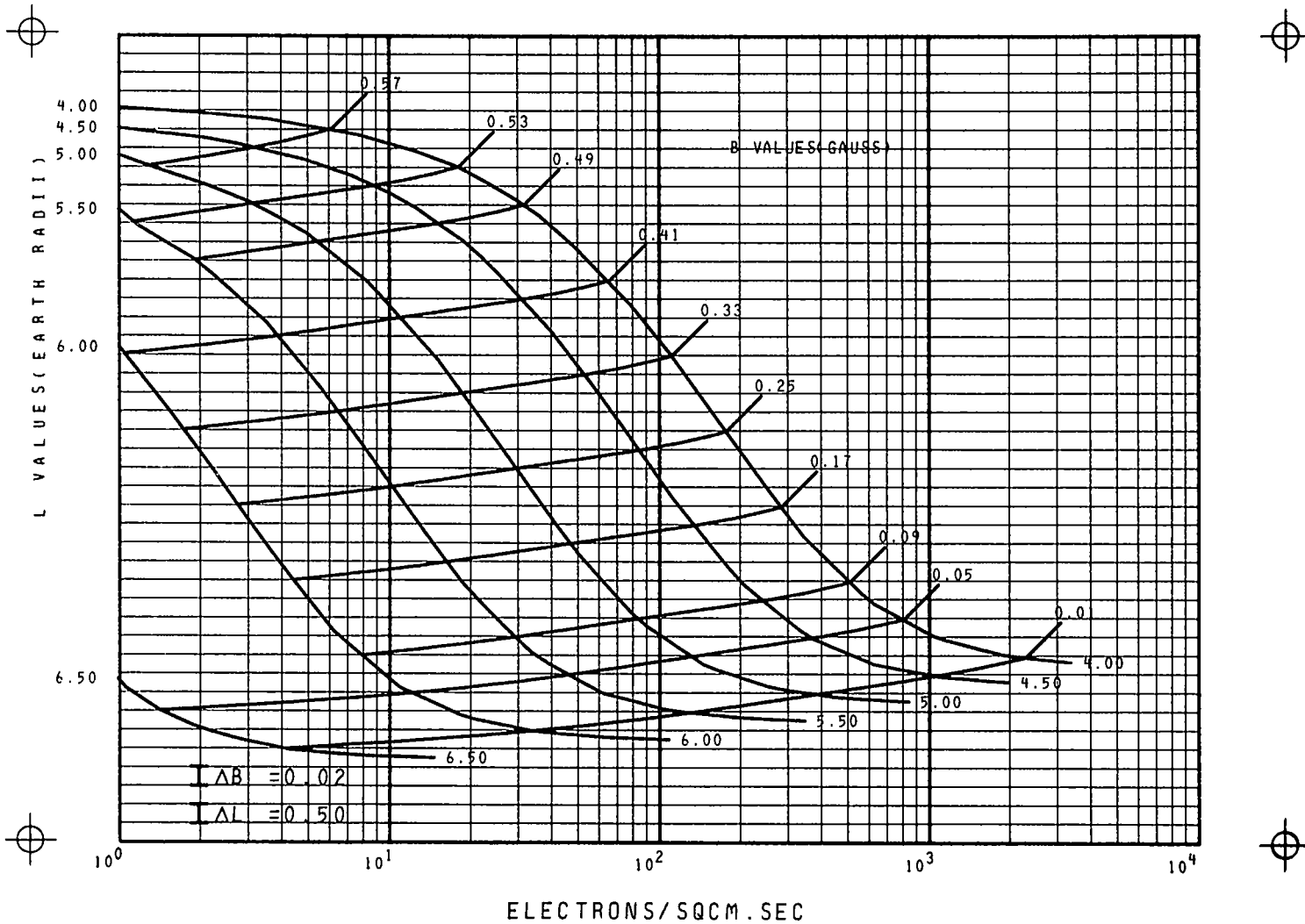
OMNIDIRECTIONAL INTEGRAL FLUX MAP
4 MEV ELECTRONS L 2.8 TO 3.8
MODEL AE4 SOLAR MINIMUM PROJECTED

FIG. 9 CONT

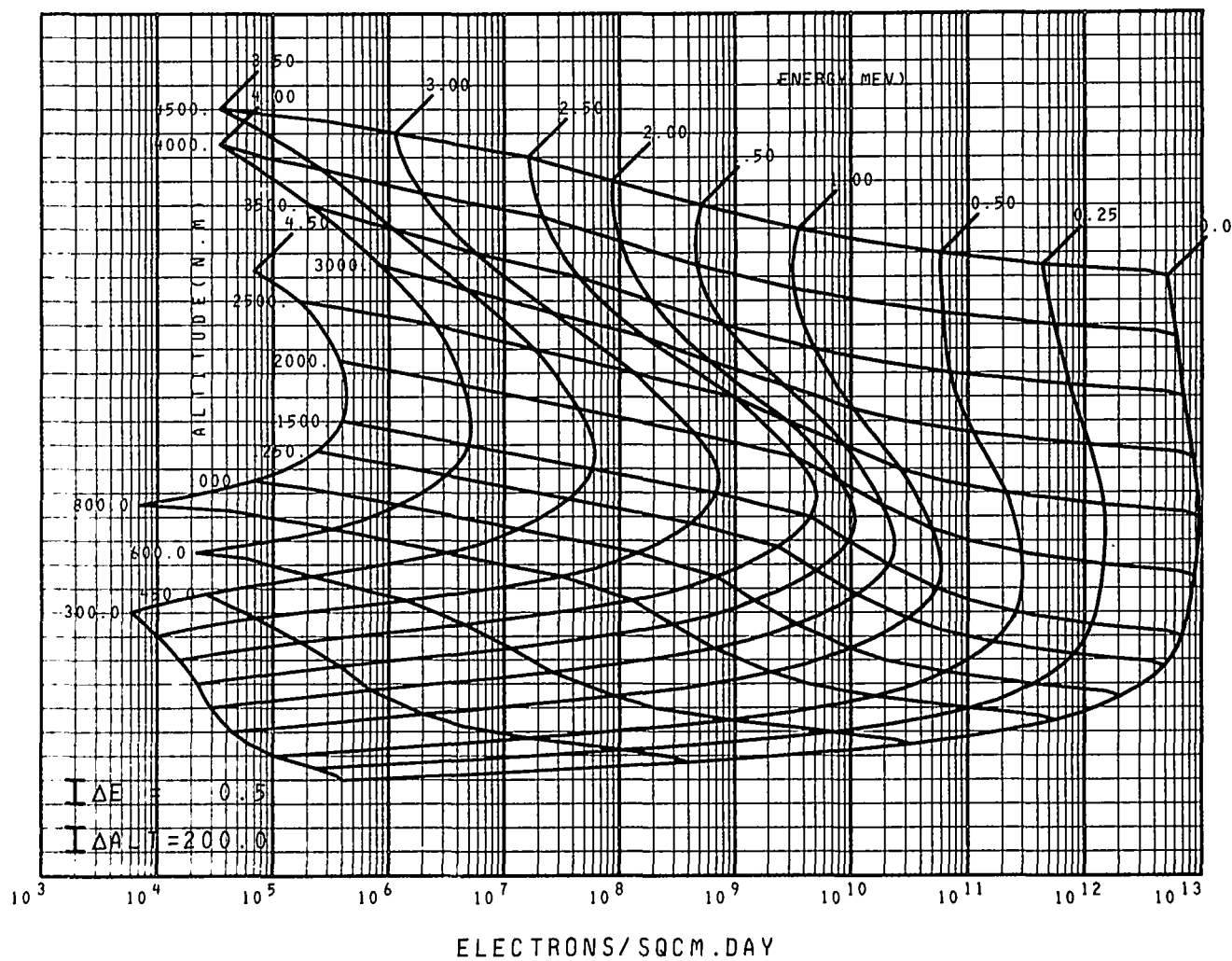


OMNIDIRECTIONAL INTEGRAL FLUX MAP
 4 MEV ELECTRONS L GE 4
 MODEL AE4 SOLAR MINIMUM PROJECTED

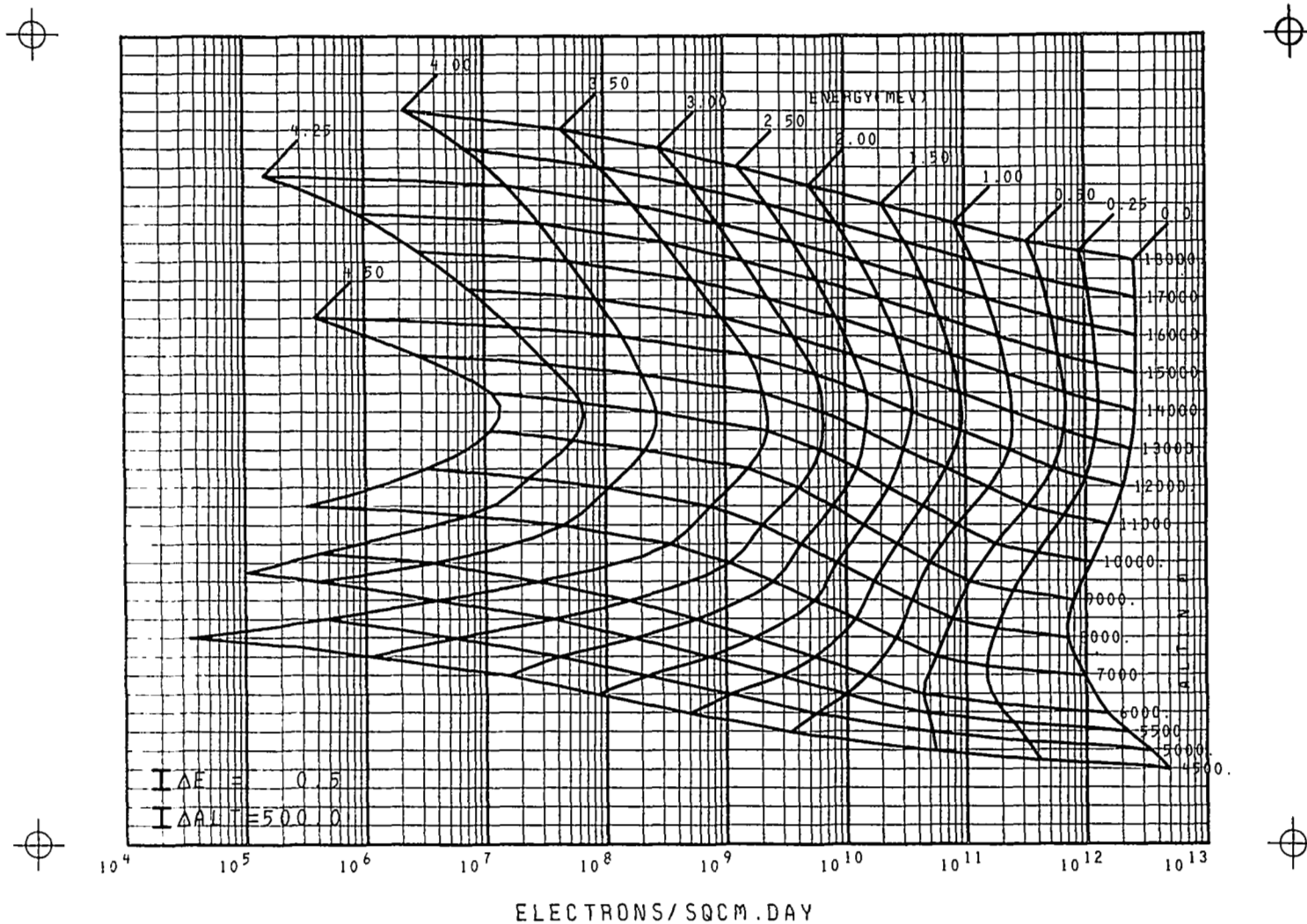
FIG. 9 CONT



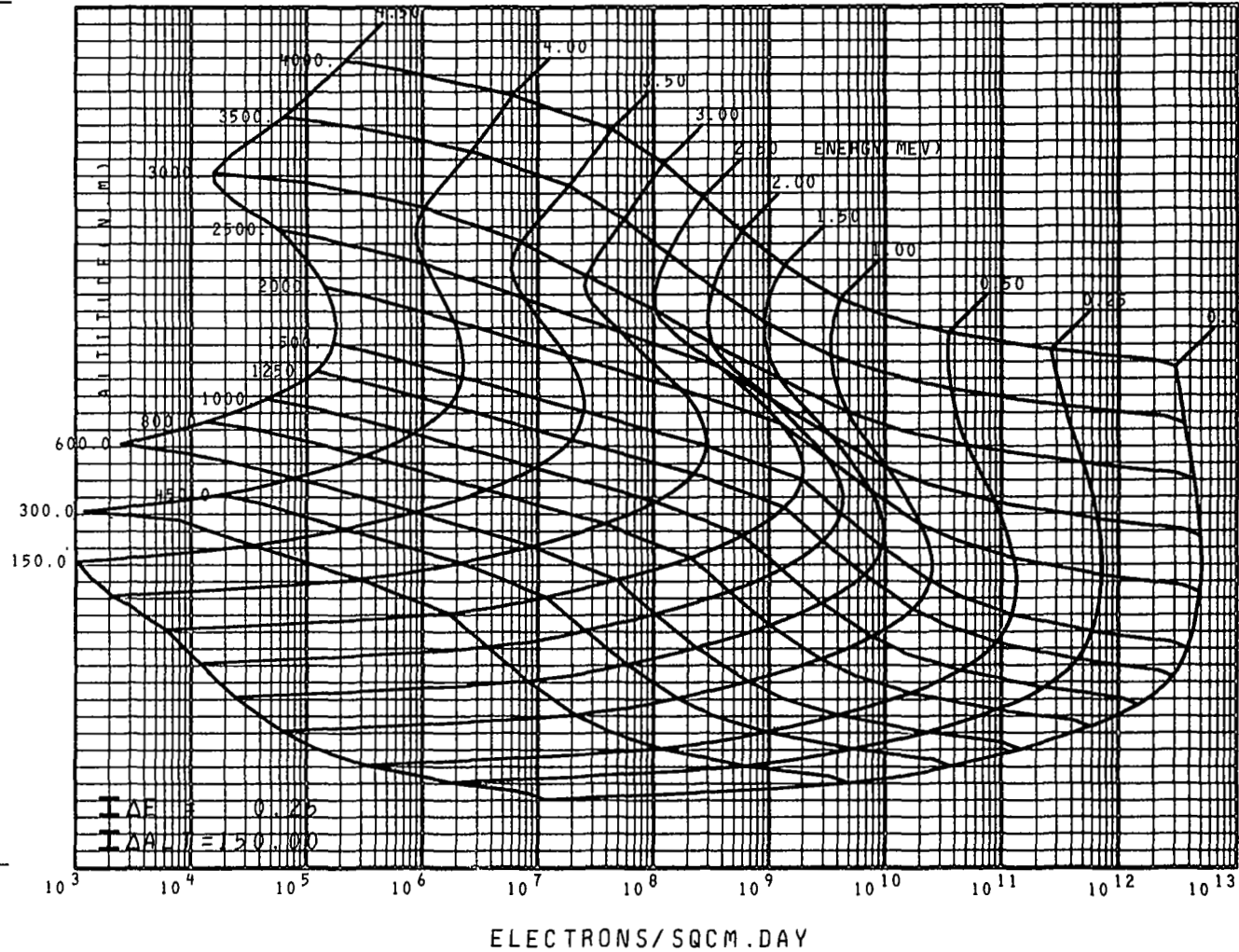
ORBITAL INTEGRATION MAP EPOCH 1975
 CIRCULAR ORBIT 0 DEG INCLINATION FIG.10
 SOLAR MINIMUM AE4 AND AE5 MODELS



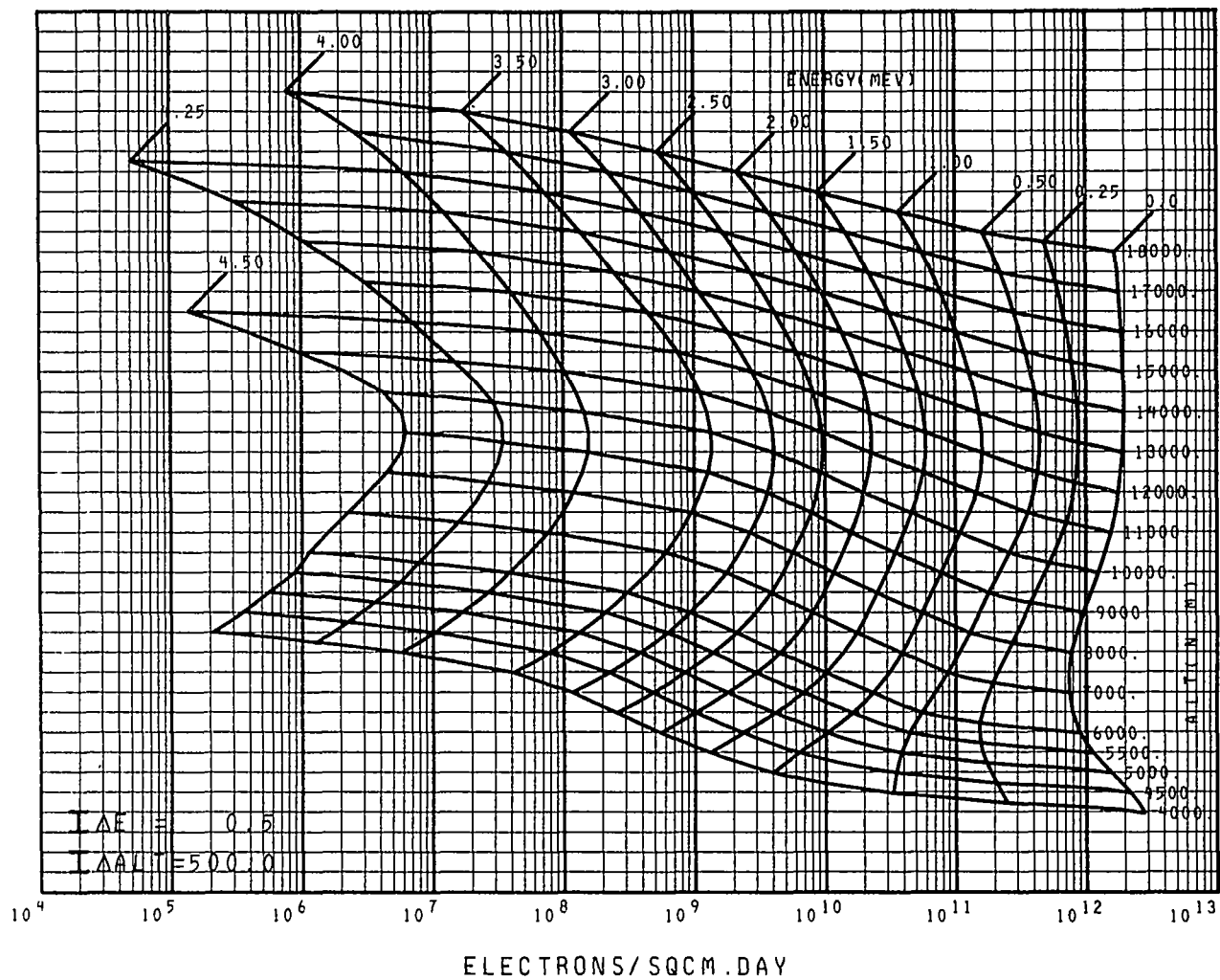
ORBITAL INTEGRATION MAP EPOCH 1975
 CIRCULAR ORBIT 0 DEG INCLINATION FIG.10 CONT
 SOLAR MINIMUM AE4 AND AE5 MODELS



ORBITAL INTEGRATION MAP EPOCH 1975
 CIRCULAR ORBIT 30 DEG INCLINATION FIG.11
 SOLAR MINIMUM AE4 AND AE5 MODELS

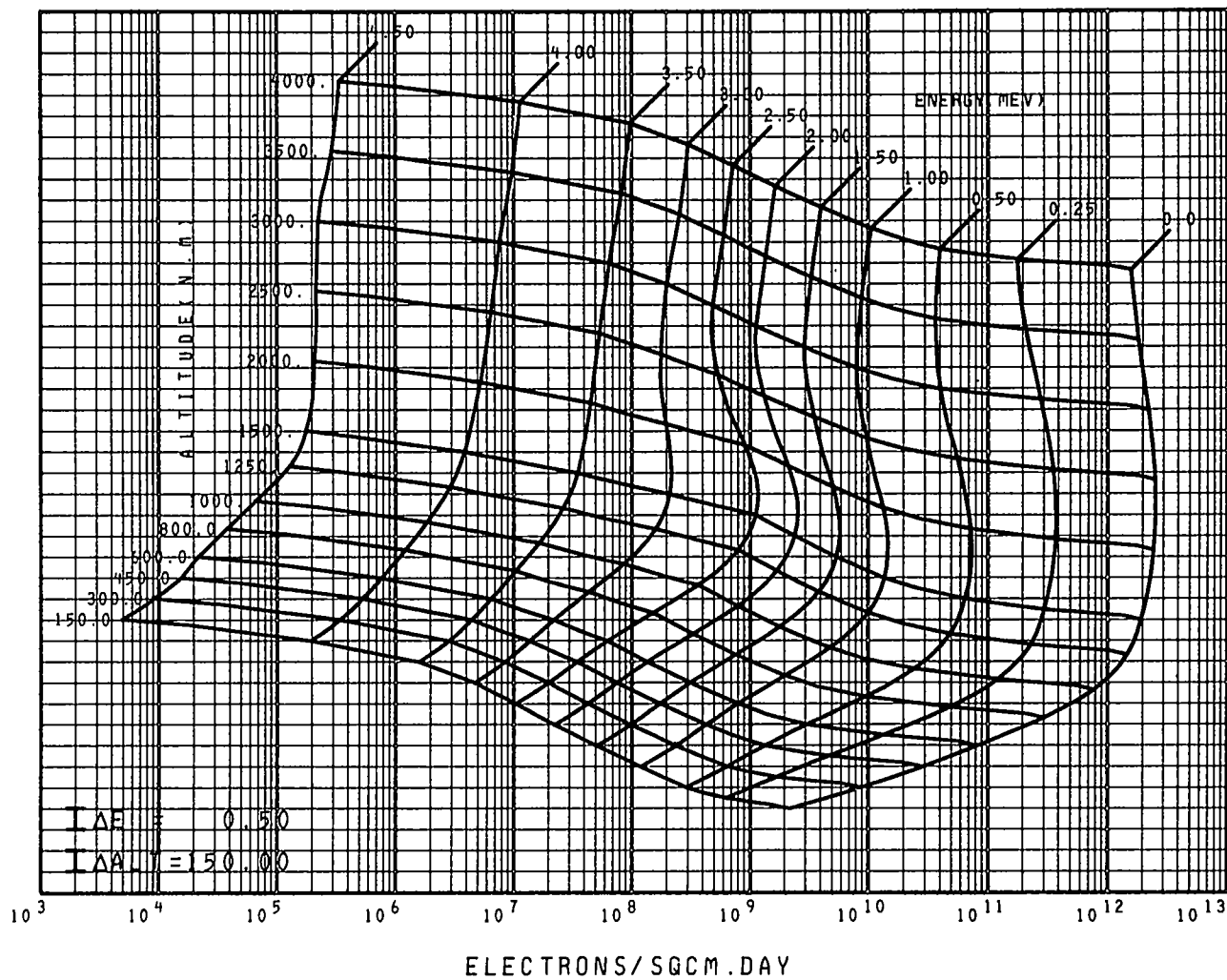


ORBITAL INTEGRATION MAP EPOCH 1975
 CIRCULAR ORBIT 30 DEG INCLINATION FIG.11 CONT
 SOLAR MINIMUM AE4 AND AE5 MODELS

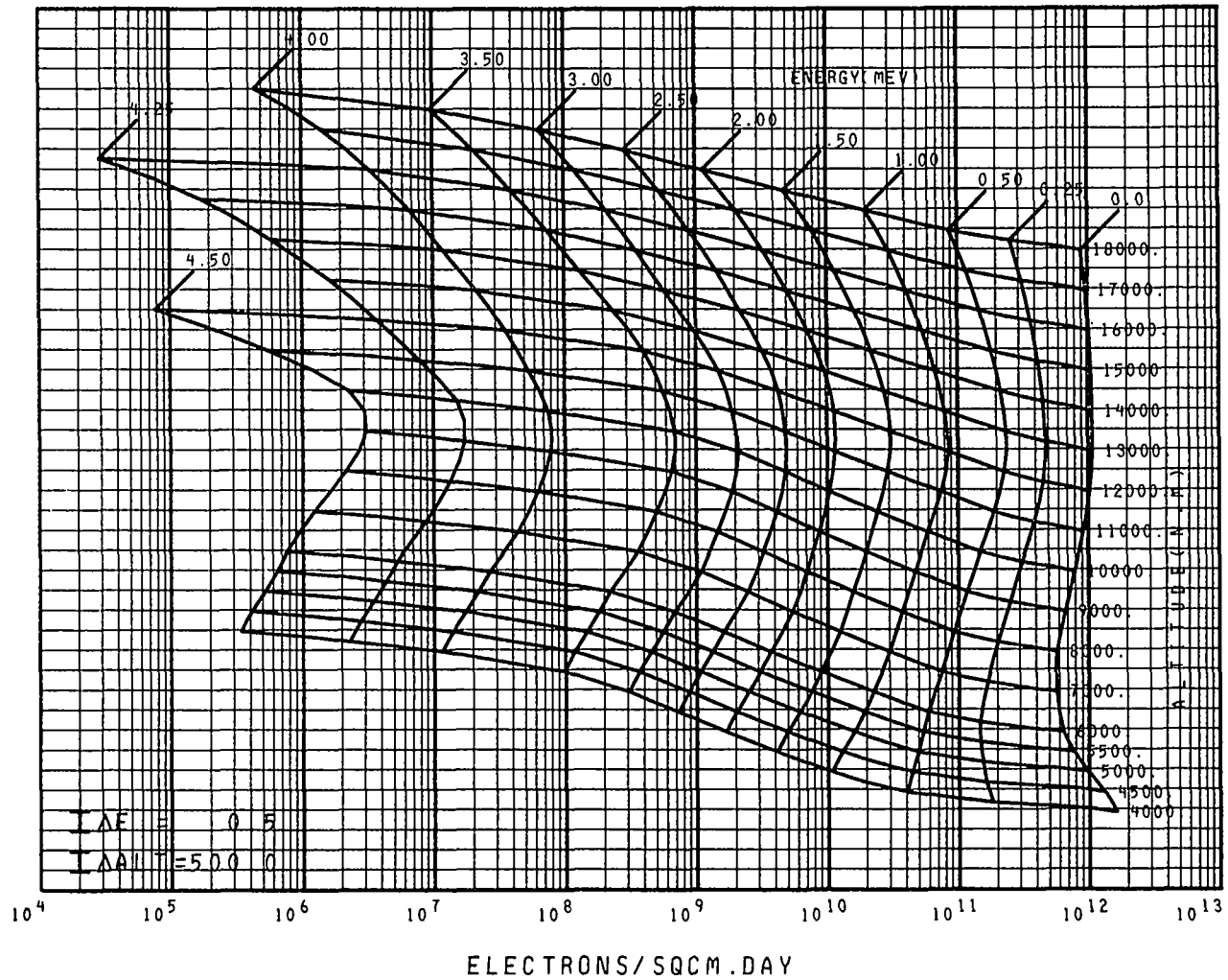


06

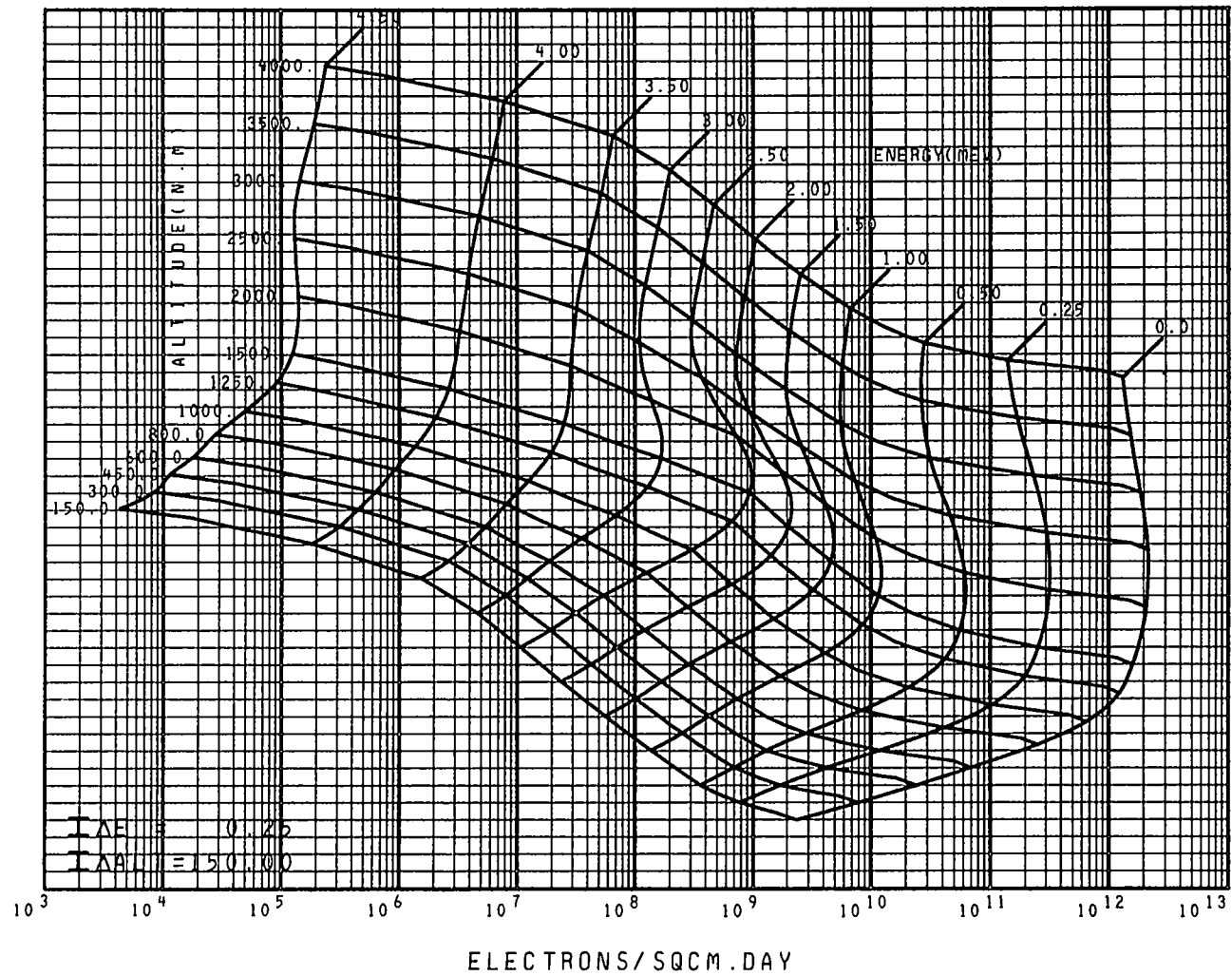
ORBITAL INTEGRATION MAP EPOCH 1975
 CIRCULAR ORBIT 60 DEG INCLINATION FIG.12
 SOLAR MINIMUM AE4 AND AE5 MODELS



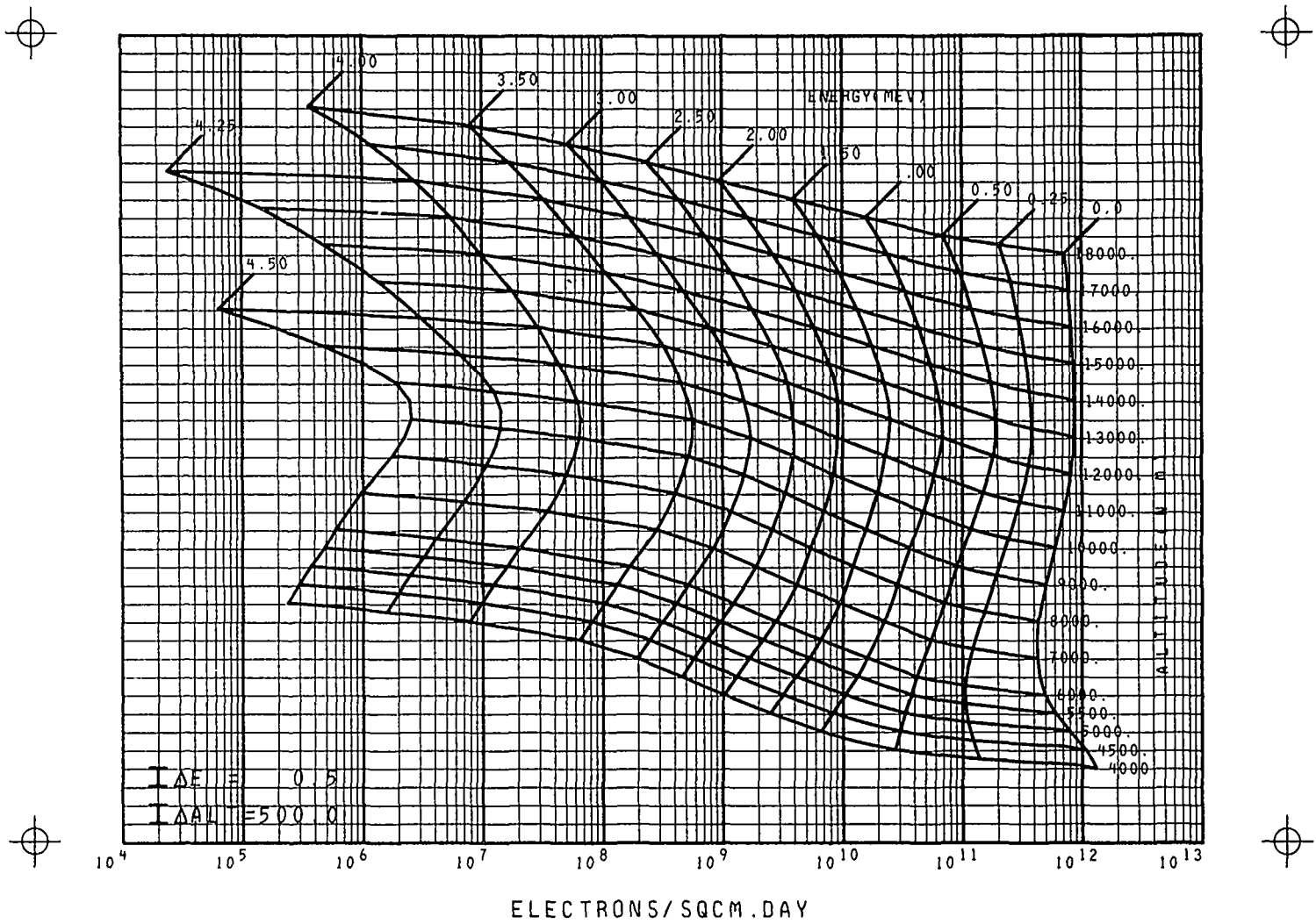
ORBITAL INTEGRATION MAP EPOCH 1975
 CIRCULAR ORBIT 60 DEG INCLINATION FIG.12 CONT
 SOLAR MINIMUM AE4 AND AE5 MODELS



ORBITAL INTEGRATION MAP EPOCH 1975
 CIRCULAR ORBIT 90 DEG INCLINATION FIG.13
 SOLAR MINIMUM AE4 AND AE5 MODELS



ORBITAL INTEGRATION MAP EPOCH 1975
 CIRCULAR ORBIT 90 DEG INCLINATION FIG.13 CONT
 SOLAR MINIMUM AE4 AND AE5 MODELS



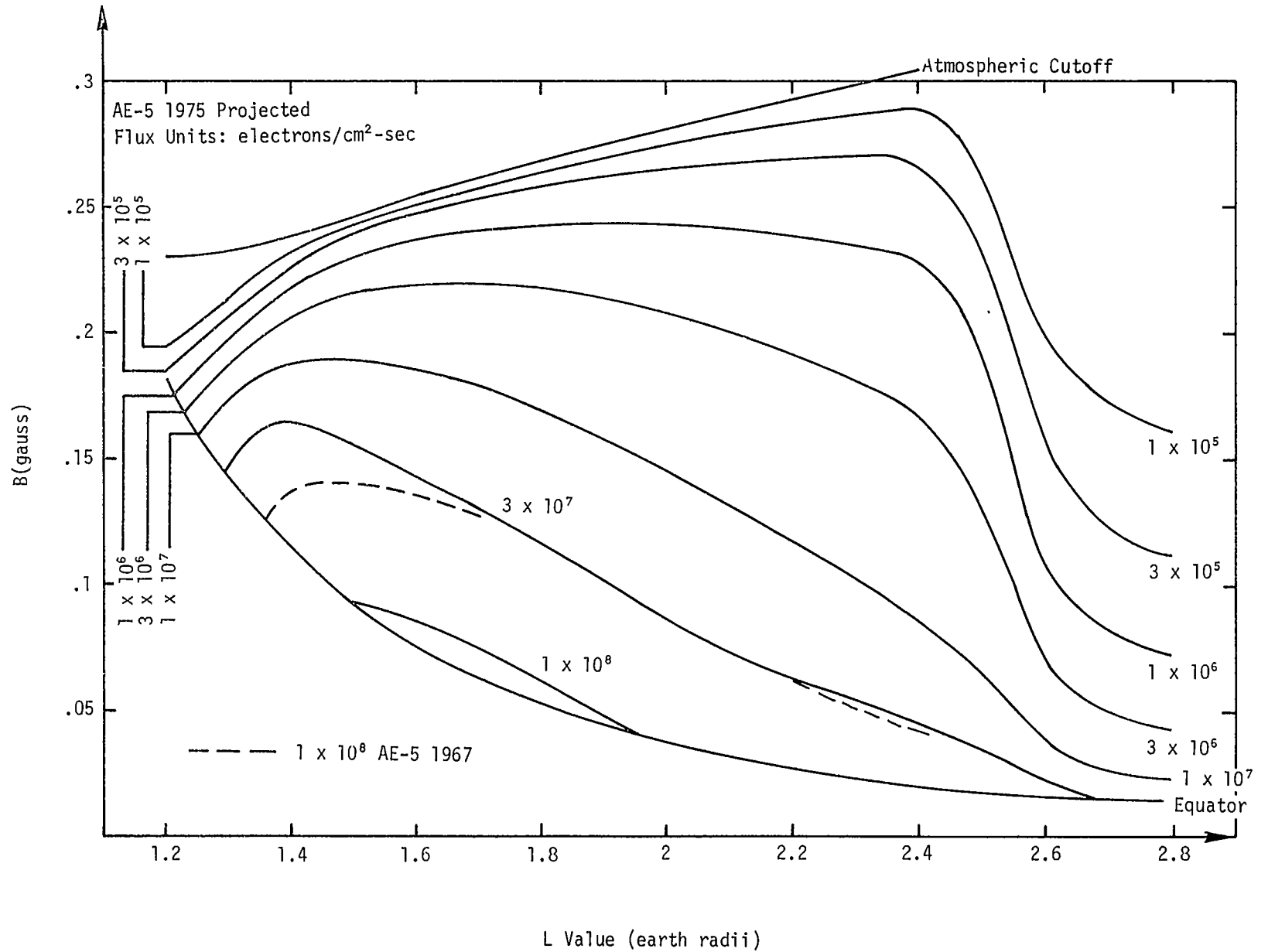


Figure 14. Omnidirectional Iso-flux Contours for 40-keV Electrons: B-L Projection

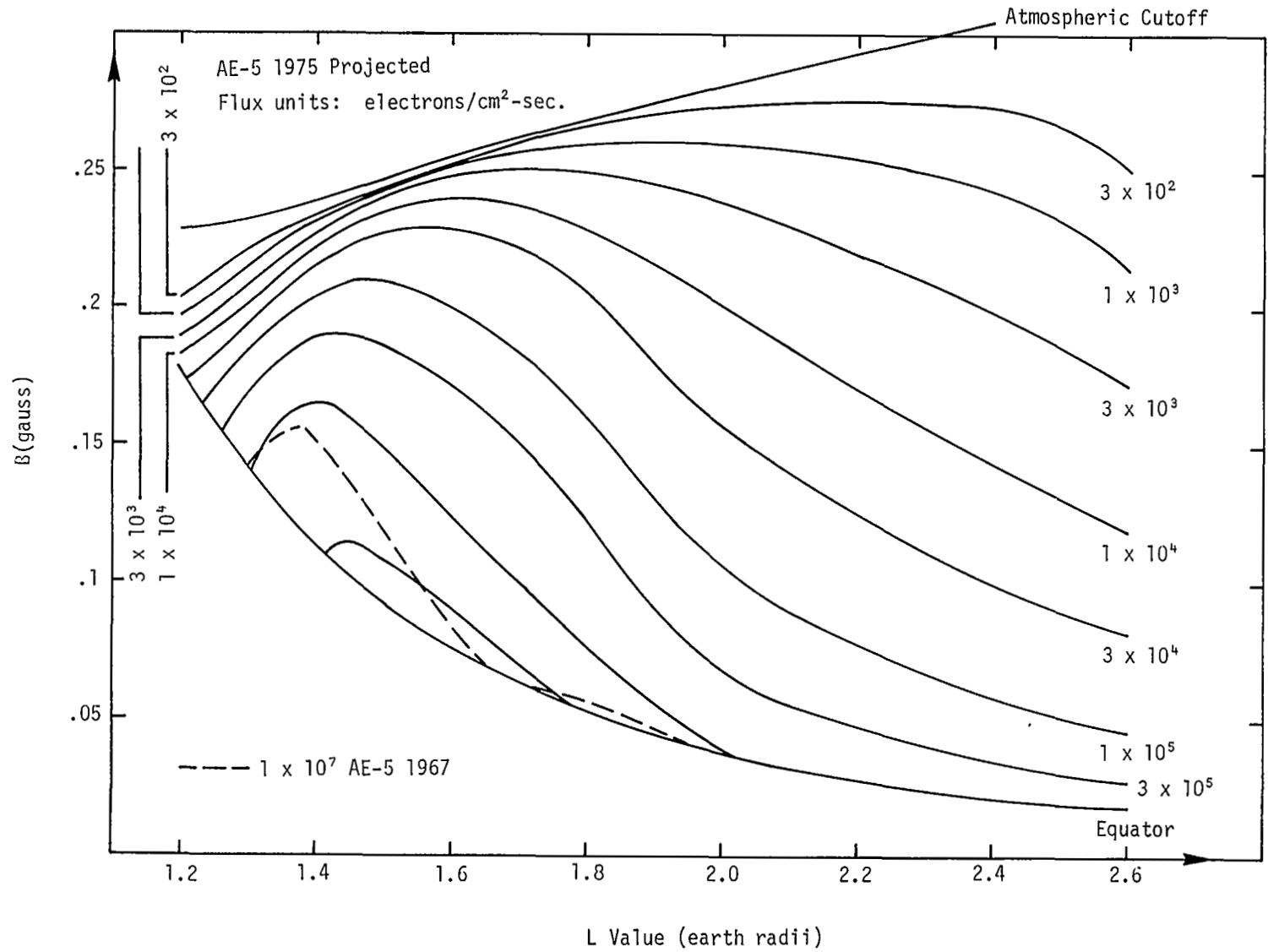


Figure 15. Omnidirectional Iso-flux Contours for 500-keV Electrons: B-L Projection

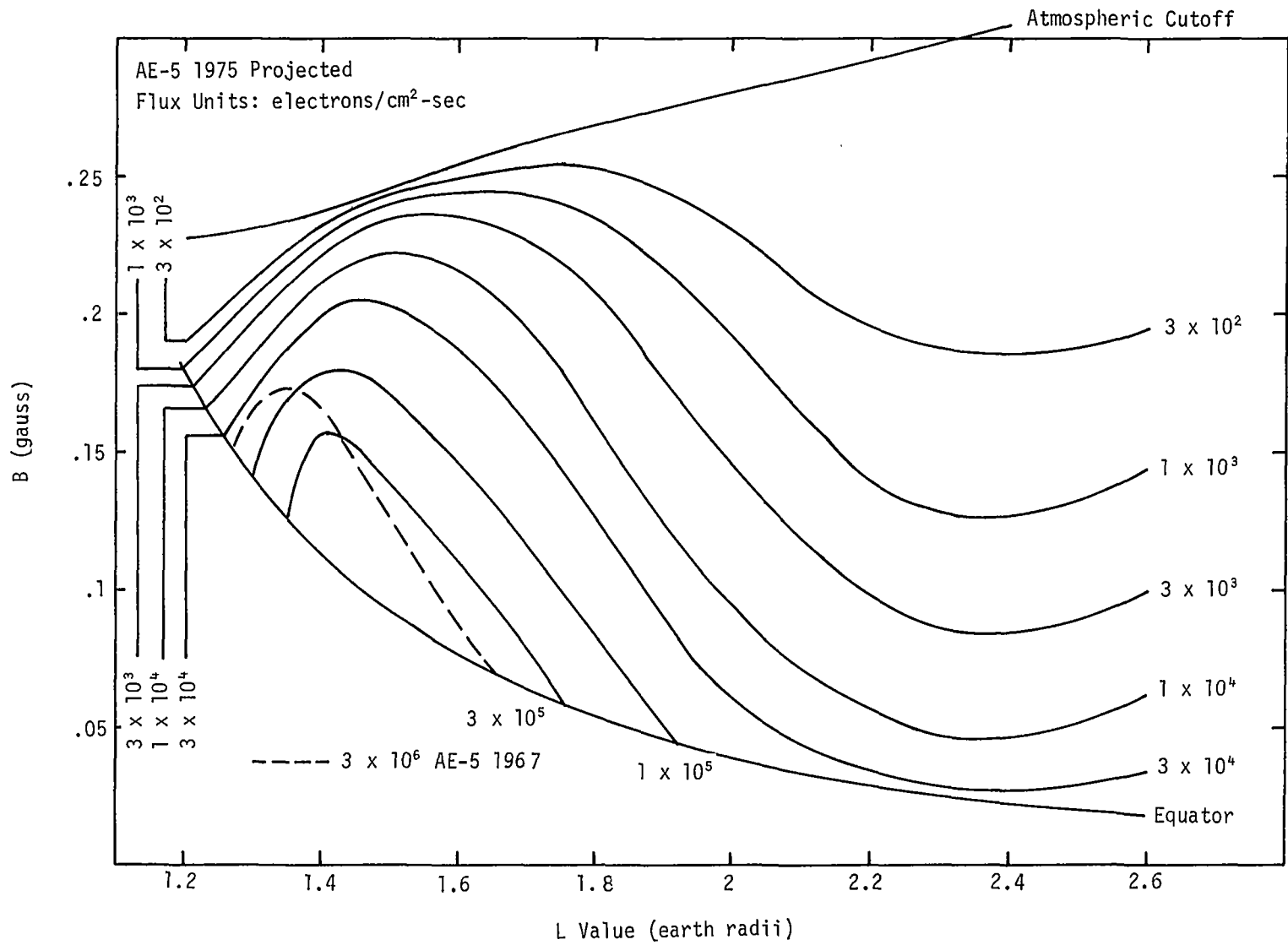


Figure 16. Omnidirectional Iso-flux Contours for 1-MeV Electrons: B-L Projection

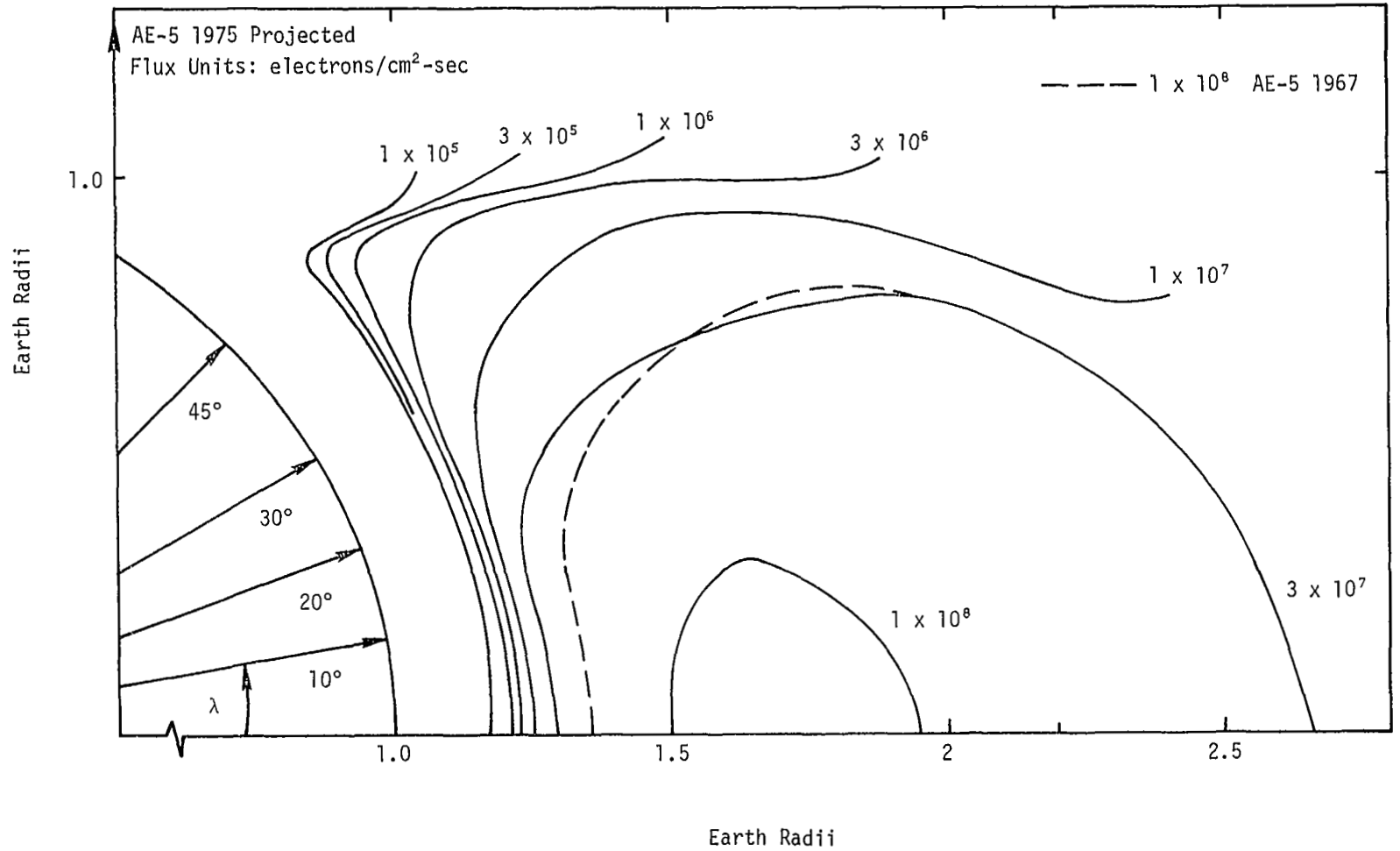


Figure 17. Omnidirectional Iso-flux Contours for 40-keV Electrons: R-λ Projection

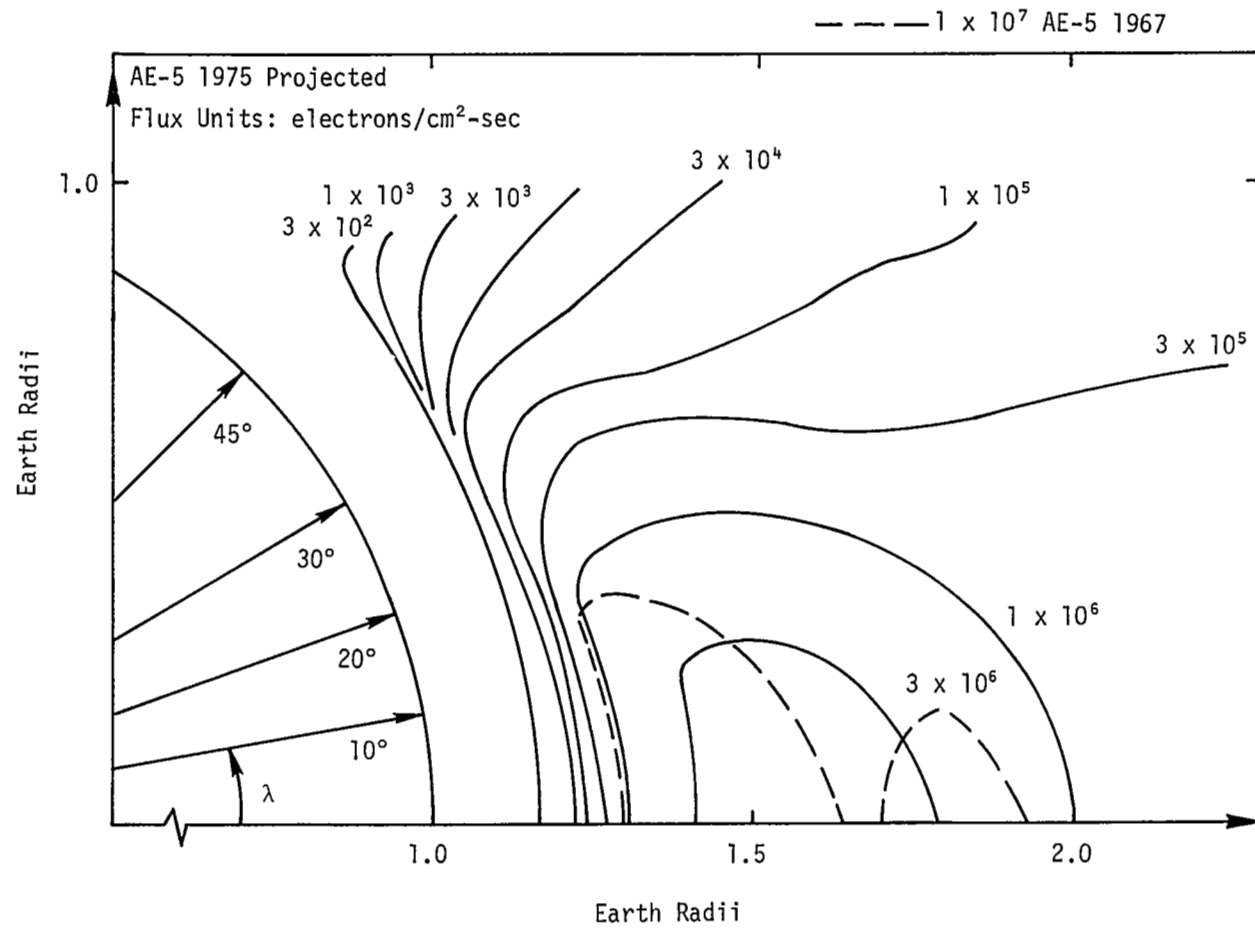


Figure 18. Omnidirectional Iso-flux Contours for 500-keV Electrons: R-λ Projection

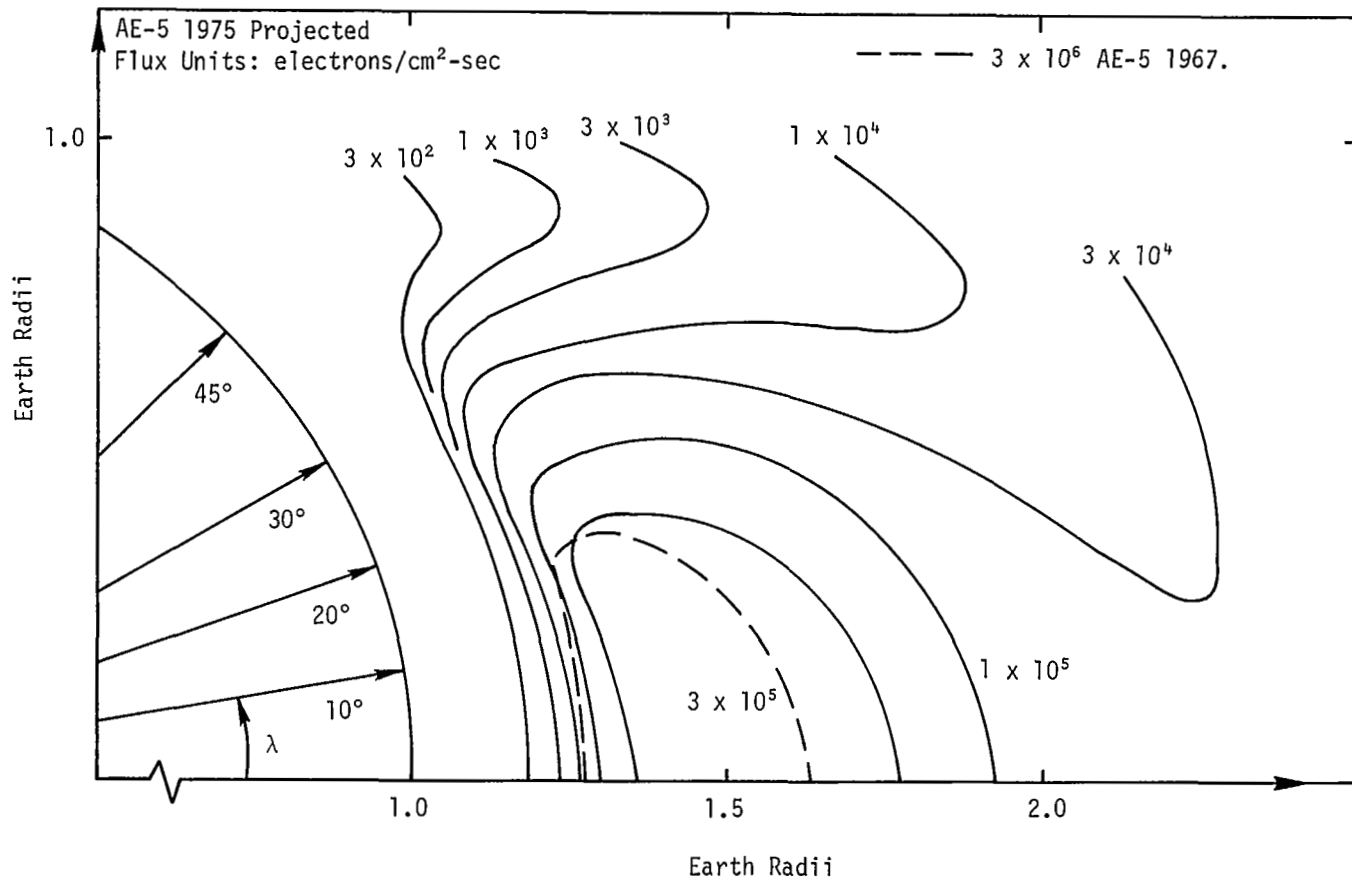


Figure 19. Omnidirectional Iso-flux Contours for 1-MeV Electrons: R- λ Projection

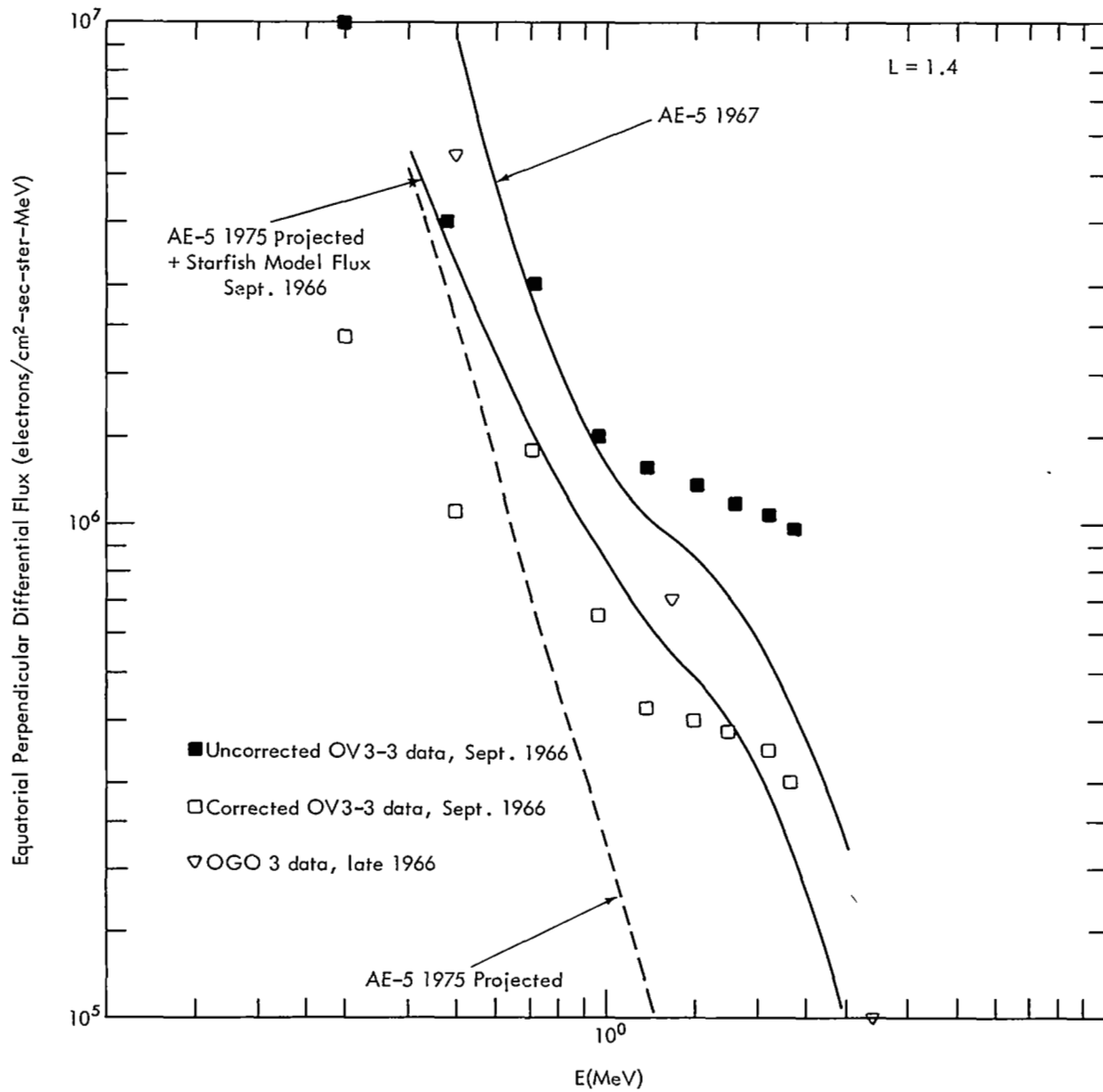


Figure 20. Effect of Revising OV3-3 Spectrometer Efficiencies

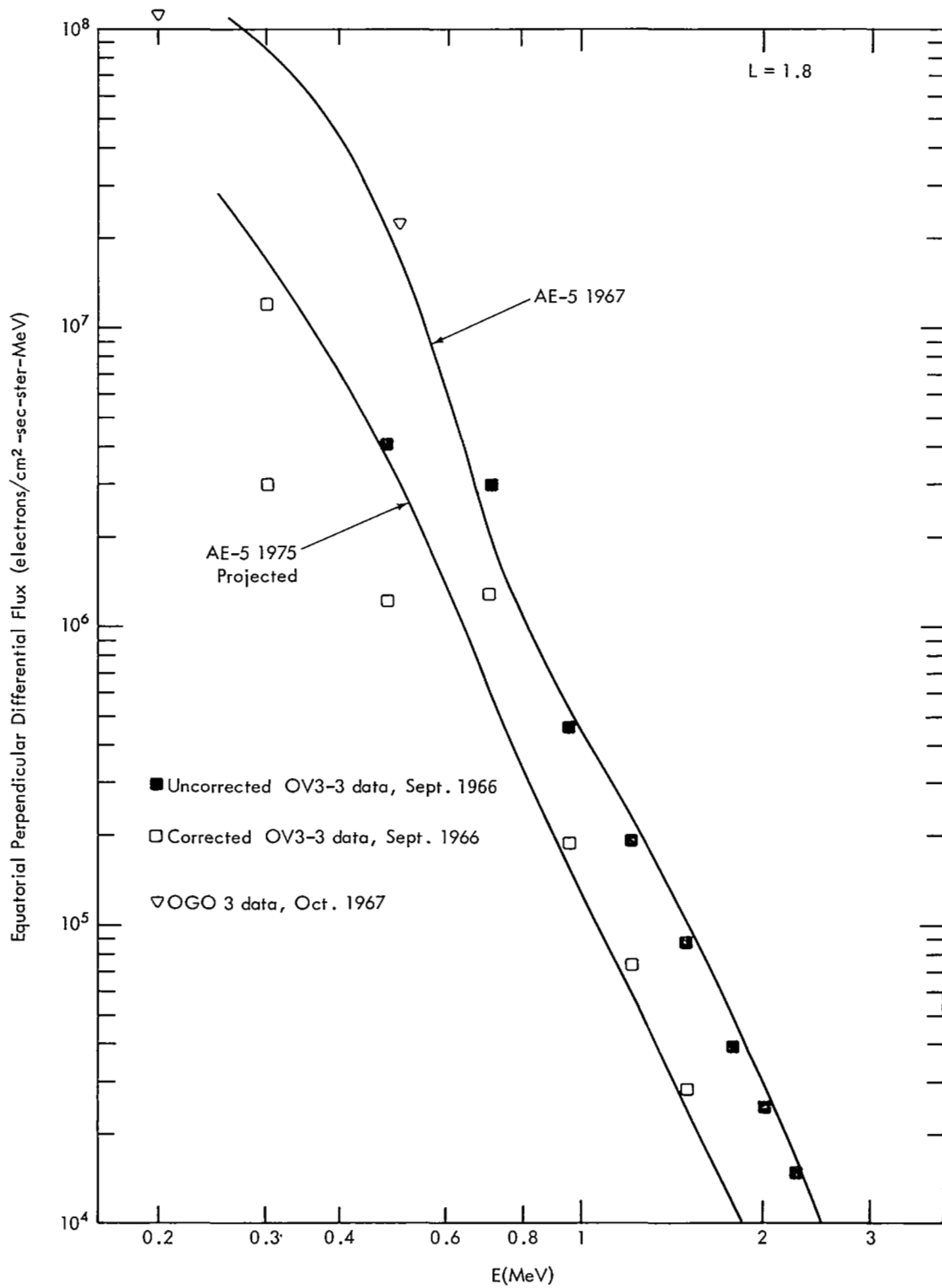


Figure 21. Effect of Revising OV3-3 Spectrometer Efficiencies

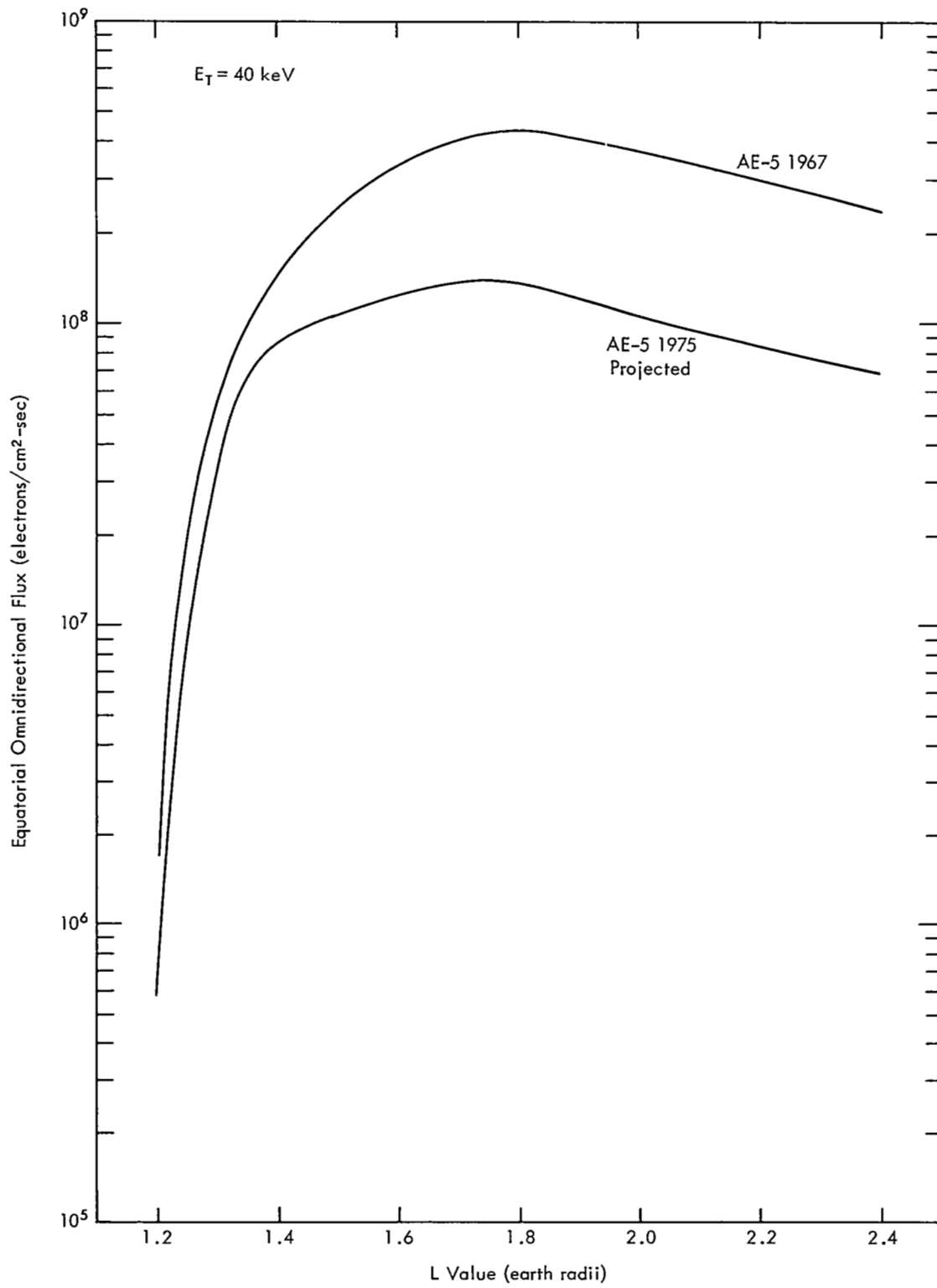


Figure 22. Inner Zone Electron Radial Profiles

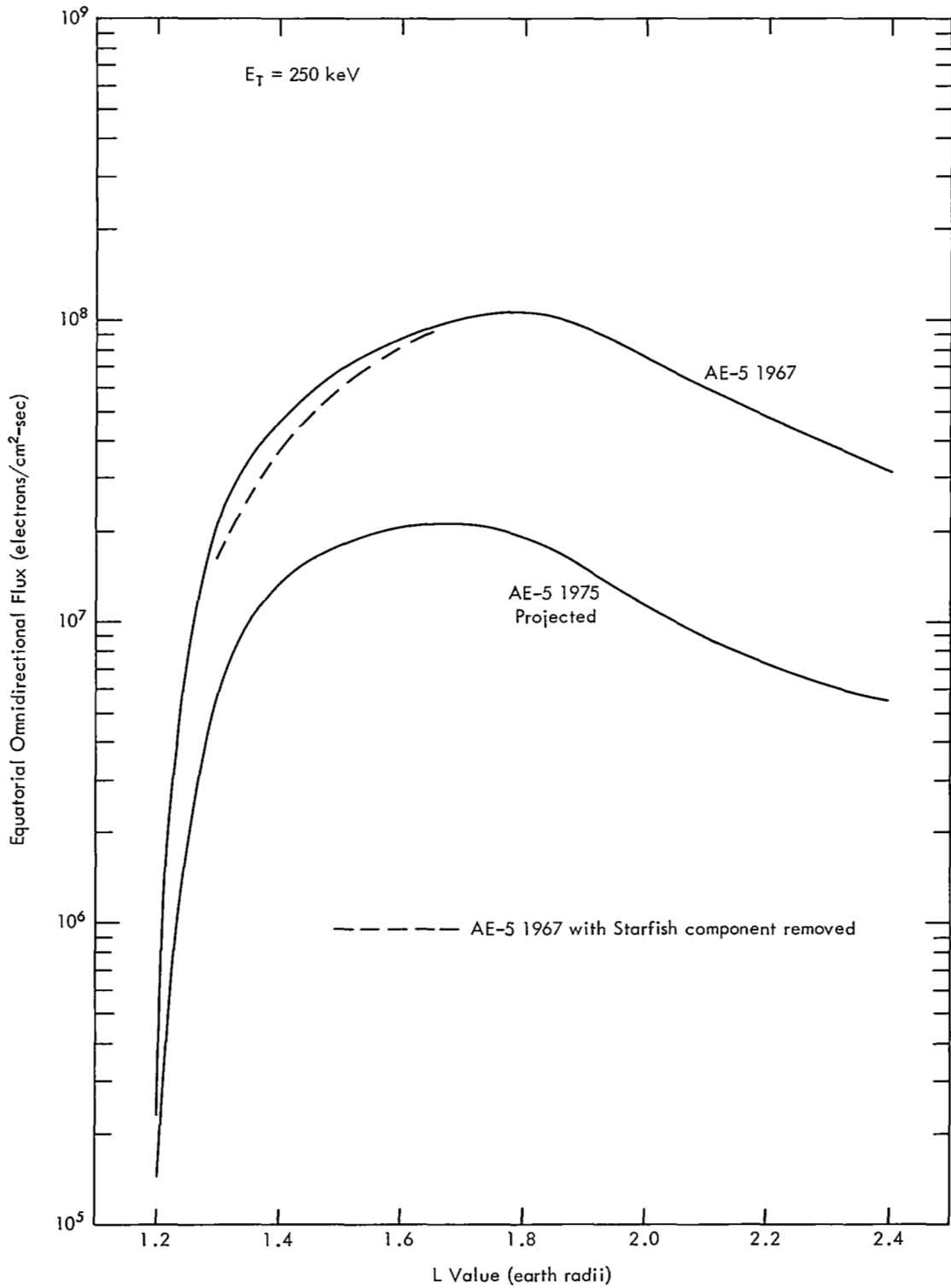


Figure 23. Inner Zone Electron Radial Profiles

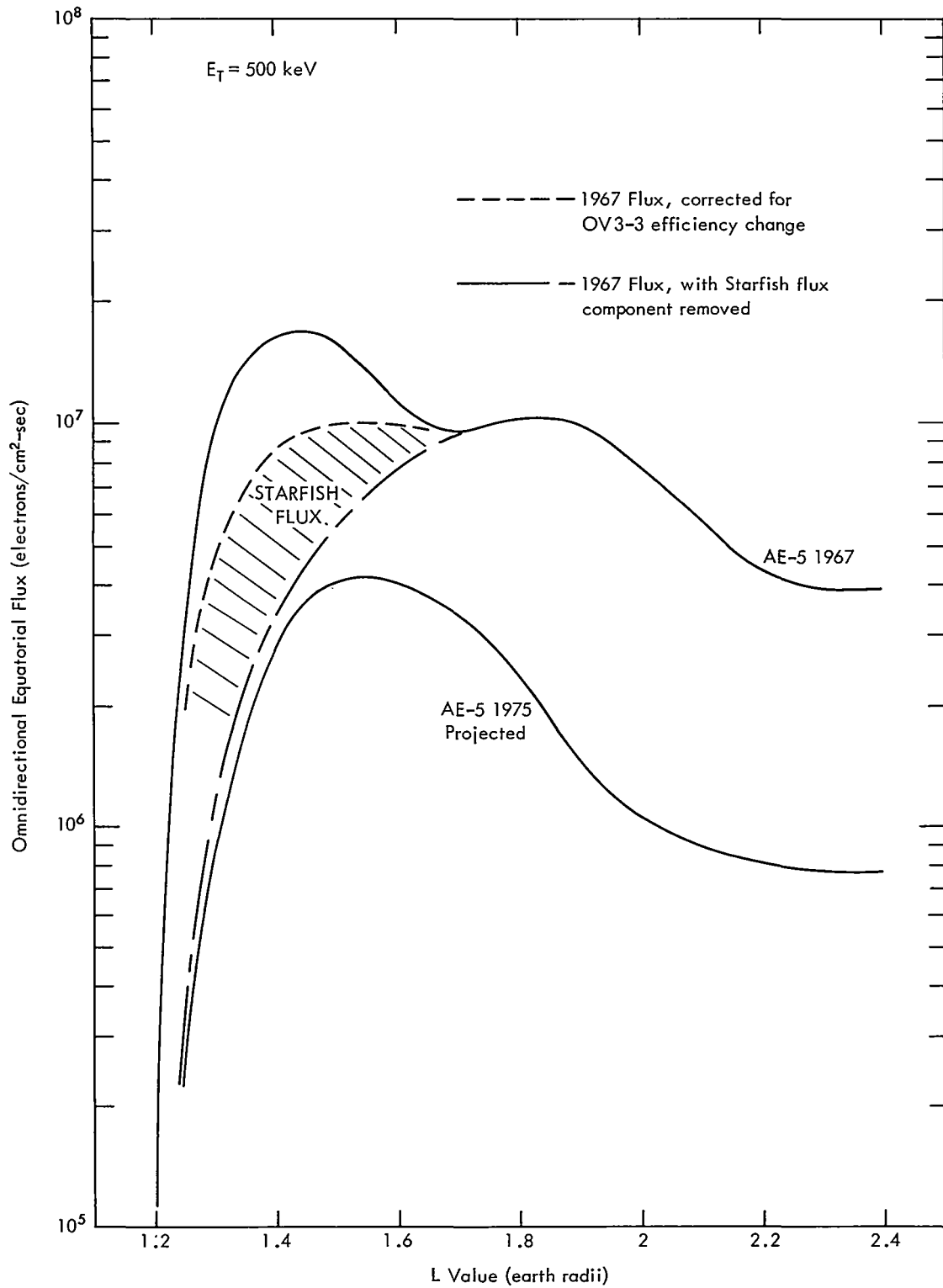


Figure 24. Inner Zone Electron Radial Profiles

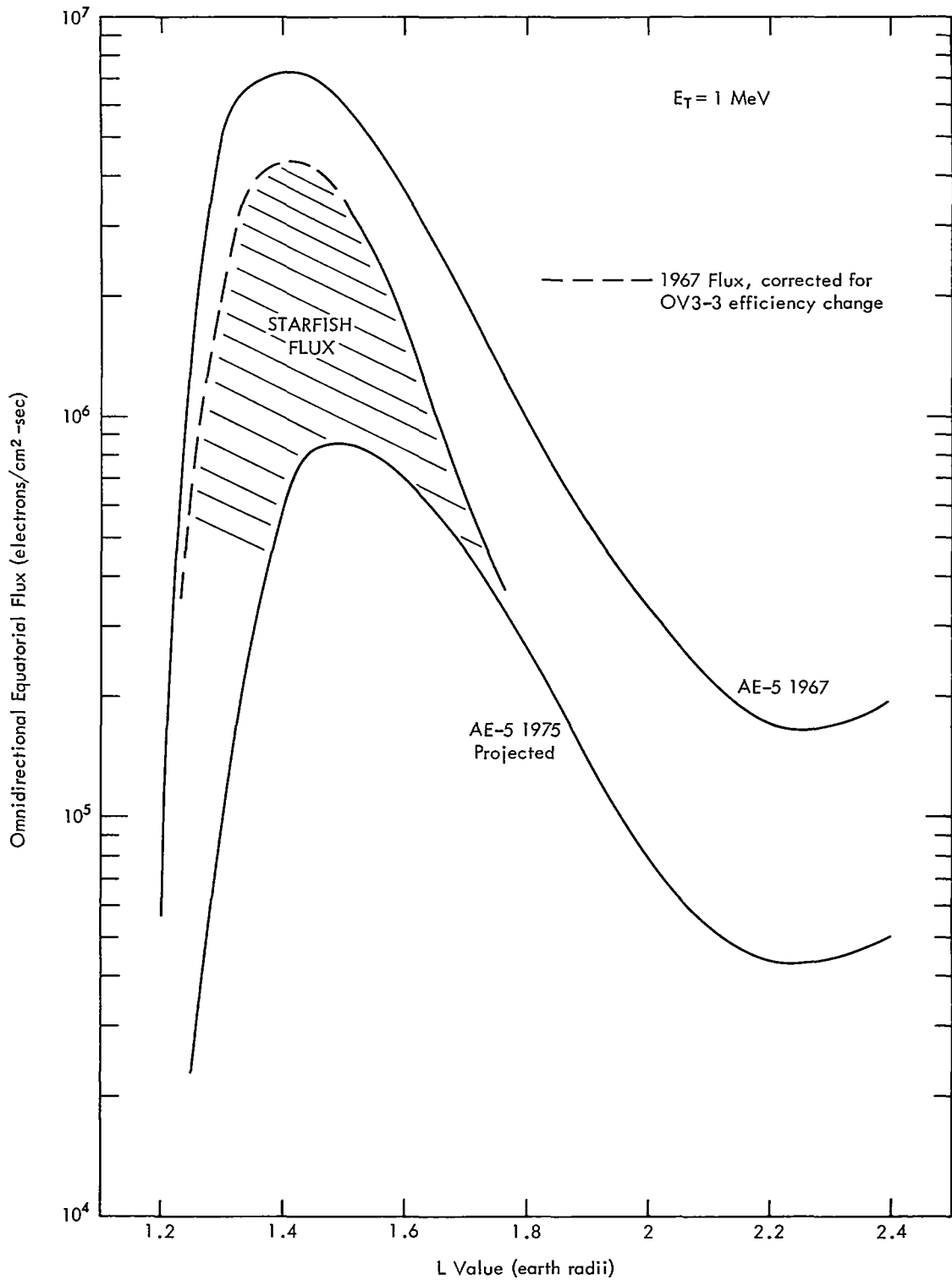


Figure 25. Inner Zone Electron Radial Profiles

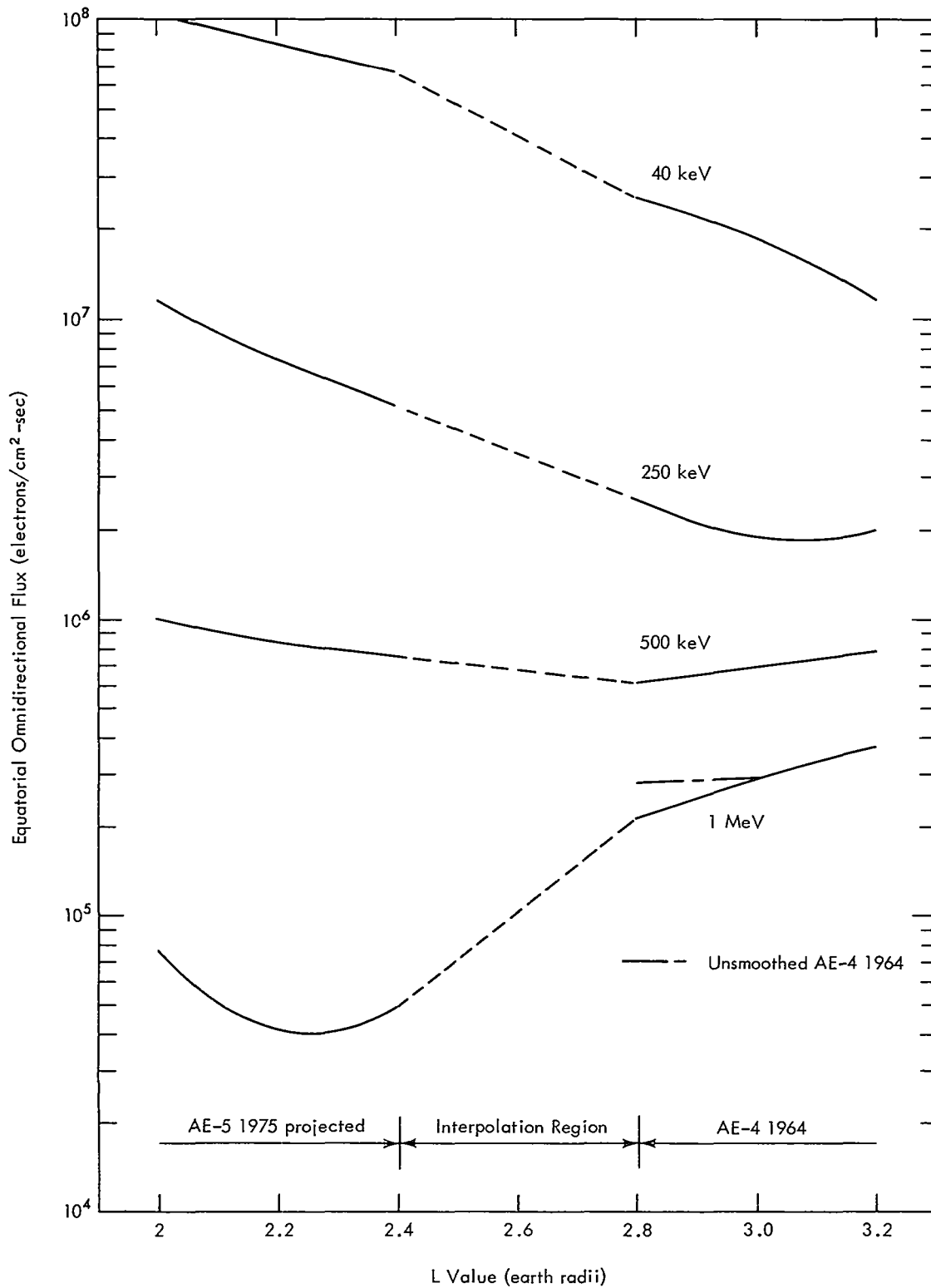


Figure 26. Radial Profiles in the Interface Region, $L \sim 2.6$

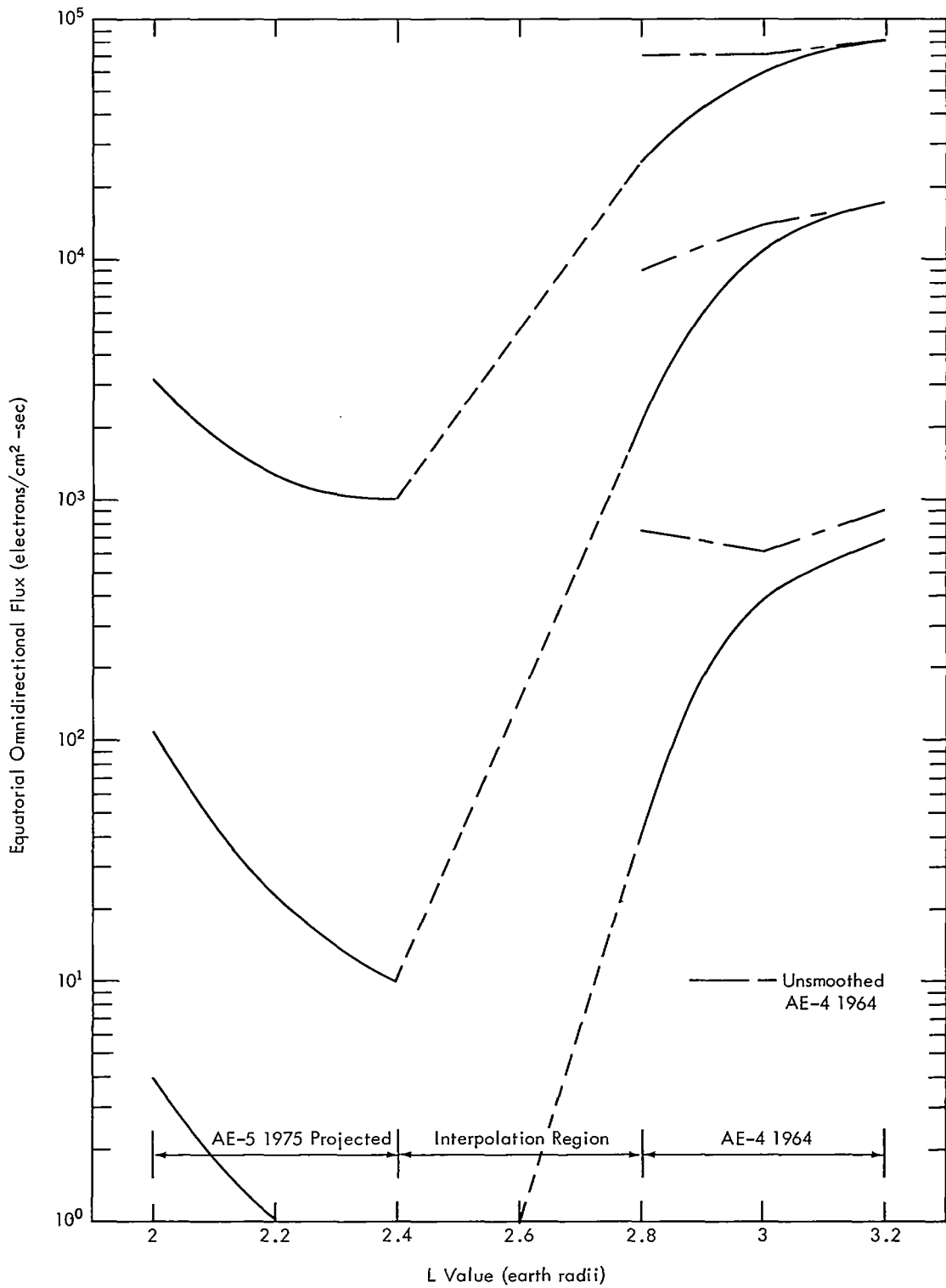


Figure 27. Radial Profiles in the Interface Region, $L \sim 2.6$

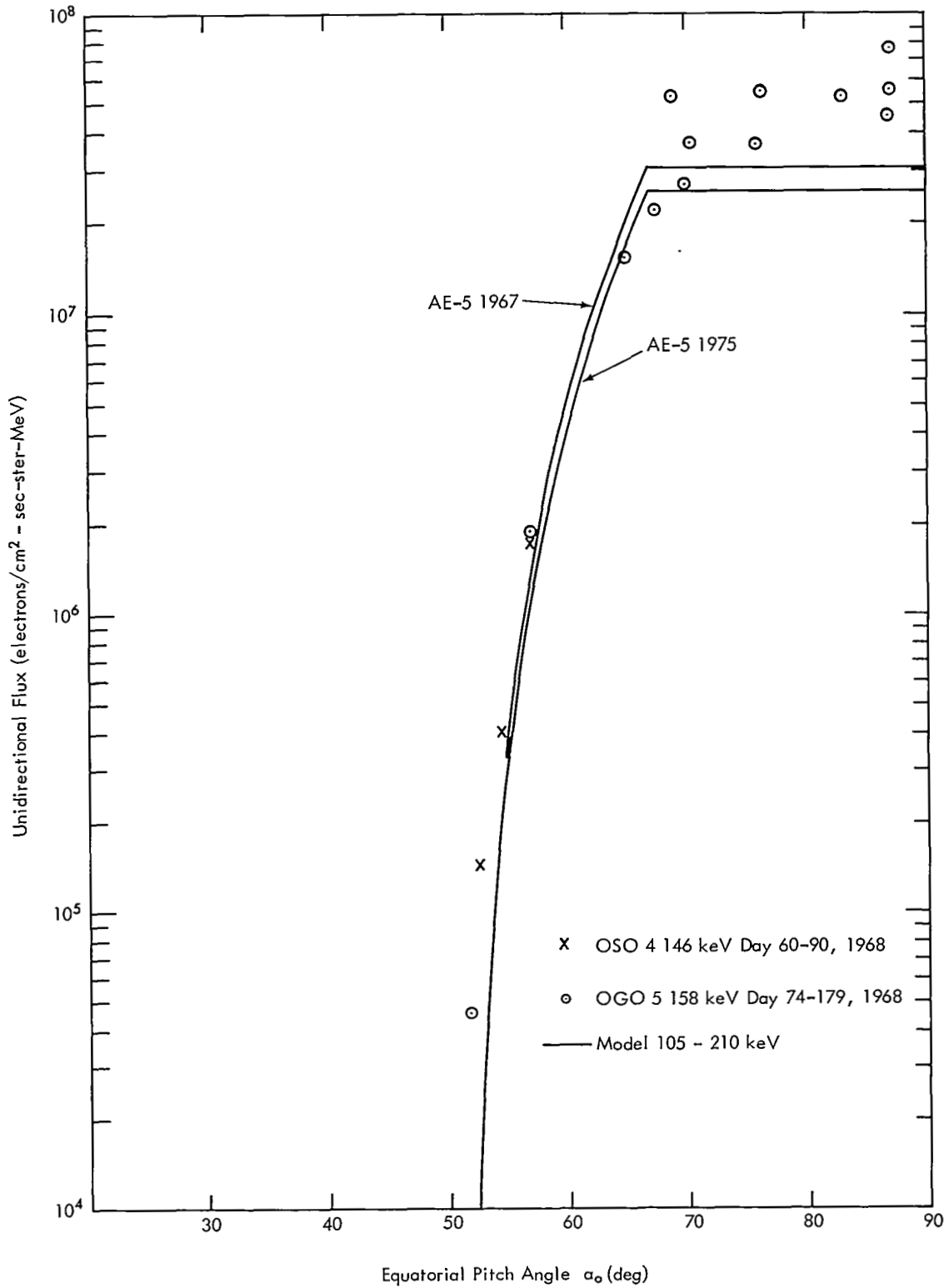


Figure 28. Equatorial Pitch Angle Distribution, L = 1.3

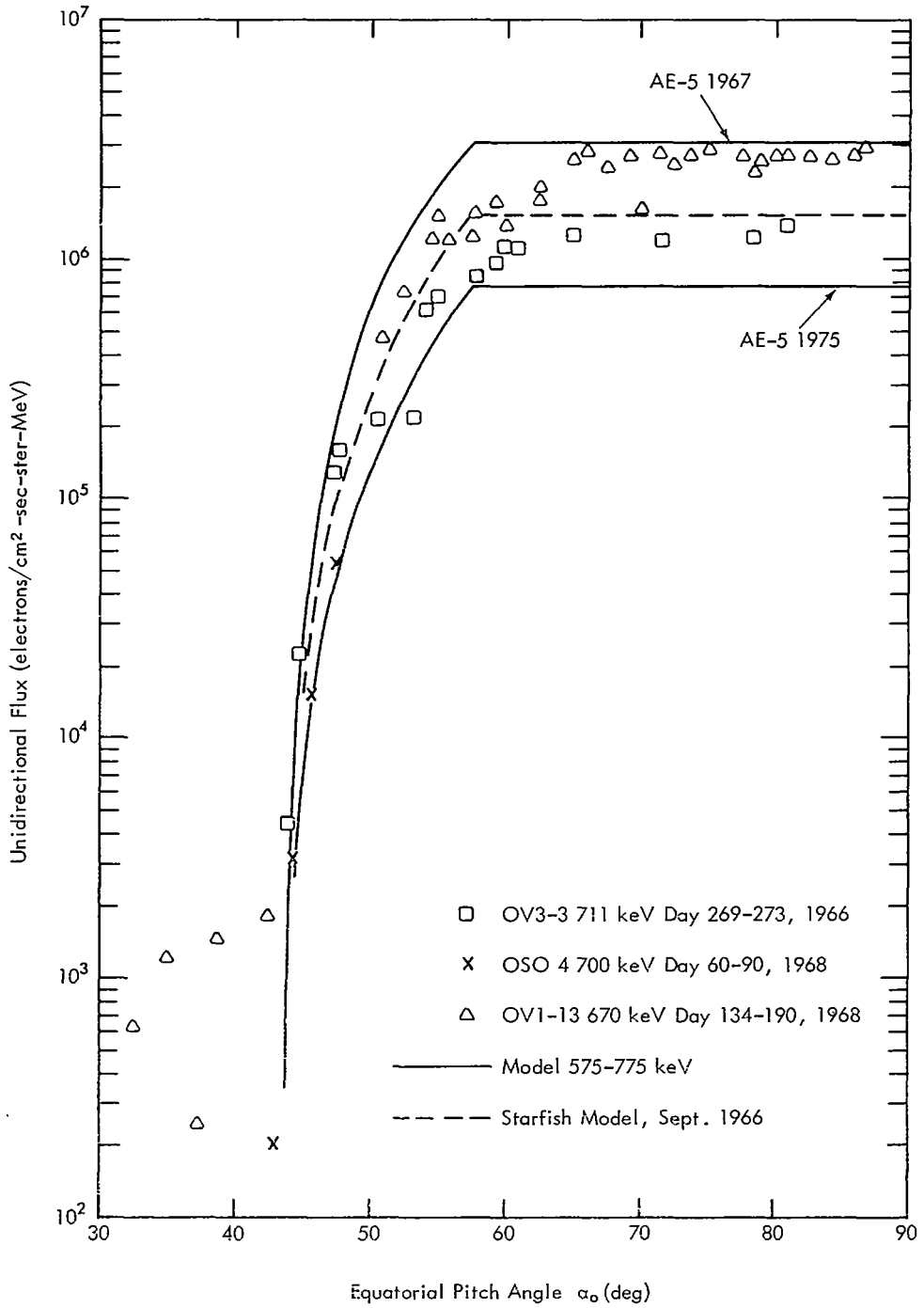


Figure 29. Equatorial Pitch Angle Distribution, L = 1.4

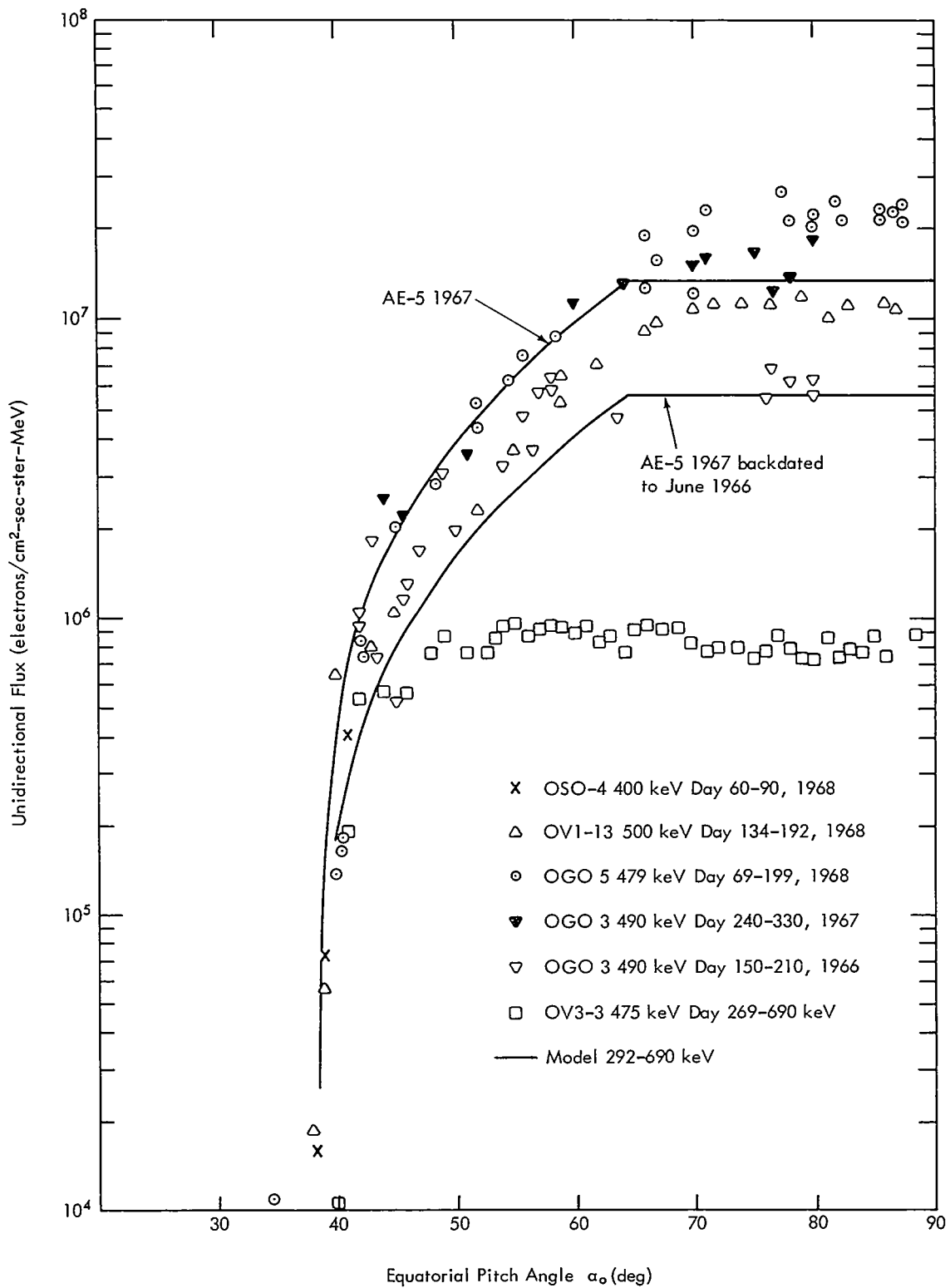


Figure 30. Equatorial Pitch Angle Distribution, L = 1.5

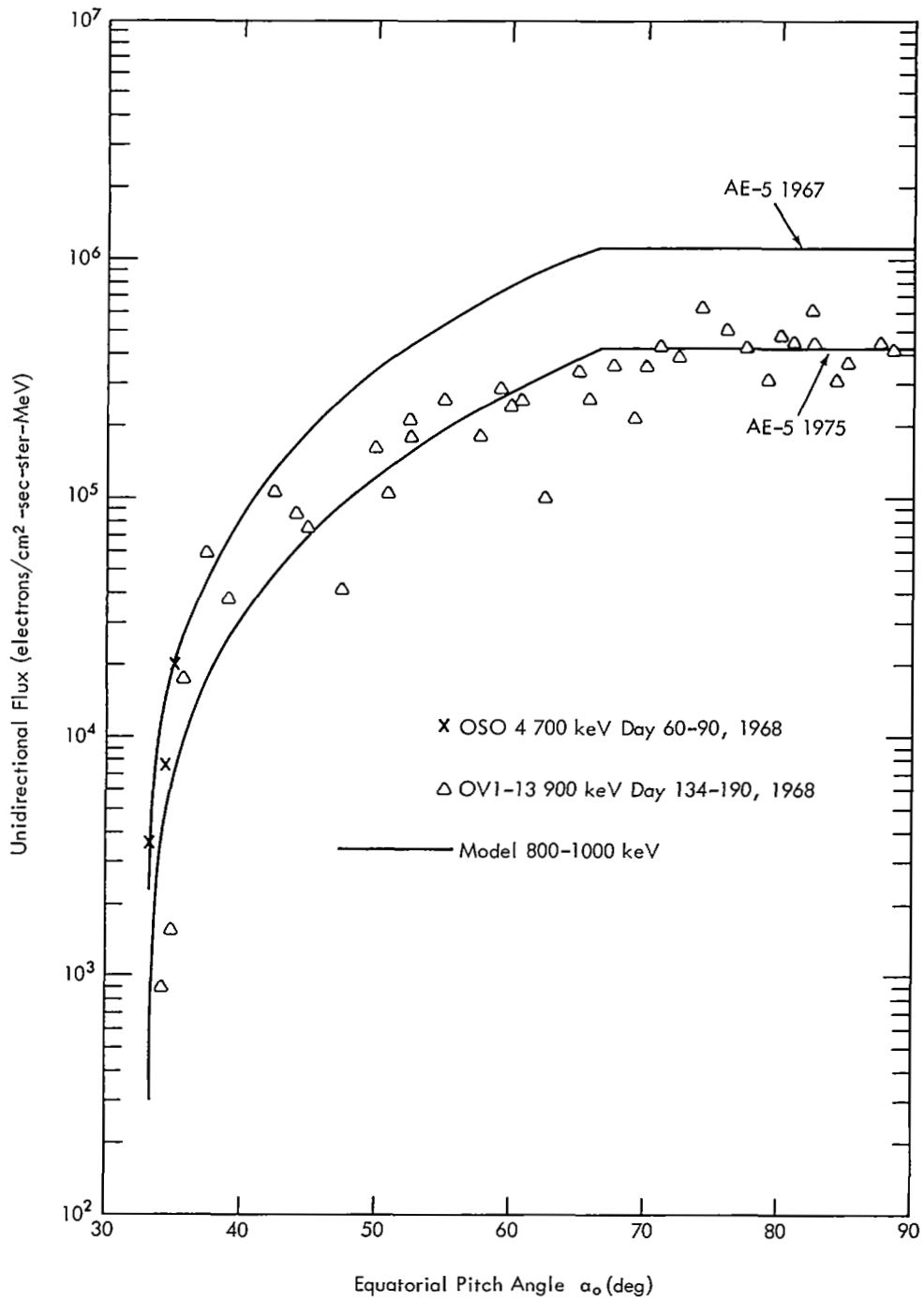


Figure 31. Equatorial Pitch Angle Distribution, L = 1.6

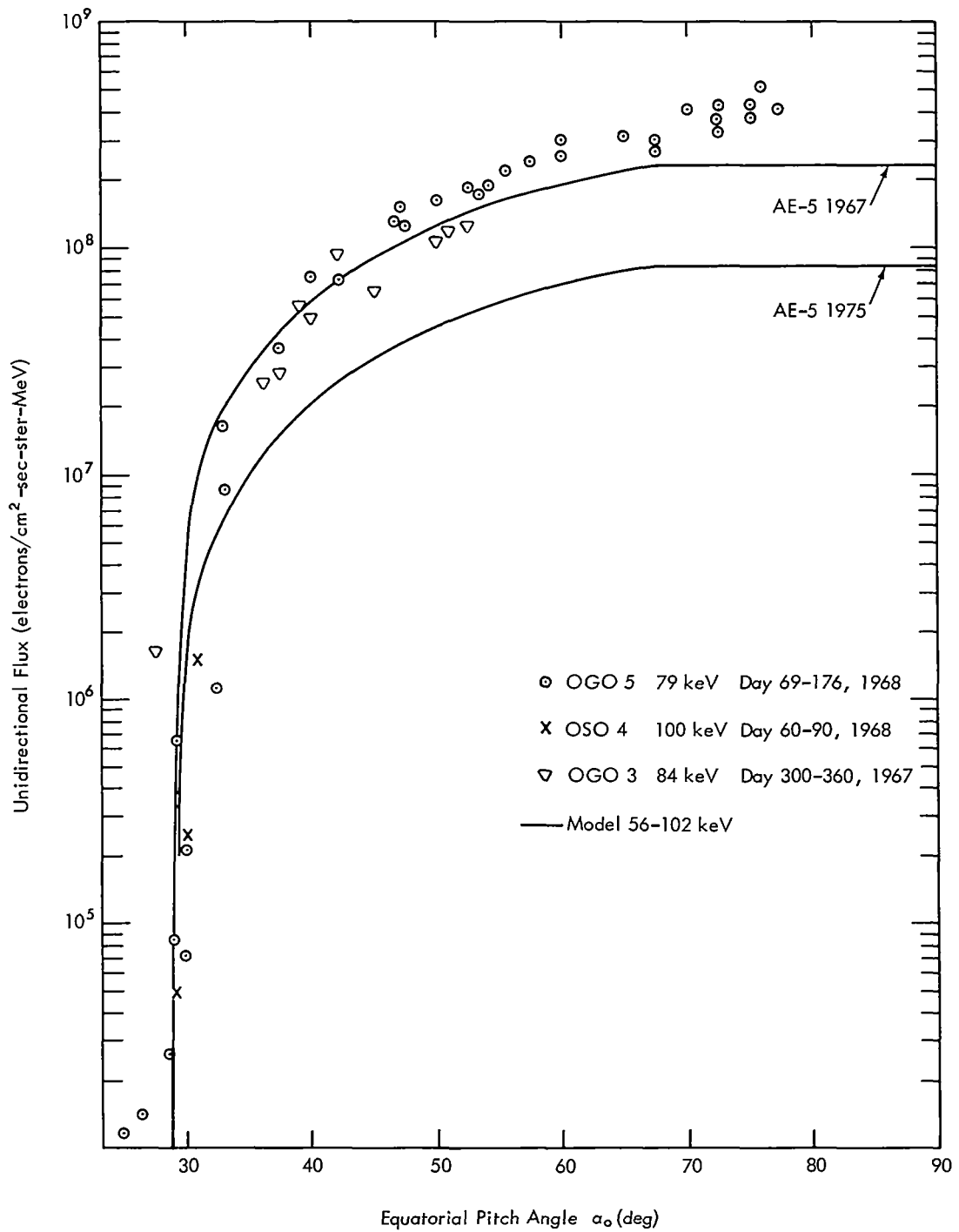


Figure 32. Equatorial Pitch Angle Distribution, $L = 1.7$

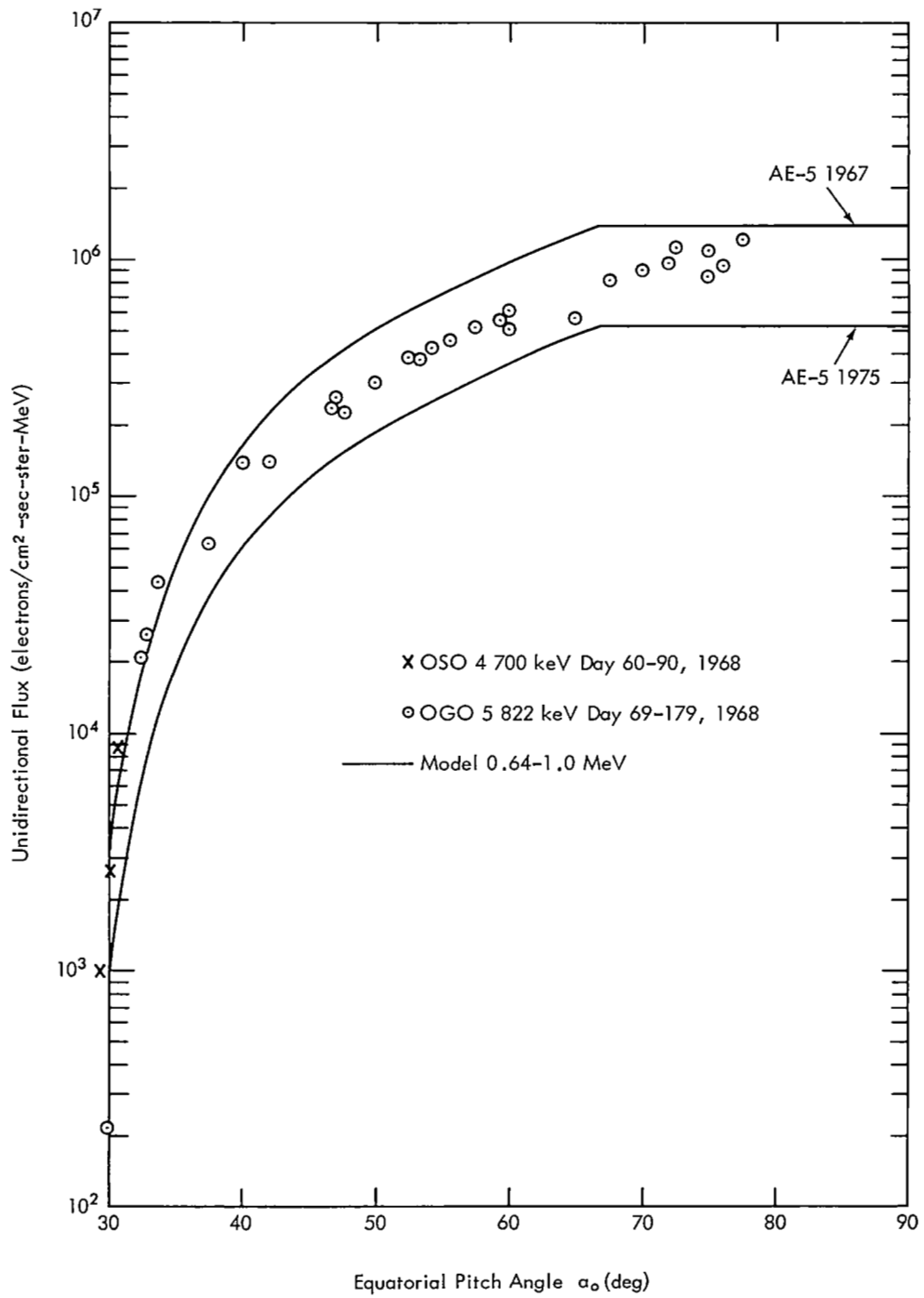


Figure 33. Equatorial Pitch Angle Distribution, L = 1.7

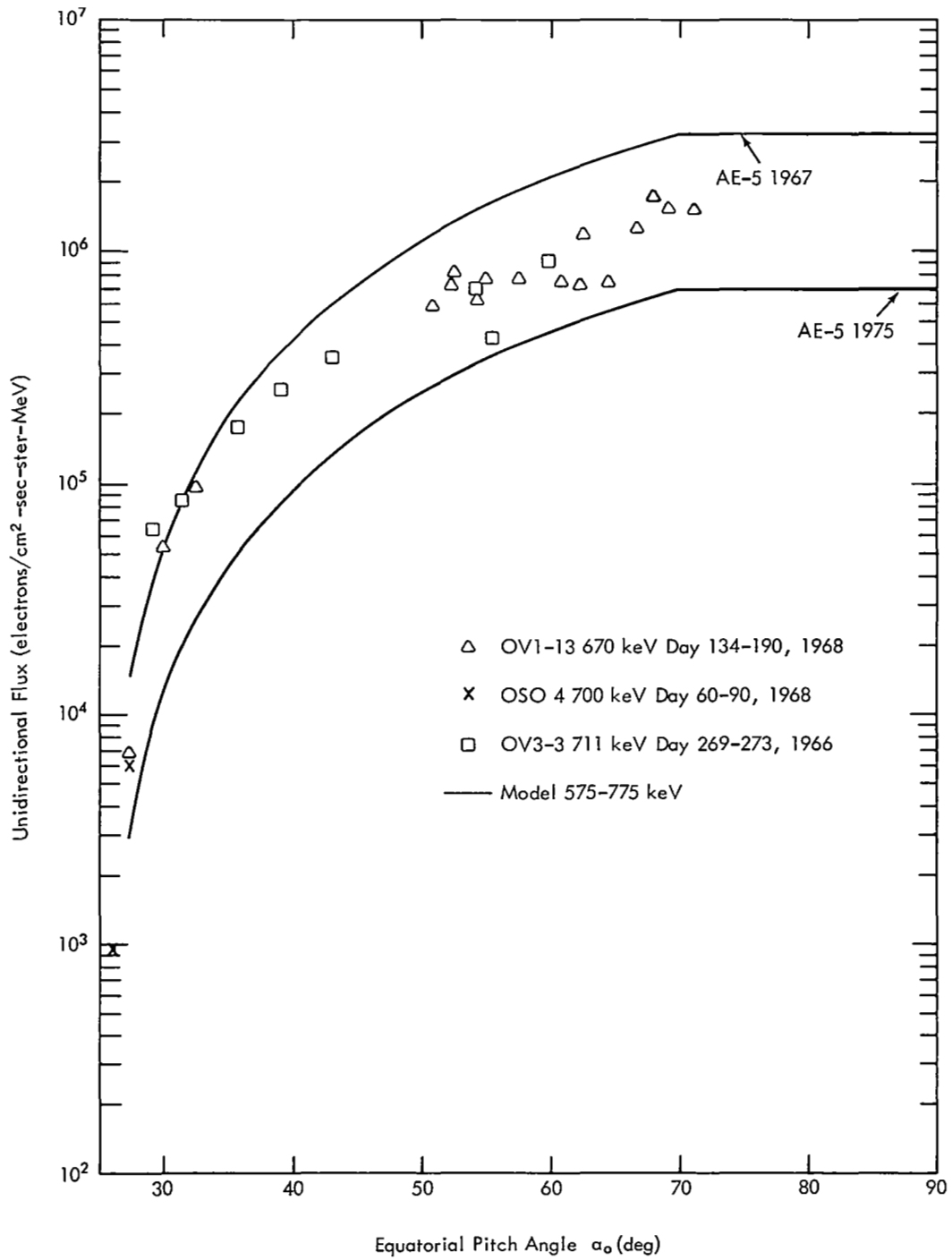


Figure 34. Equatorial Pitch Angle Distribution, L = 1.8

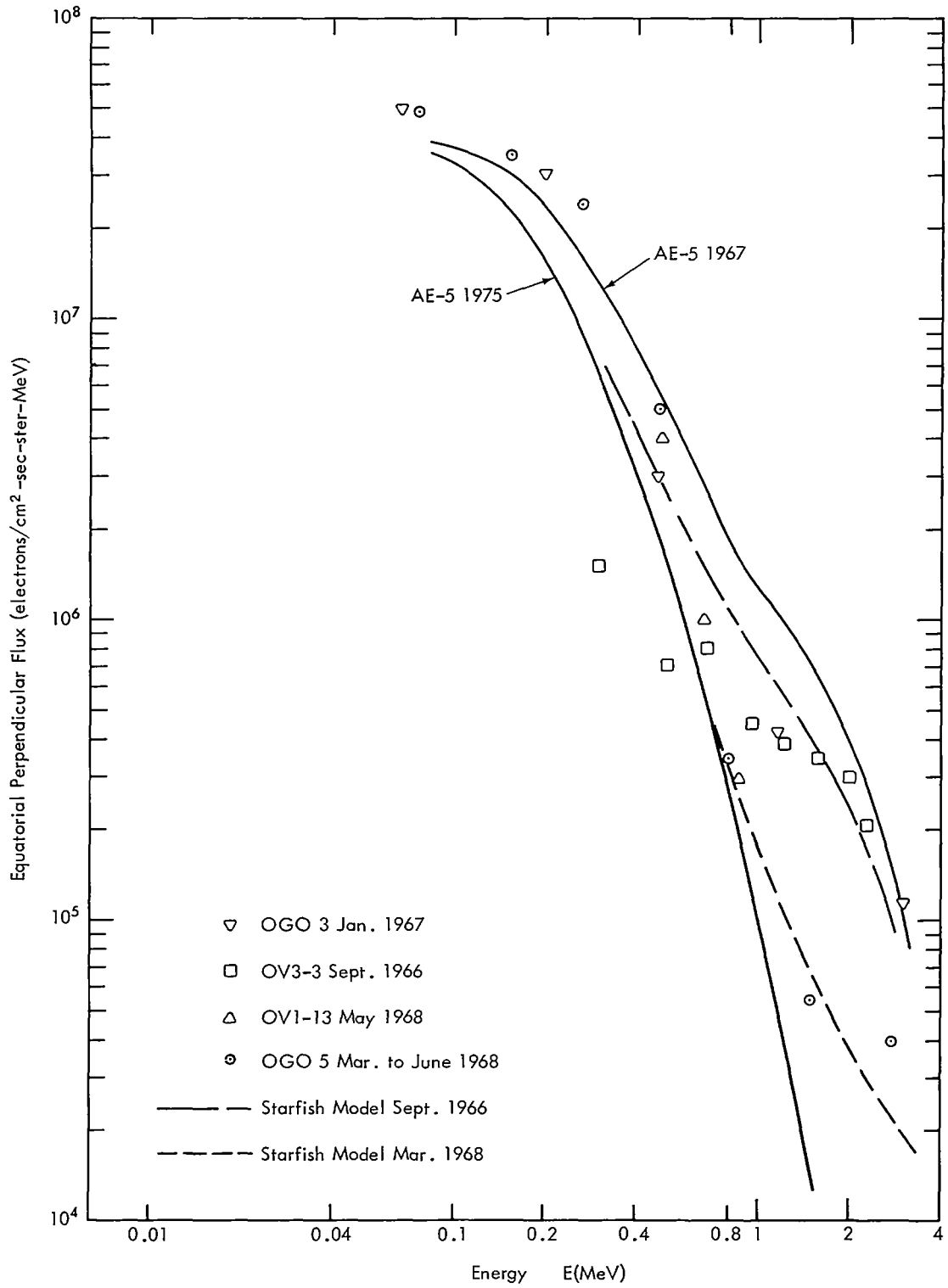


Figure 35. Differential Spectra at L = 1.3

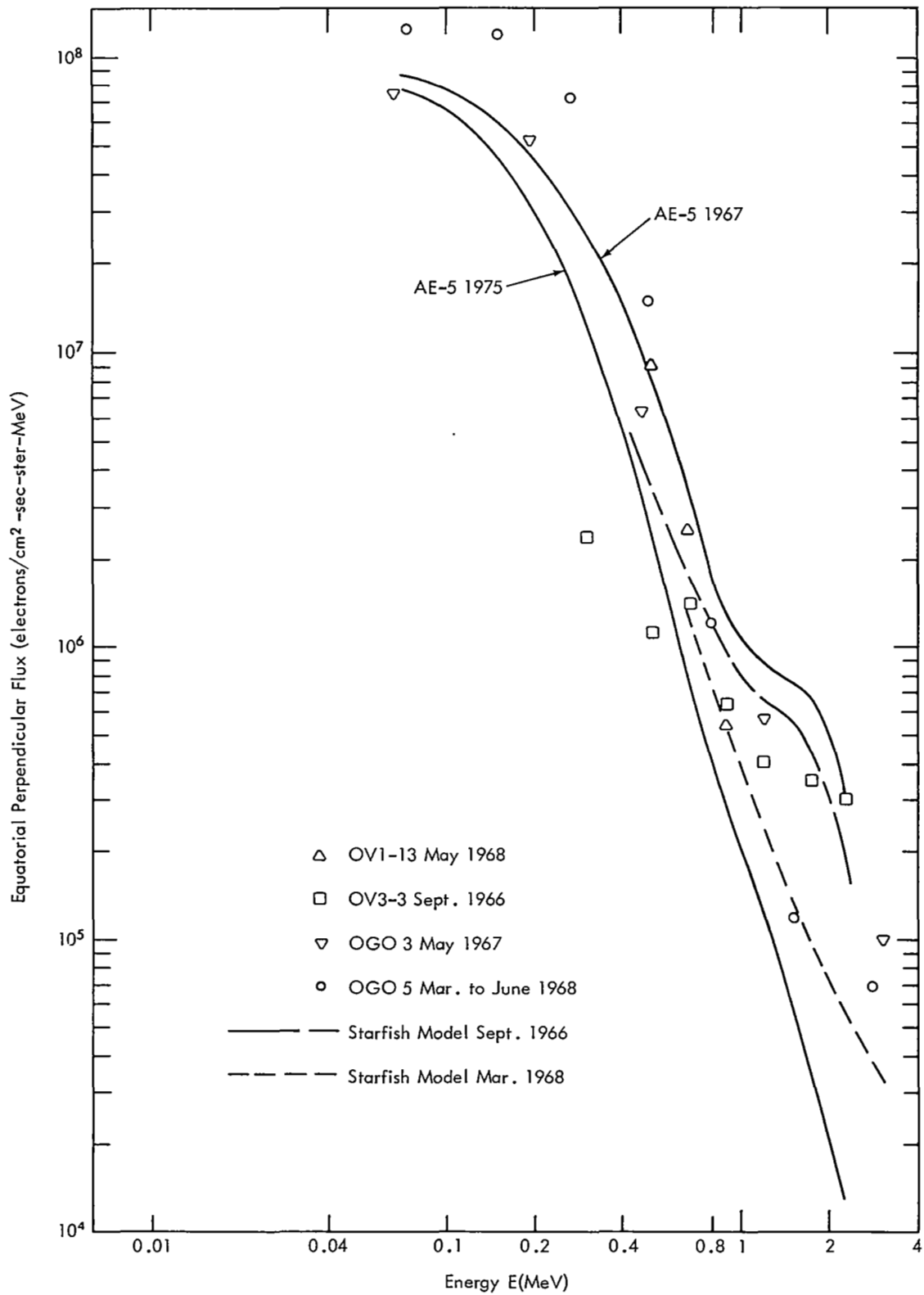


Figure 36. Differential Spectra at L = 1.4

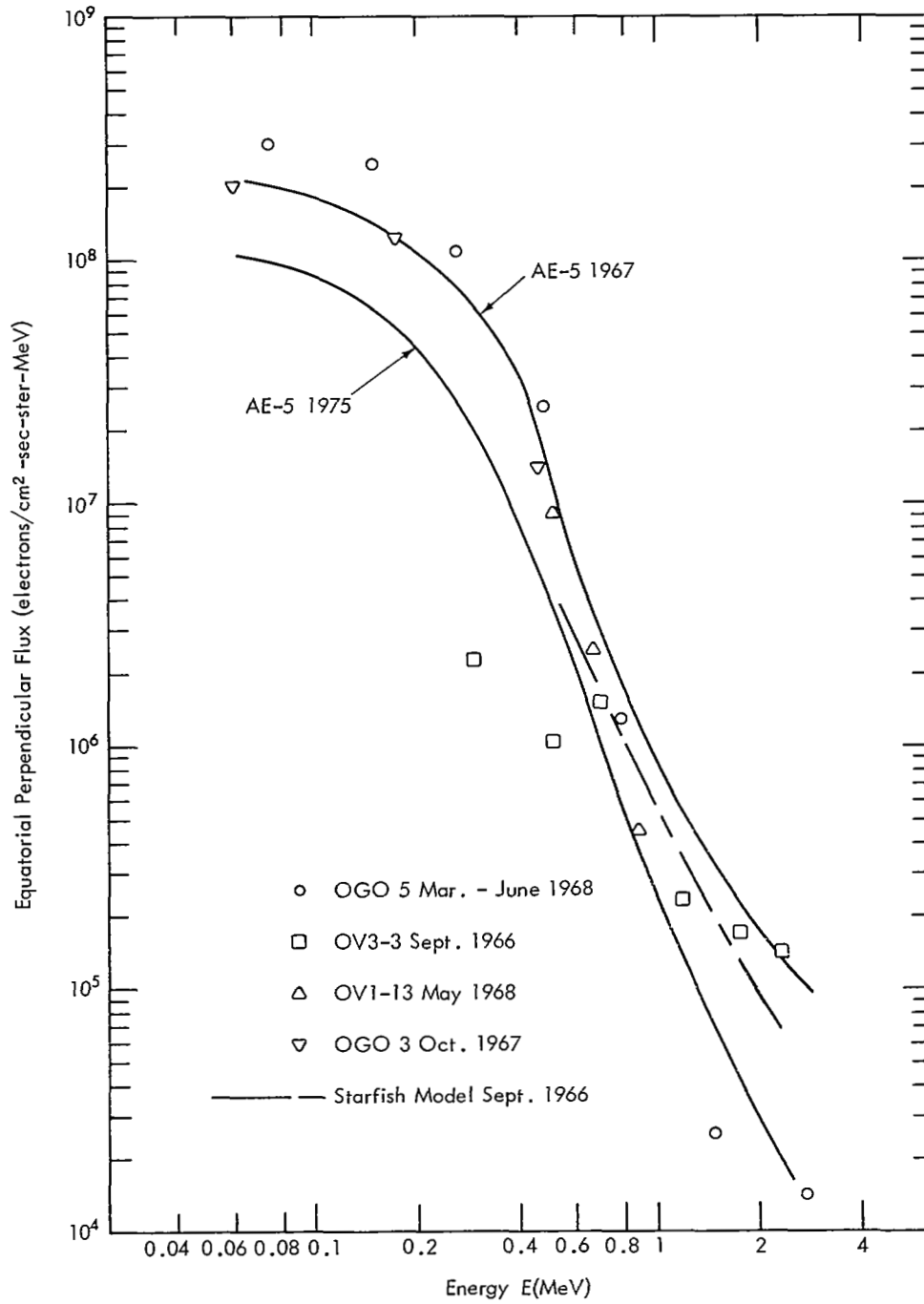


Figure 37. Differential Spectra at L = 1.6

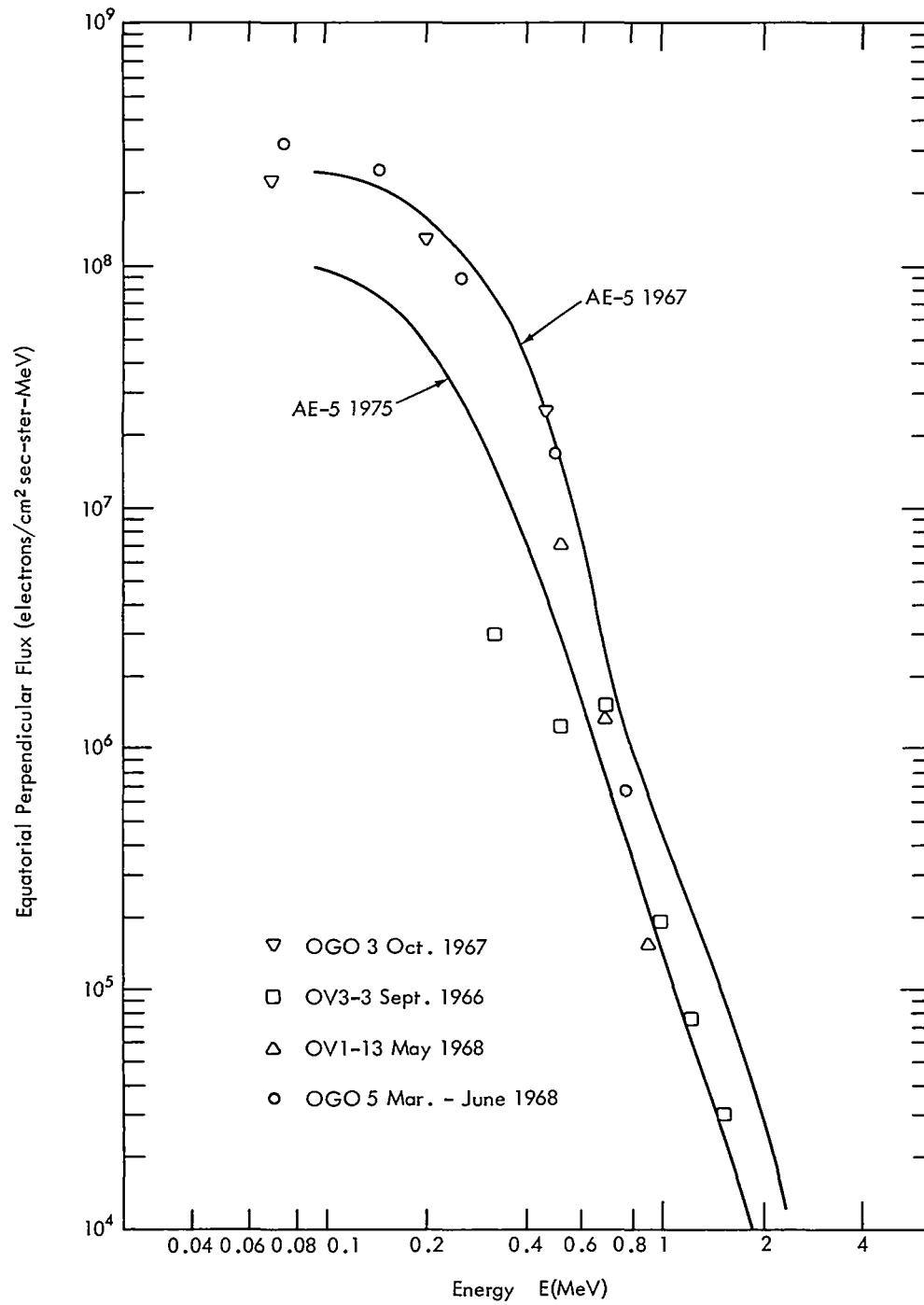


Figure 38. Differential Spectra at L = 1.8

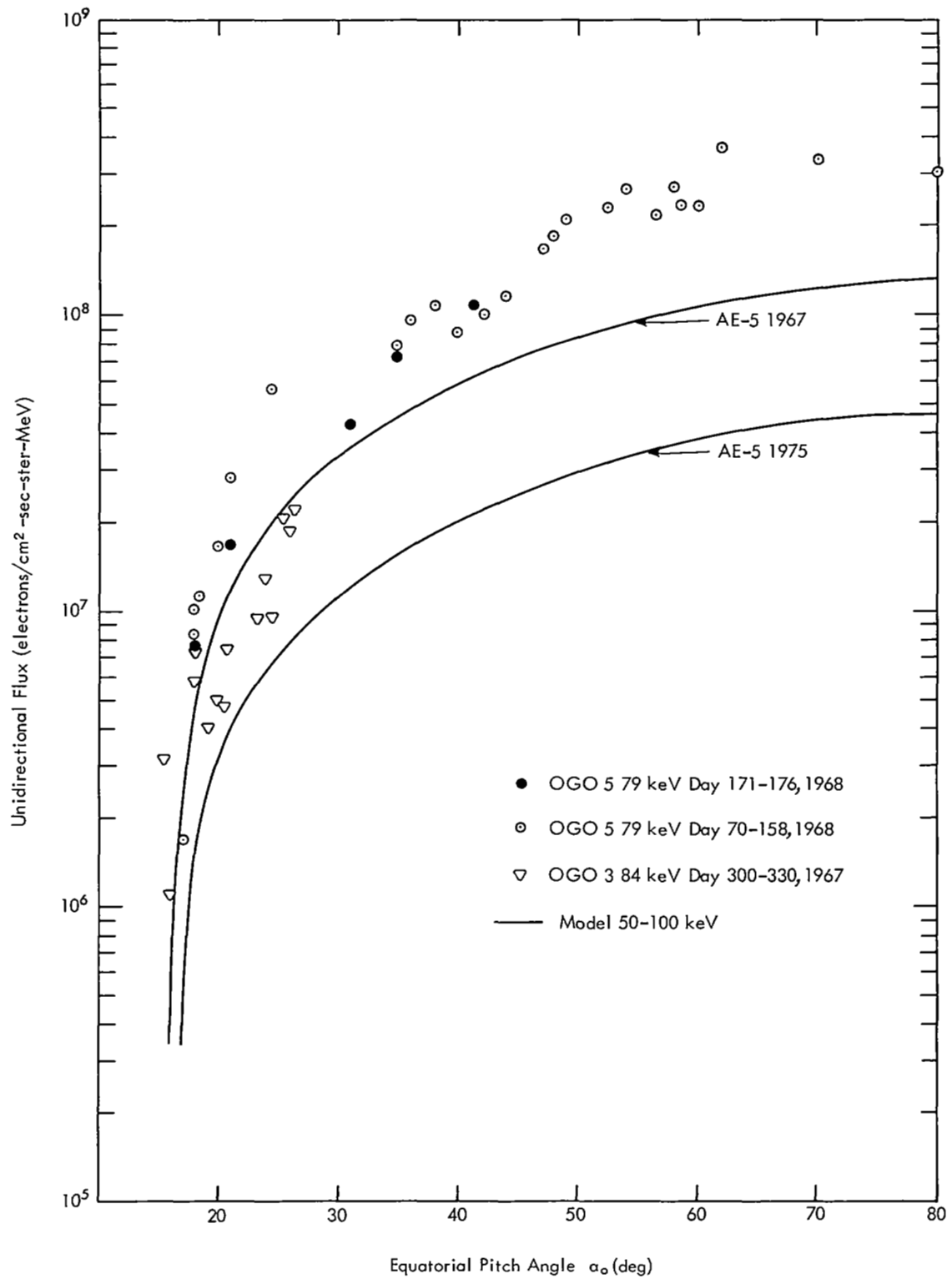


Figure 39. Equatorial Pitch Angle Distribution, L = 2.4

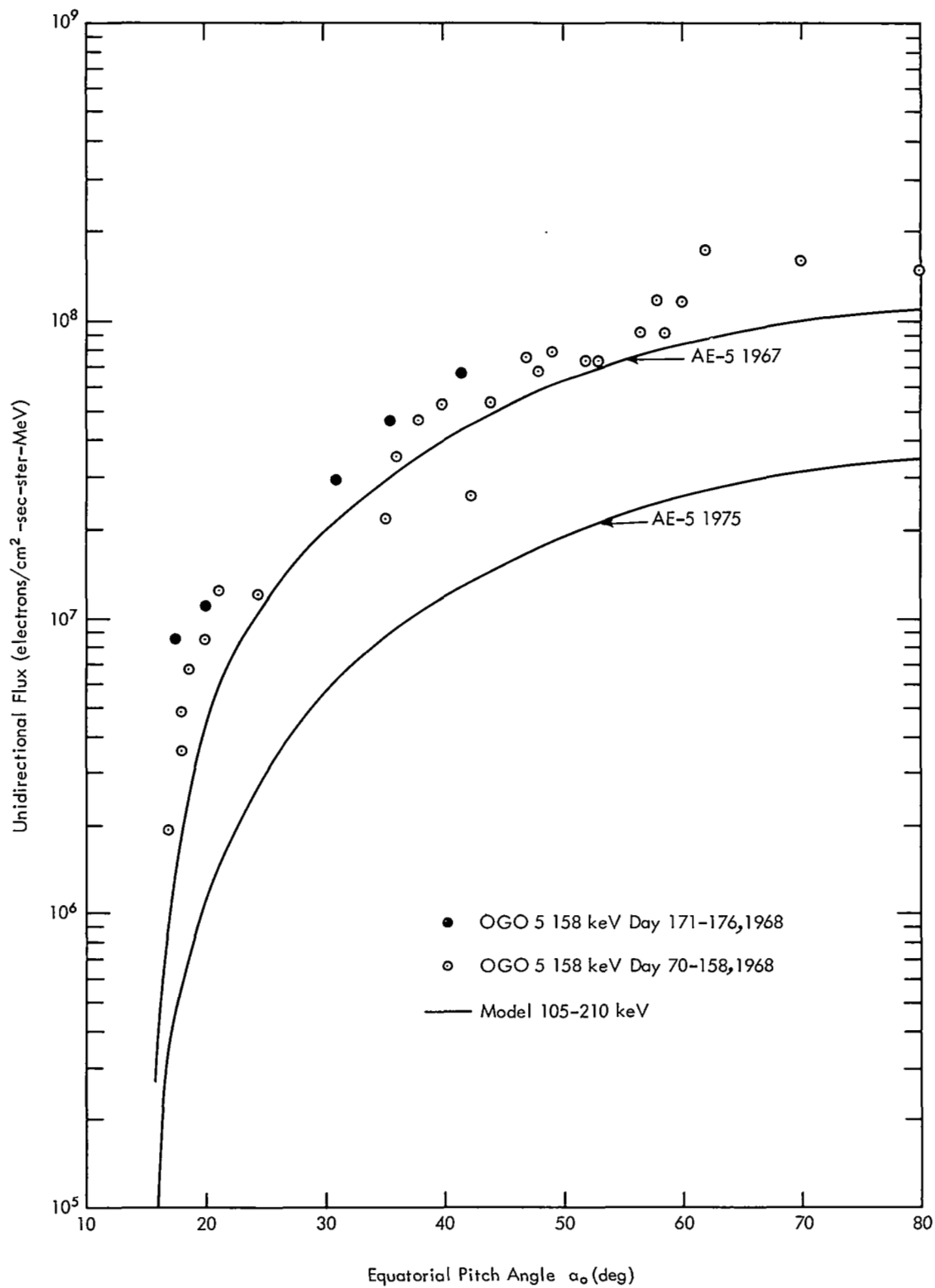


Figure 40. Equatorial Pitch Angle Distribution, L = 2.4

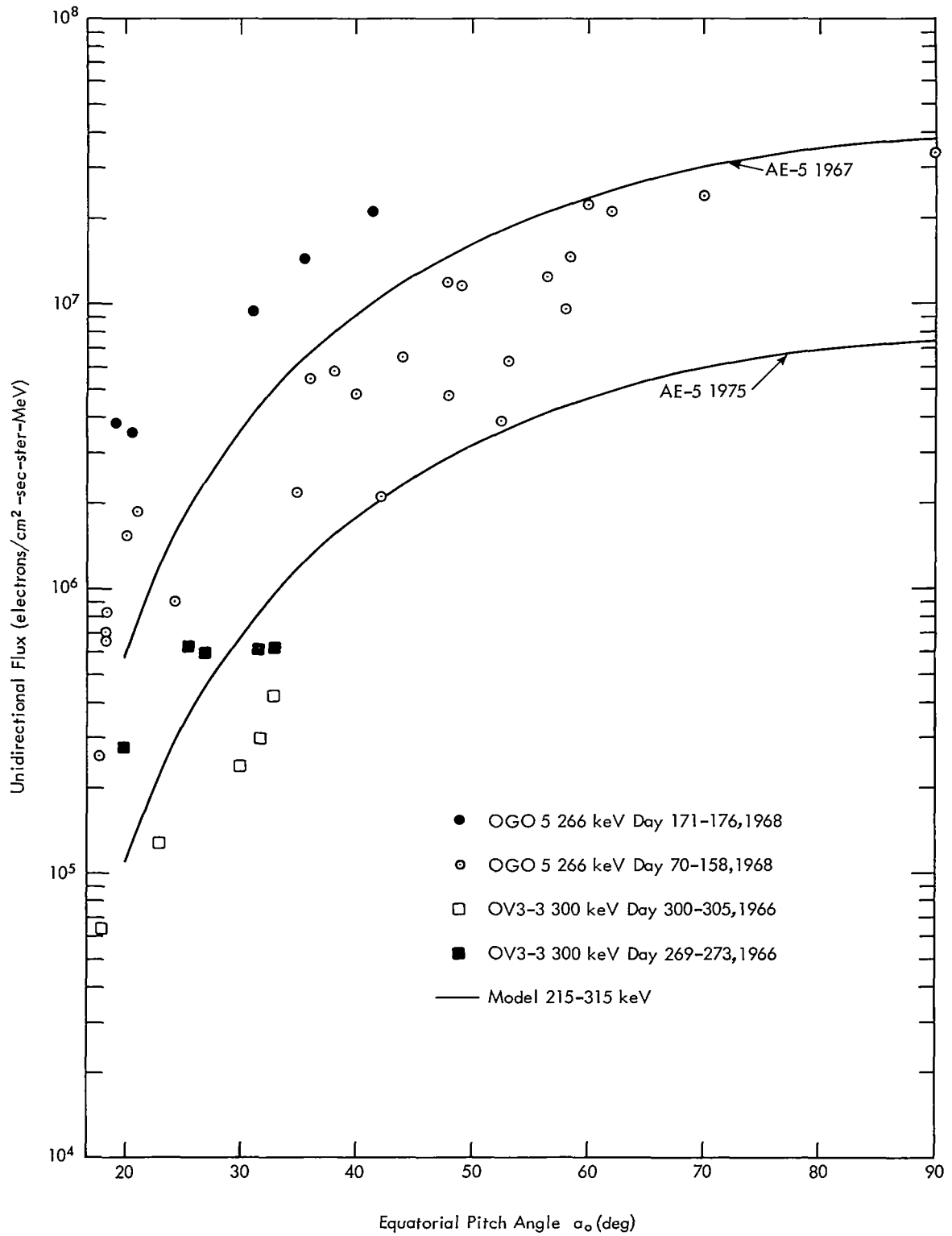


Figure 41. Equatorial Pitch Angle Distribution, $L = 2.4$

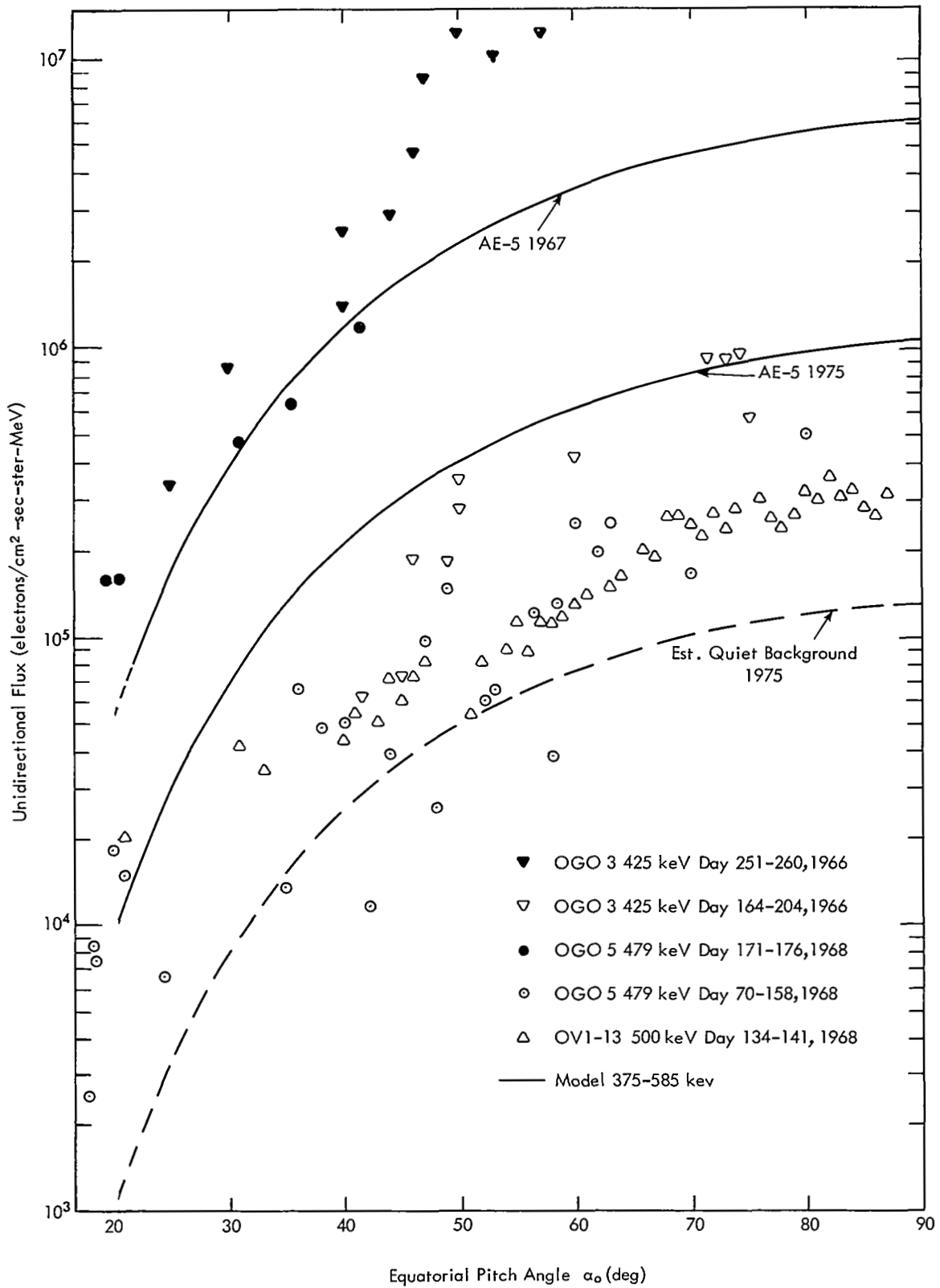


Figure 42. Equatorial Pitch Angle Distribution, $L = 2.4$

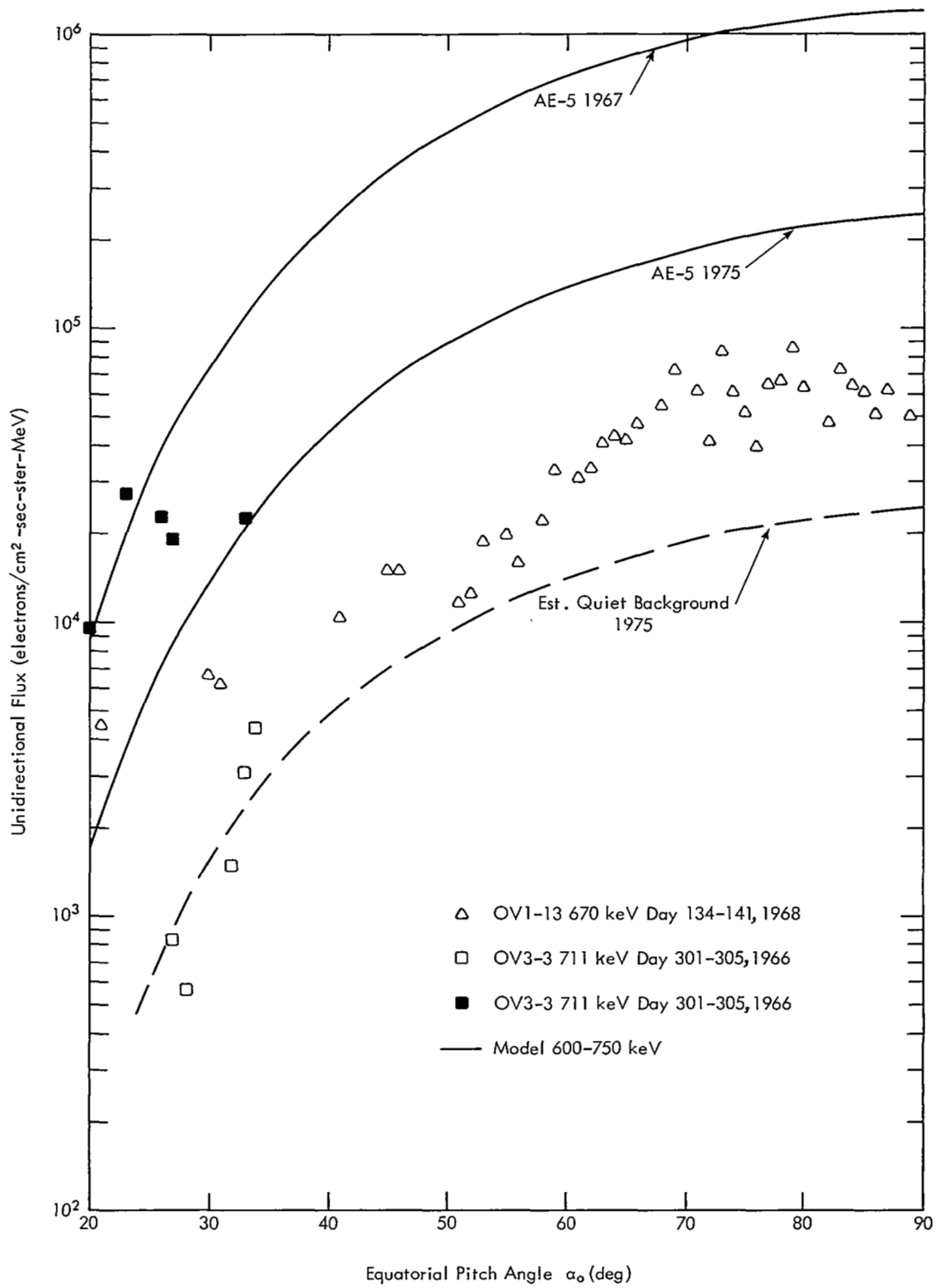


Figure 43. Equatorial Pitch Angle Distribution, L = 2.4

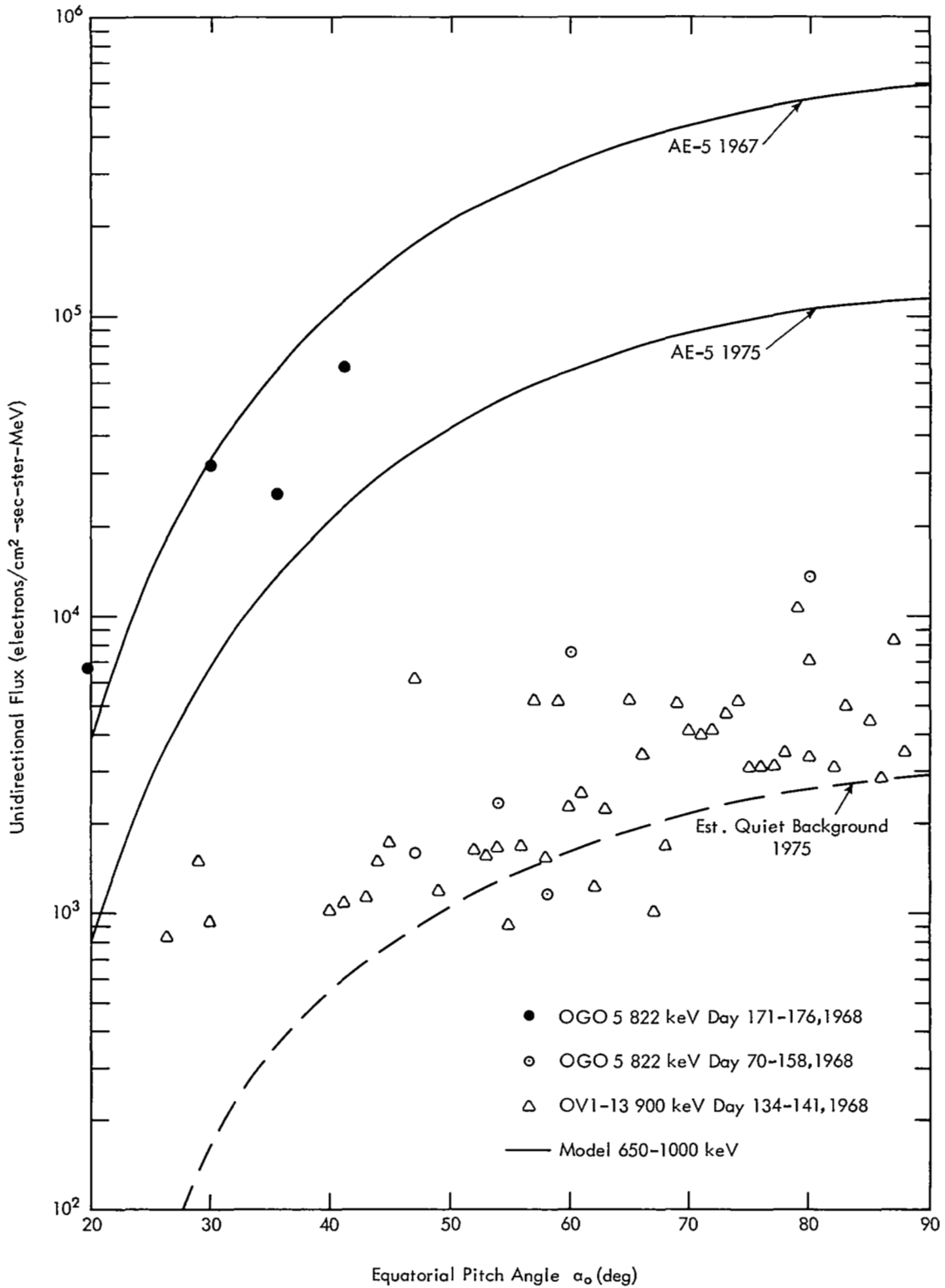


Figure 44. Equatorial Pitch Angle Distribution, L = 2.4

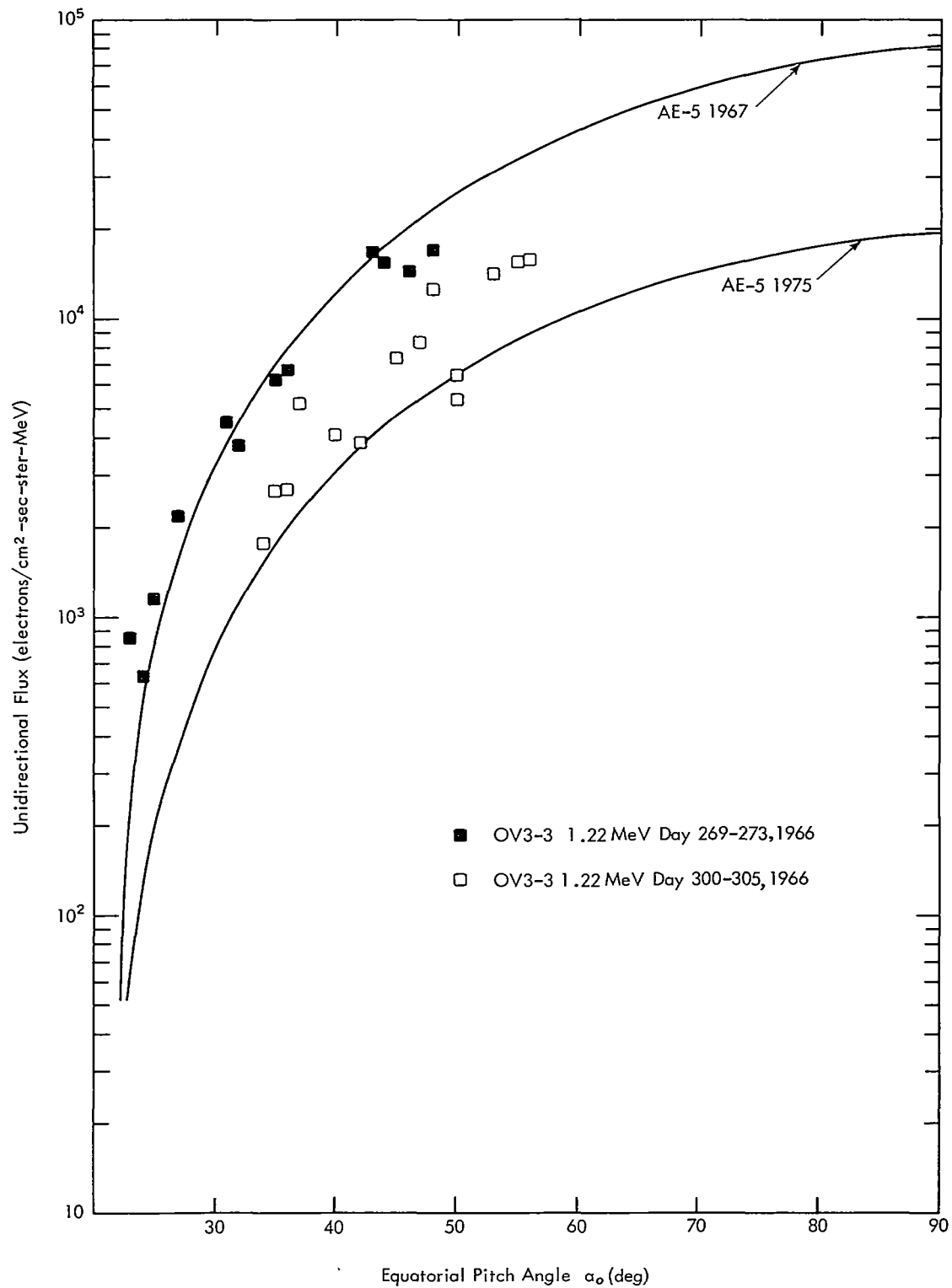


Figure 45. Equatorial Pitch Angle Distribution, L = 2.0

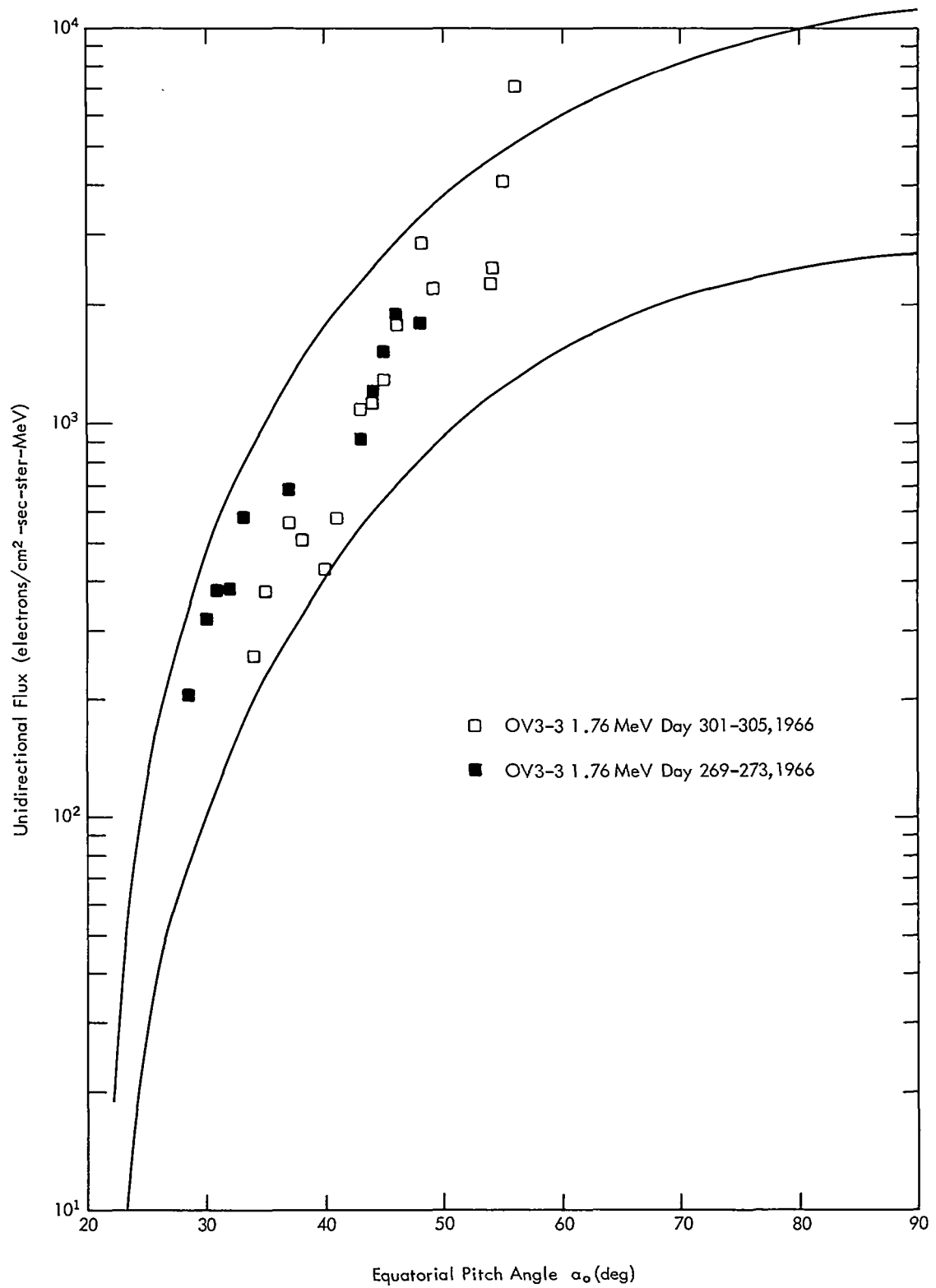


Figure 46. Equatorial Pitch Angle Distribution, L = 2.0

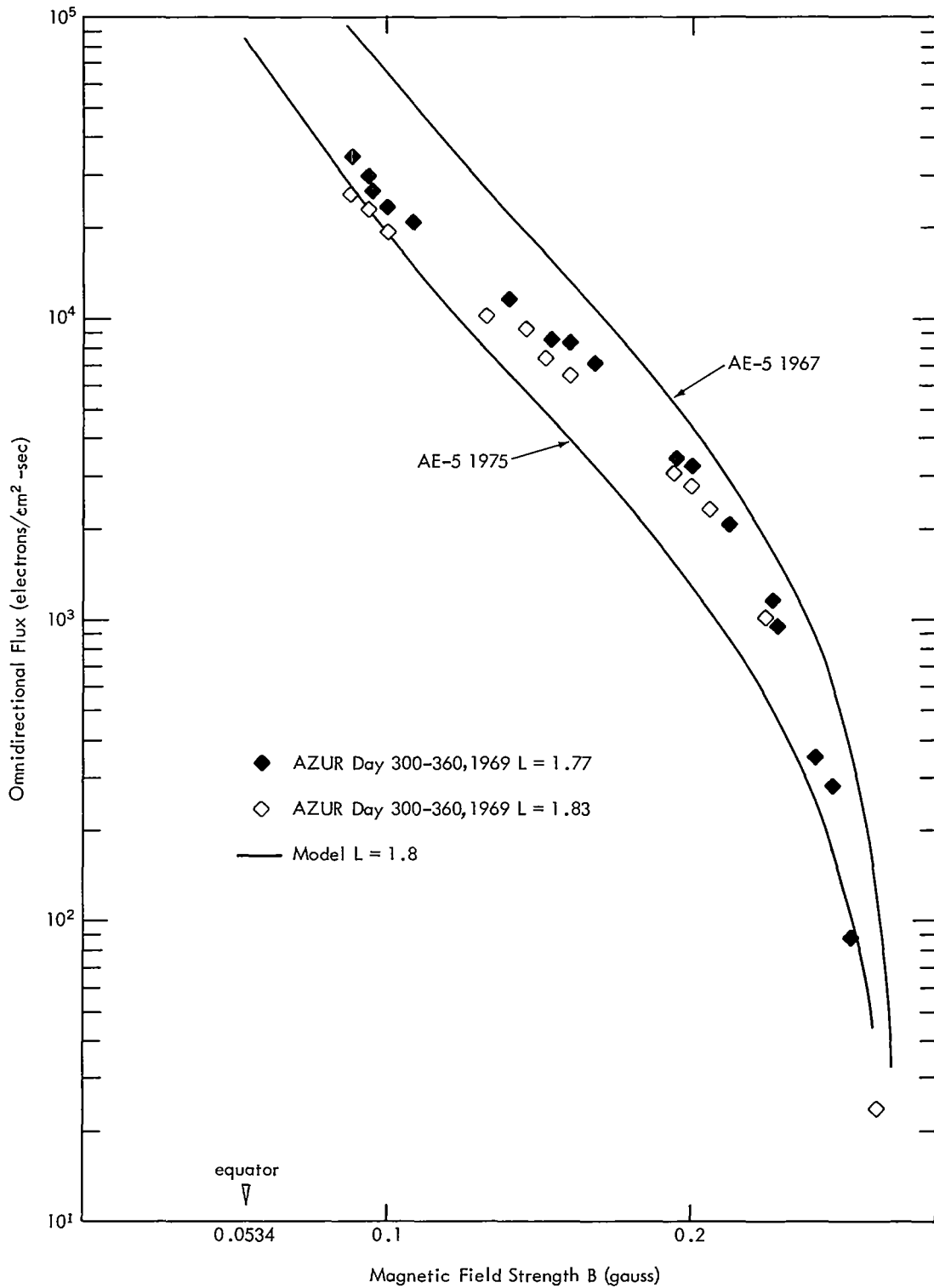


Figure 47. Omnidirectional Flux Distribution for $E > 1.5$ MeV, $L = 1.8$

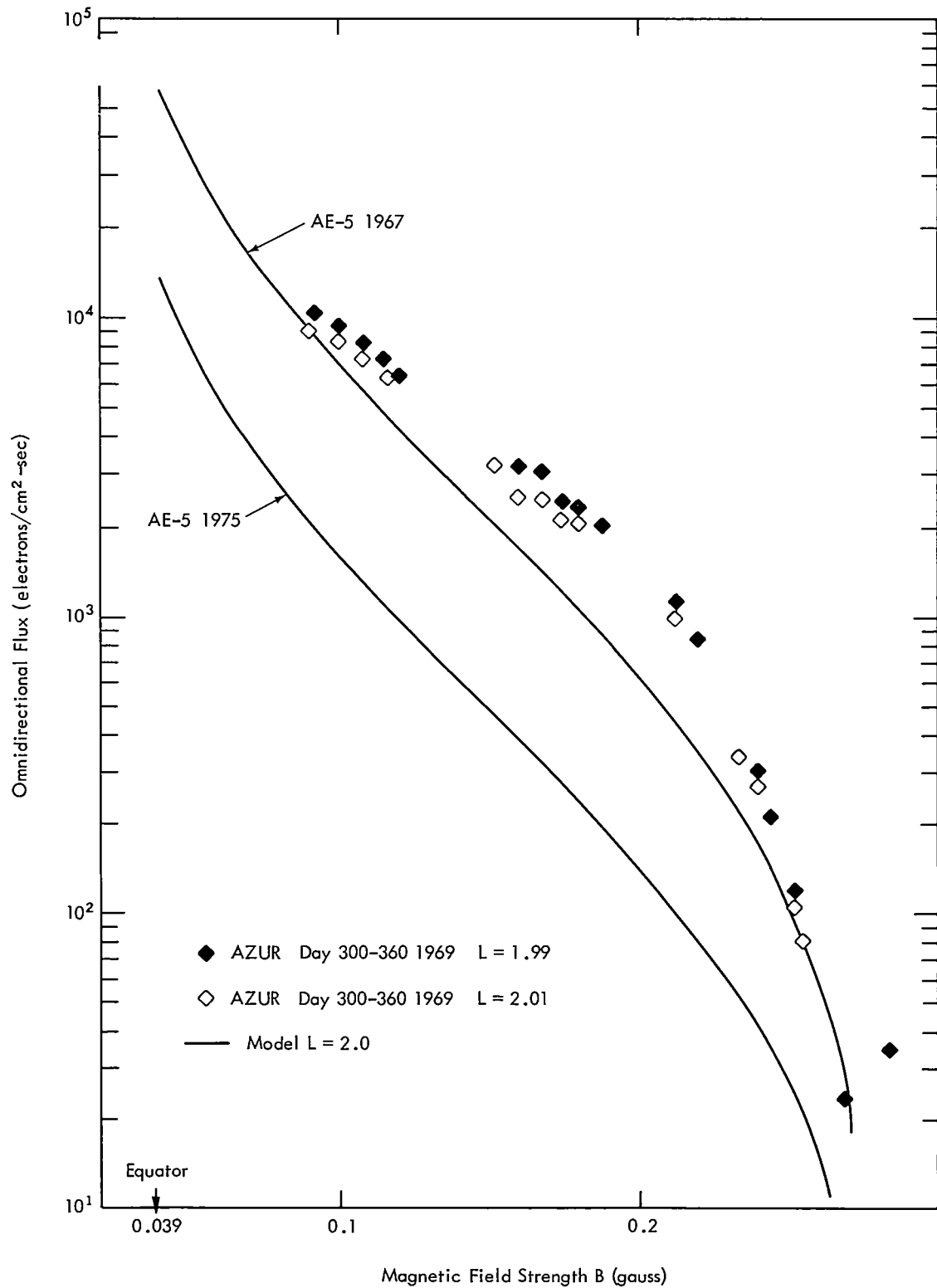


Figure 48. Omnidirectional Flux Distribution for $E > 1.5$ MeV, $L = 2$

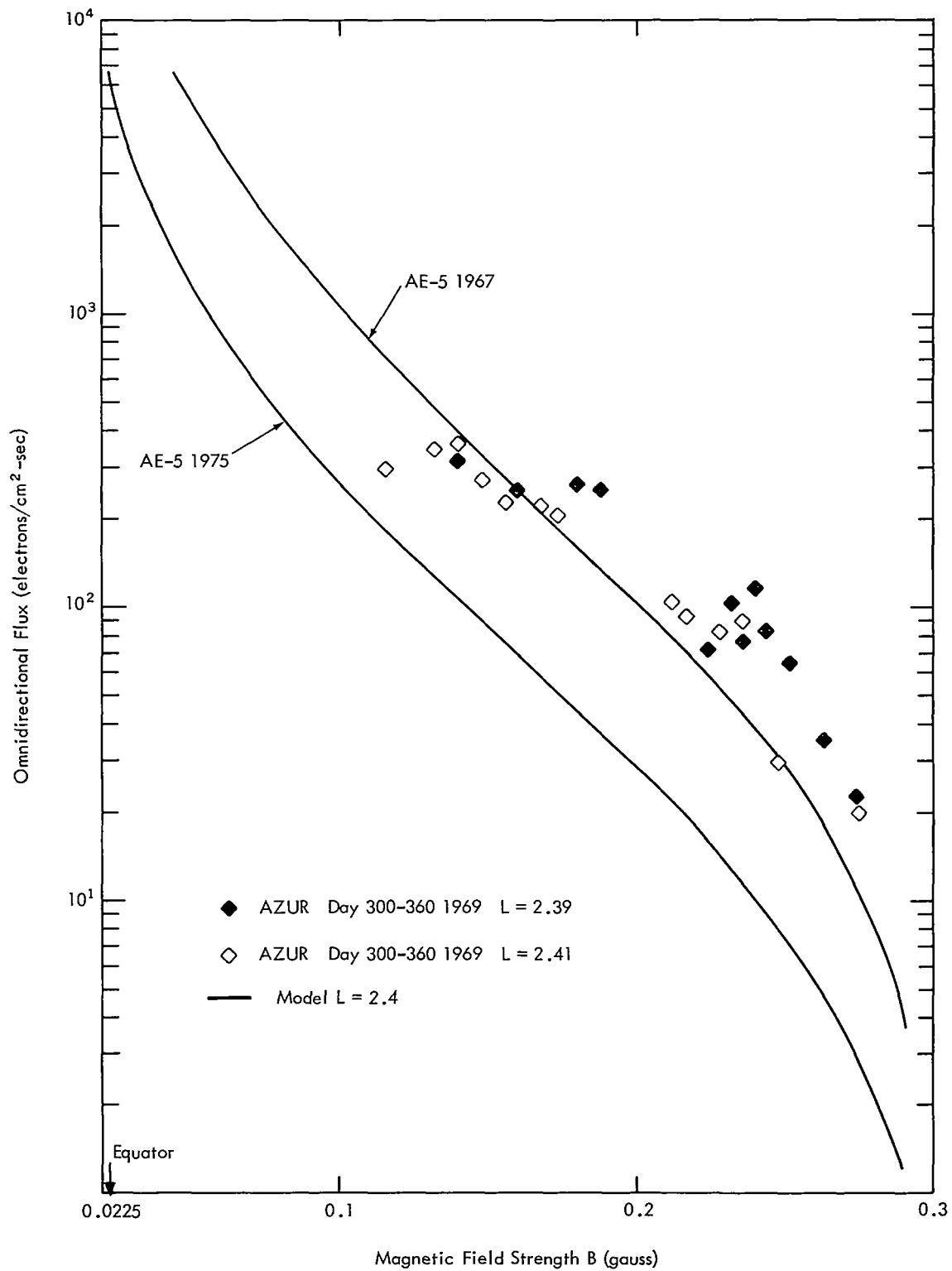


Figure 49. Omnidirectional Flux Distribution for $E > 1.5$ MeV, $L = 2.4$

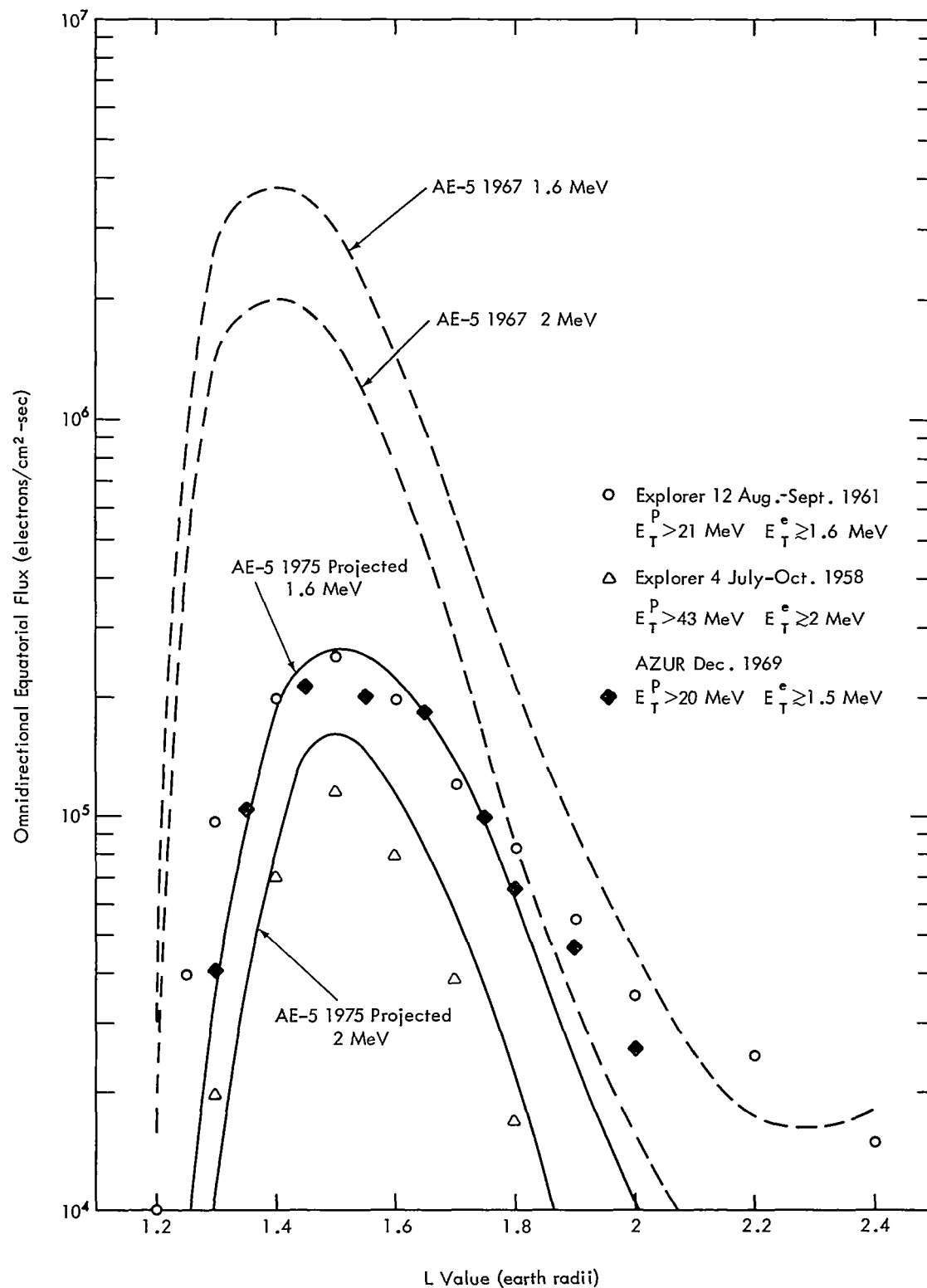


Figure 50. Pre-Starfish Radial Profiles Measured by Explorer 4 and 12

STANDARD CIRCULAR ORBIT 1500 NM ALTITUDE 90 DEG INC.

MODEL USED = AE4-SMIN

THRESHOLD ENERGIES(MEV).

LONGITUDE	LATITUDE	ALTITUDE	B	L	TIME (HRS)	INCREMENT (SEC)	0.250	0.500	0.750
297.62	-59.89	2.77E 03	0.14314	2.998	16.153	30.0	6.07E 04	2.37E 04	1.57E 04
297.50	-61.11	2.77E 03	0.14563	3.113	16.167	30.0	1.30E 05	4.97E 04	3.38E 04
297.37	-62.31	2.77E 03	0.14794	3.259	16.175	30.0	2.08E 05	8.39E 04	5.75E 04
297.25	-63.58	2.78E 03	0.15025	3.421	16.183	30.0	2.36E 05	1.01E 05	6.87E 04
297.12	-64.79	2.77E 03	0.15263	3.592	16.192	30.0	2.73E 05	1.20E 05	8.13E 04
297.00	-66.06	2.77E 03	0.15515	3.766	16.200	30.0	3.32E 05	1.43E 05	9.79E 04
296.87	-67.29	2.77E 03	0.15755	3.996	16.208	30.0	4.41E 05	1.97E 05	1.37E 05
296.75	-68.52	2.77E 03	0.15990	4.230	16.217	30.0	5.89E 05	2.86E 05	1.97E 05
296.62	-69.76	2.77E 03	0.16223	4.469	16.225	30.0	7.27E 05	4.40E 05	2.99E 05
296.50	-70.99	2.77E 03	0.16456	4.773	16.233	30.0	8.78E 05	4.78E 05	2.99E 05
296.37	-72.23	2.77E 03	0.16685	5.101	16.242	30.0	8.76E 05	4.70E 05	2.74E 05
296.25	-73.46	2.77E 03	0.16914	5.463	16.250	30.0	7.40E 05	3.59E 05	2.03E 05
296.12	-74.70	2.77E 03	0.17141	5.874	16.258	30.0	5.80E 05	2.55E 05	1.36E 05
296.00	-75.93	2.77E 03	0.17352	6.345	16.267	30.0	4.01E 05	1.49E 05	7.43E 04
295.87	-77.15	2.77E 03	0.17569	6.866	16.275	30.0	2.45E 05	7.58E 04	3.28E 04
295.75	-78.43	2.77E 03	0.17791	7.443	16.283	30.0	1.11E 05	2.45E 04	8.39E 03
295.62	-79.67	2.77E 03	0.18001	8.201	16.292	30.0	3.21E 04	3.64E 03	9.04E 02
295.50	-80.86	2.77E 03	0.18185	9.093	16.300	30.0	6.79E 03	4.02E 02	6.01E 01
295.37	-82.13	2.77E 03	0.18306	9.993	16.308	30.0	9.26E 02	1.91E 01	0.0

34 ORBIT POINTS HAVE BEEN OMITTED FROM TABLE AS BOTH B AND L WERE ZERO.

111.00	-54.67	2.77E 03	0.20875	10.170	16.600	30.0	3.43E 02	4.31E 00	0.0
110.87	-53.38	2.77E 03	0.20814	9.060	16.603	30.0	4.81E 03	2.60E 02	3.52E 01
110.75	-52.07	2.77E 03	0.20666	8.152	16.617	30.0	3.02E 04	3.55E 03	9.11E 02
110.62	-50.86	2.77E 03	0.20625	7.410	16.625	30.0	1.04E 05	2.42E 04	8.55E 03
110.50	-49.60	2.78E 03	0.20473	6.754	16.633	30.0	2.32E 05	7.40E 04	3.34E 04
110.37	-48.37	2.73E 03	0.20391	6.189	16.642	30.0	3.76E 05	1.49E 05	7.55E 04
110.25	-47.24	2.72E 03	0.20276	5.740	16.650	30.0	5.15E 05	2.34E 05	1.27E 05
110.12	-45.91	2.77E 03	0.20158	5.273	16.658	30.0	6.54E 05	3.37E 05	1.93E 05
110.00	-44.67	2.78E 03	0.19988	4.895	16.667	30.0	7.30E 05	4.01E 05	2.42E 05
109.87	-43.47	2.78E 03	0.19943	4.509	16.675	30.0	6.74E 05	3.62E 05	2.41E 05
109.75	-42.26	2.78E 03	0.19705	4.273	16.683	30.0	4.94E 05	2.44E 05	1.68E 05
109.62	-41.03	2.73E 03	0.19563	4.004	16.692	30.0	3.55E 05	1.59E 05	1.11E 05
109.50	-39.78	2.73E 03	0.19412	3.750	16.700	30.0	2.55E 05	1.10E 05	7.53E 04
109.37	-38.52	2.72E 03	0.19242	3.538	16.708	30.0	2.01E 05	8.78E 04	5.95E 04
109.25	-37.26	2.76E 03	0.19053	3.340	16.717	30.0	1.67E 05	6.95E 04	4.75E 04
109.12	-36.02	2.76E 03	0.18859	3.163	16.725	30.0	1.19E 05	4.63E 04	3.17E 04
109.00	-34.79	2.76E 03	0.18666	3.004	16.733	30.0	4.71E 04	1.71E 04	1.14E 04
108.87	-33.55	2.76E 03	0.18472	2.859	16.742	30.0	1.03E 04	2.83E 03	1.79E 03
108.75	-32.32	2.78E 03	0.18276	2.727	16.750	30.0	6.88E 03	1.51E 03	7.50E 02
108.62	-31.10	2.76E 03	0.18066	2.607	16.758	30.0	1.26E 04	2.34E 03	8.59E 02
108.50	-29.85	2.76E 03	0.17856	2.496	16.767	30.0	2.65E 04	3.60E 03	1.03E 03
108.37	-28.61	2.78E 03	0.17637	2.395	16.775	30.0	5.23E 04	5.42E 03	1.23E 03
108.25	-27.37	2.78E 03	0.17415	2.302	16.783	30.0	7.24E 04	7.01E 03	1.53E 03
108.12	-26.14	2.78E 03	0.17194	2.217	16.792	30.0	1.07E 05	9.63E 03	2.02E 03
108.00	-24.90	2.78E 03	0.16961	2.138	16.800	30.0	1.51E 05	1.28E 04	2.78E 03
107.87	-23.65	2.78E 03	0.16729	2.066	16.808	30.0	2.08E 05	1.80E 04	4.12E 03
107.75	-22.42	2.78E 03	0.16506	1.999	16.817	30.0	3.47E 05	2.57E 04	6.17E 03
107.62	-21.17	2.78E 03	0.16261	1.937	16.825	30.0	4.53E 05	3.63E 04	8.78E 03
107.50	-19.92	2.78E 03	0.16028	1.880	16.833	30.0	6.19E 05	5.47E 04	1.35E 04
107.37	-18.71	2.79E 03	0.15791	1.829	16.842	30.0	8.70E 05	8.78E 04	2.25E 04

Figure 51. Point-by-Point Table, ORP Version 2.0

L BAND SUMMARY

AVERAGE INTEGRAL FLUX WITHIN ENERGY BANDS

(PARTICLES / (CM**2 - DAY))

STANDARD CIRCULAR ORBIT 1500 NM ALTITUDE 0 DEG INC.

MODELS USED = AE4-5MIN

TOTAL TIME = 0.50 DAYS. TIME INTERVAL = 1.00 MIN.

ENERGY RANGES (MEV)	L VALUES											
	1.00 TO 1.22	1.22 TO 1.27	1.27 TO 1.32	1.32 TO 1.37	1.37 TO 1.45	1.45 TO 1.55	1.55 TO 1.65	1.65 TO 1.75	1.75 TO 1.85	1.85 TO 1.95	1.95 TO 2.05	2.05 TO 2.15
0.05- 0.25	0.0	0.0	0.0	0.0	3.05E 12	2.18E 12	3.96E 11	0.0	0.0	0.0	0.0	0.0
0.25- 0.50	0.0	0.0	0.0	0.0	4.35E 11	3.55E 11	6.17E 10	0.0	0.0	0.0	0.0	0.0
0.50- 0.75	0.0	0.0	0.0	0.0	3.22E 10	6.27E 10	1.03E 10	0.0	0.0	0.0	0.0	0.0
0.75- 1.00	0.0	0.0	0.0	0.0	2.60E 10	2.01E 10	3.14E 09	0.0	0.0	0.0	0.0	0.0
1.00- 1.25	0.0	0.0	0.0	0.0	1.13E 10	8.05E 09	1.15E 09	0.0	0.0	0.0	0.0	0.0
1.25- 1.50	0.0	0.0	0.0	0.0	6.97E 09	5.16E 09	7.14E 08	0.0	0.0	0.0	0.0	0.0
1.50- 1.75	0.0	0.0	0.0	0.0	3.78E 09	2.96E 09	3.93E 08	0.0	0.0	0.0	0.0	0.0
1.75- 2.00	0.0	0.0	0.0	0.0	2.50E 09	2.01E 09	2.62E 08	0.0	0.0	0.0	0.0	0.0
2.00- 2.25	0.0	0.0	0.0	0.0	1.54E 09	1.34E 09	1.81E 08	0.0	0.0	0.0	0.0	0.0
2.25- 2.50	0.0	0.0	0.0	0.0	1.00E 09	9.18E 08	1.19E 08	0.0	0.0	0.0	0.0	0.0
2.50- 2.75	0.0	0.0	0.0	0.0	1.39E 09	1.25E 09	1.43E 08	0.0	0.0	0.0	0.0	0.0
2.75- 3.00	0.0	0.0	0.0	0.0	5.56E 08	4.71E 08	5.22E 07	0.0	0.0	0.0	0.0	0.0
3.00- 3.25	0.0	0.0	0.0	0.0	2.65E 08	2.02E 08	2.08E 07	0.0	0.0	0.0	0.0	0.0
3.25- 3.50	0.0	0.0	0.0	0.0	7.75E 07	5.81E 07	6.41E 06	0.0	0.0	0.0	0.0	0.0
3.50- 3.75	0.0	0.0	0.0	0.0	2.27E 07	1.67E 07	1.97E 06	0.0	0.0	0.0	0.0	0.0
3.75- 4.00	0.0	0.0	0.0	0.0	6.63E 06	4.81E 06	6.06E 05	0.0	0.0	0.0	0.0	0.0
4.00- 4.25	0.0	0.0	0.0	0.0	1.98E 06	1.38E 06	1.90E 05	0.0	0.0	0.0	0.0	0.0
4.25- 4.50	0.0	0.0	0.0	0.0	5.52E 05	4.00E 05	5.57E 04	0.0	0.0	0.0	0.0	0.0
4.50- 5.00	0.0	0.0	0.0	0.0	2.14E 05	1.64E 05	2.31E 04	0.0	0.0	0.0	0.0	0.0
5.00	0.0	0.0	0.0	0.0	0.0	0.0	0.0	0.0	0.0	0.0	0.0	0.0
TOTAL =	0.0	0.0	0.0	0.0	3.67E 12	2.64E 12	4.74E 11	0.0	0.0	0.0	0.0	0.0
NP1 =	0	0	0	0	411	252	56	0	0	0	0	0
NP2 =	0	0	0	0	411	252	56	0	0	0	0	0
NSIZE =	0	0	0	0	411	252	56	0	0	0	0	0

NP1 = NUMBER OF ORBIT POINTS FOR WHICH NON ZERO FLUX WAS ENCOUNTERED ABOVE 0.05 MEV
 NP2 = NUMBER OF ORBIT POINTS FOR WHICH NON ZERO FLUX WAS ENCOUNTERED ABOVE 0.50 MEV
 NSIZE = NUMBER OF ORBIT POINTS LYING IN L BAND.

Figure 52. L-Band Summary Table, ORP Version 2.0

133

INTENSITY SUMMARY

AVERAGE INTEGRAL FLUX WITHIN ENERGY BANDS

STANDARD CIRCULAR ORBIT 1500 NM ALTITUDE 0 DEG INC.

MODELS USED = AE4-5MIN

TOTAL TIME = 0.50 DAYS. TIME INTERVAL = 1.00 MIN.

ENERGY RANGES	INTENSITY RANGES								
	1.E2 OR LESS	1.E2 TO 1.E3	1.E3 TO 1.E4	1.E4 TO 1.E5	1.E5 TO 1.E6	1.E6 TO 1.E7	1.E7 TO 1.E8	1.E8 & OVER	
0.05 - 0.25	0.0	0 0.0	0 0.0	0 0.0	0 0.0	0 0.0	0 5.62E 12	719 0.0	0
0.25 - 0.50	0.0	0 0.0	0 0.0	0 0.0	0 0.0	0 3.42E 11	314 5.60E 11	405 0.0	0
0.50 - 0.75	0.0	0 0.0	0 0.0	0 0.0	0 0.0	0 1.55E 11	719 0.0	0 0.0	0
0.75 - 1.00	0.0	0 0.0	0 0.0	0 0.0	0 4.92E 10	719 0.0	0 0.0	0 0.0	0
1.00 - 1.25	0.0	0 0.0	0 0.0	0 0.0	0 2.05E 10	719 0.0	0 0.0	0 0.0	0
1.25 - 1.50	0.0	0 0.0	0 0.0	0 1.90E 03	16 1.27E 10	703 0.0	0 0.0	0 0.0	0
1.50 - 1.75	0.0	0 0.0	0 0.0	0 5.00E 09	553 2.13E 09	166 0.0	0 0.0	0 0.0	0
1.75 - 2.00	0.0	0 0.0	0 0.0	0 4.78E 09	719 0.0	0 0.0	0 0.0	0 0.0	0
2.00 - 2.25	0.0	0 0.0	0 0.0	0 3.06E 09	719 0.0	0 0.0	0 0.0	0 0.0	0
2.25 - 2.50	0.0	0 0.0	0 0.0	0 2.09E 09	719 0.0	0 0.0	0 0.0	0 0.0	0
2.50 - 2.75	0.0	0 0.0	0 0.0	0 2.79E 09	719 0.0	0 0.0	0 0.0	0 0.0	0
2.75 - 3.00	0.0	0 0.0	0 2.14E 08	202 3.67E 06	517 0.0	0 0.0	0 0.0	0 0.0	0
3.00 - 3.25	0.0	0 0.0	0 4.83E 03	719 0.0	0 0.0	0 0.0	0 0.0	0 0.0	0
3.25 - 3.50	0.0	0 4.31E 06	44 1.37E 06	675 0.0	0 0.0	0 0.0	0 0.0	0 0.0	0
3.50 - 3.75	0.0	0 4.14E 07	719 0.0	0 0.0	0 0.0	0 0.0	0 0.0	0 0.0	0
3.75 - 4.00	5.96E 05	56 1.15E 07	663 0.0	0 0.0	0 0.0	0 0.0	0 0.0	0 0.0	0
4.00 - 4.25	3.55E 06	719 0.0	0 0.0	0 0.0	0 0.0	0 0.0	0 0.0	0 0.0	0
4.25 - 4.50	1.01E 06	719 0.0	0 0.0	0 0.0	0 0.0	0 0.0	0 0.0	0 0.0	0
4.50 - 5.00	4.01E 05	719 0.0	0 0.0	0 0.0	0 0.0	0 0.0	0 0.0	0 0.0	0
5.00	0.0	719 0.0	0 0.0	0 0.0	0 0.0	0 0.0	0 0.0	0 0.0	0

INTENSITY RANGES HAVE UNITS OF PARTICLES PER SQCM SEC FOR THE ENERGY RANGES IN LEFT COLUMN.
 THE ACCUMULATED FLUXES HAVE UNITS OF PARTICLES PER SQCM DAY FOR THE ENERGY RANGES IN LEFT COLUMN.
 TOTALS FOLLOWING THE ACCUMULATED FLUXES INDICATE THE NUMBER OF FLUXES ENCOUNTERED IN BIN.
 THESE TOTALS HAVE MAX VALUES OF 9999.

Figure 53. Intensity Summary Table, ORP Version 2.0

PEAK FLUX PER ORBIT TABLE

STANDARD CIRCULAR ORBIT 1500 NM ALTITUDE 90 DEG INC.

MODELS USED = AE4-5MIN

ENERGY = 0.50 MEV

TOTAL TIME = 1.00 DAYS. TIME INTERVAL = 0.50 MIN. NOMINAL PERIOD = 2.418 HRS.

ORBIT NO.	PEAK ENCOUNTERED	LONGITUDE	LATITUDE	ALTITUDE	TIME (HRS)	FIELD (E) (GAUSS)	LINE (L) (E.R.)	TOTAL FLUX/ORBIT (PARTICLES/CM**2)	S-N EQUATORIAL CROSSING (DEG)
1	4.052E 06	324.50	-8.50	2785.5	2.36667	0.09021	1.511	6.977E 09	360.00
2	4.013E 06	266.87	-15.75	2784.2	4.74167	0.09401	1.492	5.380E 09	323.62
3	3.604E 06	252.12	-11.90	2785.1	7.19167	0.10384	1.448	5.088E 09	287.25
4	3.230E 06	52.62	-1.16	2783.7	6.49167	0.11121	1.450	5.276E 09	250.87
5	3.767E 06	16.75	3.64	2784.5	10.88333	0.10029	1.460	5.634E 09	214.50
6	4.055E 06	339.75	-2.74	2787.4	13.35000	0.09223	1.501	6.113E 09	178.12
7	4.055E 06	302.25	-14.05	2784.8	15.85000	0.09125	1.506	5.753E 09	141.75
8	3.760E 06	266.00	-12.97	2784.6	18.26666	0.10041	1.460	5.429E 09	105.37
9	3.534E 06	32.75	0.20	2785.6	21.81667	0.10405	1.462	5.794E 09	69.12
10	3.566E 06	32.50	2.68	2785.4	21.83333	0.10401	1.448	PARTIAL ORBIT	

Figure 54. Peak Flux per Orbit Table, ORP Version 2.0

BROUWER ORBIT GENERATOR.

AXIS(RF) = 0.10435549D 01
 ECCENTRICITY = 0.10000000D-06
 INCLINATION(DIG) = 0.30000000D 02
 MEAN(RAD) = 0.0
 PERIGEE(RAD) = 0.0
 NODE(RAD) = 0.0

TIME INTERVAL BETWEEN ORBIT POINTS = 120.00 SECS TOTAL ORBIT TIME = 24.00 HRS

STANDARD CIRCULAR ORBIT 150 NM ALTITUDE 30 DEG INC.

LONGITUDE (DEGS)	LATITUDE (DEGS)	ALTITUDE (KM)	B (GAUSS)	L	TIME (HR)
0.35512315D 01	-0.23111170D-01	0.27915114D 03	0.25700467D 00	0.10765937D 01	0.0
0.004320535D 01	0.39889503D 01	0.28120775D 03	0.27534821D 00	0.10482624D 01	0.33333333D-01
0.12581175D 02	0.77371334D 01	0.27998406D 03	0.23643221D 00	0.10283783D 01	0.06666667D-01
0.19631425D 02	0.11765100D 02	0.28003229D 03	0.29846132D 00	0.10209100D 01	0.10000000D 00
0.26461173D 02	0.15392581D 02	0.28104931D 03	0.31329465D 00	0.10264785D 01	0.13333333D 00
0.33770440D 03	-0.95034038D 01	0.28310700D 03	0.23693144D 00	0.11337945D 01	0.23666667D 02
0.34430367D 03	-0.55348750D 01	0.28041160D 03	0.24094222D 00	0.11144893D 01	0.23900000D 02
0.35082089D 03	-0.15745487D 01	0.28148739D 03	0.25535368D 00	0.10857558D 01	0.23933333D 02
0.35712930D 03	0.23550274D 01	0.28320214D 03	0.26532292D 00	0.10644500D 01	0.23966667D 02

-100.

NUMBER OF ORBIT POINTS = 720

AVERAGE ALTITUDE(KMS) = 0.27795039D 03

NOMINAL PERIOD(HRS) = 0.14936665D 01

Figure 55. ORB Output